universität innsbruck

Polarons and their Mediated Interactions in Fermi-Bose and Fermi-Fermi Mixtures of Lithium and Potassium

Cosetta Baroni, MSc

Doctoral thesis submitted to the faculty of
Mathematics, Computer Science and Physics
at the University of Innsbruck

in partial fulfillment of the requirements for the degree of
DOCTOR OF PHILOSOPHY (PhD)

Carried out at the Institute for Quantum Optics and Quantum Information and
the Institute of Experimental Physics under the supervision of
UNIV.-PROF. DR. RUDOLF GRIMM
with the co-supervison of
UNIV.-PROF. DR. ORIOL ROMERO-ISART

Innsbruck, March 2023

SUMMARY

In this Thesis, I present experimental investigations concerning the physics of impurities in strongly interacting Fermi-Bose and Fermi-Fermi mixtures. Our system consists of a bath of degenerate fermionic ^{6}Li, in which either bosonic ^{41}K or fermionic ^{40}K impurities are embedded. Thus, we investigate the quasi-particles formed by K impurities, obeying different quantum statistics, interacting with a Fermi sea of Li atoms: Fermi polarons.

We first studied Fermi polarons formed by bosonic impurities. We investigated the two cases of thermal impurities and of impurities forming a partial Bose-Einstein condensate. In the thermal case, and for the thermal part of the partial condensate, we found good agreement between the recorded energy spectrum and the theory for isolated polarons. Moreover, we observed hints of mediated interactions between polarons for increasing impurity concentration. In the case of condensed impurities, we observed the emergence of an additional branch in the impurity energy spectrum, which can be explained by the presence of Bose polarons created by fermionic Li impurities in the K condensate. In our system we can thus observe the coexistence of Fermi and Bose polarons.

In a new generation of precise measurements, we investigated more closely the effect of increasing the impurity concentration on the impurity energy spectrum.

Summary

This work led to the first observation of the mediated polaron-polaron interaction. In order to understand how this effect is affected by different quantum statistics, we employed either bosonic or fermionic thermal impurities. In the single impurity limit, we did not observe any difference in the respective energy spectra, as expected for single impurities. For higher impurity concentration we observed the experimentally challenging weak effect of the mediated polaron-polaron interaction. In particular, we unambiguously detected the influence of the quantum statistics, which manifests itself as a sign inversion in the mediated polaron-polaron interaction.

CONTENTS

LIST OF FIGURES

LIST OF TABLES

CHAPTER

INTRODUCTION AND OUTLINE 1

If you want to find the secrets of the universe,
think in terms of energy, frequency and vibration.
N. Tesla

Wave-particle duality is a key concept at the basis of quantum mechanics. It states that matter can be described both in terms of particles and in terms of waves. Whether one or the other description applies better is determined by the wavelength associated with the object, the de Broglie wavelength [Bro25]. For instance, a gas of atoms is described in terms of particles if the distance between its components is smaller than their de Broglie wavelength. When the de Broglie wavelength of the particles becomes comparable with their interparticle separation, the waves corresponding to each particle start to overlap and quantum-statistical effects appear: We reach degeneracy. Different phenomena then arise, depending on the nature of the constituent of the gas. In the field of ultracold atoms we exploit dilute gases at temperatures as low as few nK, in order to investigate such effects. In nature there are two fundamentally distinct families of particles: bosons and fermions. Bosons have integer spin, and follow the Bose-Einstein statistics. Thus, there is no limit at the number of indistinguishable bosons that can occupy the same quantum state. In

this case, reaching degeneracy corresponds to a phase transition into a Bose-Einstein condensate (BEC), where the atoms *condense* in the same quantum state and behave as a whole particle. The BEC was first observed in 1995 in a gas of ^{87}Rb at JILA [And95], of ^{23}Na at MIT [Dav95], and of ^{7}Li at Rice University [Bra95; Sac97]. Fermions, instead have half integer spin, and obey to Fermi-Dirac statistics. This means that two indistinguishable fermions cannot occupy the same quantum state. This effect is called Pauli exclusion principle [1]. For fermions, reaching degeneracy is less spectacular since a phase transition does not occur. In this case, the atoms fill all the energy levels available up to the so called *Fermi energy*. Fermionic degeneracy was achieved for the first time in 1999, in an ultracold Fermi gas of ^{40}K at JILA [DeM99].

One of most amazing features of ultracold atoms systems is the enormous control that we can have on them: To a large extent, we can vary the temperature, the atom number, the internal and external atomic states, the trapping geometries and dimensionality [Blo08; Mis22], and we can tune the interatomic interactions thanks to Feshbach resonances (FR) [Chi10; Kok15]. In particular, via FRs we can tune the scattering length between two particles almost at will, spanning from zero to very large values, both negative or positive. At the center of such resonances the interparticle scattering length diverges and the system can be descibed in an universal way, independently of the details of the interatomic potential. This regime, named *unitarity*, is of particular interest because the gas is at the same time dilute (the range of the interatomic potential is much smaller than the interparticle distance) and strongly interacting (the interparticle scattering length is much larger than the interparticle distance).

This great control, together with the fact that in these systems both time and length scales are experimentally accessible, allows to exploit ultracold atoms as simulators for other systems that can be hardly investigated experimentally, and for which numerical

[1] Recently *crystals* formed due to this exquisitely quantum effect have been realized in Ref. [Hol21].

simulations are impossible or extremely time consuming on classical computers. That is, we can use ultracold atoms systems as quantum analog simulators. The idea of using more controllable analog systems in order to understand the behavior of less accessible ones is not new. A famous example is given by the large alternating current (AC) power systems, which in the first half of the twentieth century were modelled and studied on AC network analyzers. Such network analyzers were essentially a scale model of the electrical properties of a specific power system, with all the real elements replaced by miniature electrical components with scale values in proportion to the modeled system [Eam90].

A natural application of ultracold systems as quantum analog simulators is the mapping of solid state systems [Lew07; Blo12; Sch20; Alt21], but such platforms are not limited to this, and can serve as test bed for several many-body systems, such as neutron matter [Bak99; Sch05; Gez08; Bal08; Gez11; Gez12; Krü15], quantum gravity [Dan17], biological systems [Dor12], even in understating the early universe [Opa13], and as architectures for quantum computing [Kas22]. In particular, ultracold atoms experiments can be exploited to study polarons, a key concept in solid state physics [App68], and the interaction between them. A polaron is a *quasi-particle* created when an impurity strongly interacting with the environment in which it is embedded, dresses itself with the environmental excitations generated by such interactions. A famous example is an electron dressed by phonons while moving in a metal [Lan33]. In the following, I would like to give a succinct historical overview on how the ultracold community started to look at the polaron problem.

While seminal experimental works on ultracold gases were aimed to investigate the newly realised BEC (see for example Refs. [Jin96; And97; Mat99; Blo99]), soon the scientific interest embraced fermionic systems as well, and the quest for fermionic superfluidity started. The goal was to study the crossover between a condensate of bosonic molecules formed by two fermions on the repulsive (BEC) side of the FR and

the superfluidity due to the emergence of Cooper pairs on the attractive (BCS, from Bardeen–Cooper–Schrieffer) side, and investigate the intermediate regime of unitarity between the two [Gri07; Blo08; Gio08; Tör15].

On the theoretical side, while for bosonics systems, thanks to the implementation of the Gross-Pitaevskii equation [Dal99], the many-body physics at low temperature and small density can be accurately described, an analogous description for the fermionic systems across the BEC-BCS crossover is still missing [Gio08], and efforts have been made to adapt the BCS theory to the new ultracold atoms systems [Eag69; Leg80; Noz85; Gio08].

Experimentally, the investigation of the BEC-BCS crossover started with the realization of strongly interacting Fermi gases via FR in Ref. [OHa02], and proceeded with the creation of a BEC of molecules on the BEC side [Joc03; Gre03; Zwi03], and the observation of superfluidity on both sides of the resonance [Zwi05]. These experiments were carried out with an equal amount of atoms of equal masses in two different spin states, that is, with mass- and spin-balanced systems.

New physics emerges in the presence of a spin imbalance. In this case, the Fermi surfaces of the two components do not match and new phenomena, such as the appearance of exotic states [Ful64; Lar65; Sar63], can emerge. By increasing the spin imbalance, the system would eventually undergo a phase transition between a superfluid and a normal phase [Clo62; Cha62]. In a harmonic trap, where the density distribution of the gas is not uniform, this effect leads to the emergence of a shell structure with a superfluid core at the center of the trap surrounded by a normal gas [Lob06], and was observed in Ref. [Zwi06]. This scenario raised the interest in the physics of an impurity immersed in a Fermi sea as the limit of only one particle of one spin component in the normal phase of the other spin component: the Fermi polaron [Che06b].

A further step in order to obtain more intriguing phenomena is to change the mass

ratio between the atoms in the system, that is, to create a mass-imbalance system. This can be achieved by creating heteronuclear mixtures of different atomic species. Mixing different species, other than providing a mass imbalance, allows to study the effect of the interplay of quantum statistics, being possible to obtain Fermi-Fermi, Bose-Bose and Fermi-Bose mixtures. In addition, the response of each species to external fields may be different, opening the possibility of having pinned impurities and, in general, mixed dimensional systems, e.g. by using a species-selective optical lattice [LeB07]. When combined with spin imbalance, mass imbalance gives a richer phase diagram for the Fermi gas [Gub09; Baa10] and, in the impurity limit, opens the door to study phenomena otherwise difficult to access, such as the Kondo effect [Kon64; Hew93; Nis13] and Anderson's orthogonality catastrophe [And67; Goo11; Kna12; Sin13], and to have a better insight into polaron physics [Mat11; Baa12; Sch18; Fri21; Bar23].

OUTLINE

In this Thesis, I report the characterization of the Fermi polaron formed by bosonic impurities, and the first observation of the mediated polaron-polaron interaction in the case of both bosonic and fermionic impurities.

The first two Chapters are devoted to provide the reader with the knowledge needed to understand the main experimental results.

In Chapter 2, I will give an introductory overview of some topics that are at the base of the results presented in this Thesis. In Section 2.1, the theory of scattering at ultralow temperature is summarized, the concept of mean field effect introduced, and the physics of Feshbach resonances illustrated. Section 2.2 gives a review of the theory of atom-field interaction and discusses radio frequency spectroscopy.

In Chapter 3, the concept and the properties of polarons are explained, focusing on the phyisics of the Fermi polaron. After a general introduction of the Fermi polaron in Section 3.1, I will give a theoretical presentation of the properties of an isolated polaron in Section 3.2, and of the mediated interaction that can arise between polarons in Section 3.3. Finally, the main experimental observations of polaronic properties present in literature are summarized in Section 3.4.

Chapter 4 has the two fold aim of introducing our laboratory to the reader and gather together some technicalities that are in common between the two experiments presented in the main Chapters. In Section 4.1, I will quickly review the history of our laboratory, in Section 4.2, I will discuss our choice of using Li-K mixtures. In Section 4.3, I will give a succinct description of our experimental setup and present the radio frequency control in our laboratory, of crucial importance for the realization of our experiments. In Section 4.4, I will describe the preparation of the atomic samples exploited in the experiments presented in this Thesis.

In the following two Chapters, I present the experimental results that I obtained during my PhD.

In Chapter 5, I will report on the observation and characterization of Fermi polarons formed by bosonic impurities in a mixture of ^{6}Li and ^{41}K. These results have been published in Ref. [Fri21]. For this work I contributed in the design of the experiment, in the data acquisition, and only marginally in the data analysis and in paper writing.

In Chapter 6, I will report on the first observation of the mediated polaron-polaron interaction in the field of ultracold atoms. These results, which led to the publication manuscript (in the final stage of preparation at time of submission of the present Thesis) in Ref. [Bar23], have been achieved by measuring the impurity con-

centration dependence of the Fermi polaron energy in the case of both bosonic and fermionic impurities in an ultracold mixture of fermionic ^{6}Li and either bosonic ^{41}K, or fermionic ^{41}K. For this work, the design of which is similar to the one presented in Chapter 5, I took and analyzed all the data, and had a major role in paper writing.

I will finally conclude this Thesis by discussing possible future experiments that are realizable in the near future in our laboratory.

CHAPTER

INTERACTIONS IN ULTRACOLD ATOMIC GASES 2

One of the most interesting properties of ultracold atoms is the possibility to tune the interactions between them almost at will, and to manipulate their internal and external states. In order to understand how this is possible, in this Chapter, I will review how they interact.

In Section 2.1, I will give a short summary of the theory of the scattering between two particles at ultralow temperature (Section 2.1.1), introduce the concept of *mean field* with a simple example (Section 2.1.2), and show how the scattering length can be tuned via *Feshbach resonances* (Section 2.1.3). In Section 2.2, I will discuss how atoms interact with an external field, starting from the theory of a two-level atoms coupled to a classical field (Section 2.2.1), and concluding with introducing the powerful tool of *radio frequency spectroscopy* (Section 2.2.2).

2.1 SCATTERING THEORY AND FESHBACH RESONANCES

Feshbach resonances (FR) are a powerful and ubiquitous tool in ultracold atoms experiments. Given their importance, I here recall their physical origin, starting with some basic results of scattering theory. For a comprehensive description on scattering

theory in ultracold atomic gases, in general, I refer the reader to [Wal19], and for Feshbach resonances, in particular, to [Chi10; Kok15].

2.1.1 Two-body scattering

In this Section, I will give a short introduction on the theory of the scattering between two particles at ultralow temperature, following the description of Ref. [Mas14].

Ultracold atomic gases have low density and low temperature. Low density means that the typical interparticle distance is much larger than the range of the interparticle potential, of the order of the van der Waals length, $r_{\mathrm{vdW}} \lesssim 100\, a_0$ for alkali-alkali interactions (a_0 being the Bohr radius) [Wal19]. We can then assume that only two particles are involved in each interaction. Ultralow temperatures, together with the fact that the interparticle potential is short-range, lead to the approximation that only s-wave scattering is relevant.

Let's consider the scattering between two particles of mass m and M, respectively. Outside the scattering region, the scattering wave function of two scattering particles is given by the superposition of the incident plane wave and the scattered wave function:

$$\psi(\boldsymbol{r}) = e^{ikz} + f(k)\frac{e^{ikr}}{r}. \tag{2.1}$$

Here k is the relative momentum between the two particles, and $f(k)$ is the s-wave channel scattering amplitude, which for low momenta can be written as

$$f(k) = -\frac{1}{k\cot\delta + ik} \approx -\frac{1}{1/a - r_{\mathrm{eff}}k^2/2 + ik}, \tag{2.2}$$

where δ is the scattering phase shift, which incorporates the effect of the whole potential on the collision event. For ultracold s-wave collisions, this phase shift can be

written as

$$k \cot \delta(k) = -1/a + r_{\text{eff}} k^2/2. \tag{2.3}$$

This is an important result: For ultralow temperatures the scattering amplitude depends only on the scattering length a and the effective range r_{eff}. Remarkably, different microscopic interactions can lead to the same scattering amplitude, allowing for a description in terms of an effective interaction parameterized only by these two parameters.

We can write the effective range in a more handy way by introducing the *range parameter* R^* as

$$R^* = -r_{\text{eff}}/2. \tag{2.4}$$

For $R^* > 0$, the scattering amplitude (2.2) admits a single pole for $a > 0$, which describes a dimer with binding energy

$$E_d = -\frac{\hbar^2}{2m_r a_*^2} \tag{2.5}$$

where $m_r = \frac{mM}{m+M}$ is the reduced mass of the two particles and $a_* = 2R^*/(\sqrt{1 + 4R^*/a} - 1)$. It is worth noting here that when $R^* \ll a$ we recover the universal dimer energy $E_d = -\hbar^2/(2m_r a^2)$, while for $R^* \gg a$ we have $E_d = -\hbar^2/(2m_r R^* a)$.

When the scattering length diverges ($|a| \to \infty$) the scattering amplitude (2.2) for $k \ll 1/|R^*|$ follows the universal law $f(k) = i/k$ and does not depend on the interaction: This regime is called the *unitary regime*.

2.1.2 Scattering length and mean field shift

A useful concept exploited in describing interacting ultracold atoms is the *mean field shift*, which allows to reduce the problem of a particle weakling interacting with many others to the one of a particle experiencing a shift due the potential generated

by the others.

An instructive way to obtain this result is to use a *refractive index* approach, as described in Ref. [Dal98] and presented in the following. Let's assume to have a cloud of atoms of mass m in the dilute regime ($n|a|^3 \ll 1$) and cold enough that only s-wave scattering occurs. Let's consider how a particle of mass M and momentum $\hbar\mathbf{K} \neq \mathbf{0}$ parallel to z is scattered when crossing with a normal angle a slice of this atomic cloud (Fig. 2.1). Let's further assume that the atoms in the cloud remain at rest during the process. This assumption, together with the diluteness of the cloud, assures that we can treat independently each collision of the incident particle with atoms from the cloud.

The incident state is a plane wave $\psi_i(z) \propto e^{iKz}$. The transmitted wave is a superposition of the incident wave and of all the scattered waves resulting from the collisions:

$$\psi_t(z) = e^{iKz} + n \int \frac{f(k)}{|\mathbf{r} - \mathbf{r_s}|} e^{ik\frac{|\mathbf{r}-\mathbf{r_s}|}{2}} e^{iK\frac{(z+z_s)}{2}} d^3r_s, \tag{2.6}$$

where the integration is performed over the slice of the atomic cloud $\mathbf{r}_s = [x_s, y_s, z_s]$ and k is the relative momentum between the two particles. This integral can be exactly calculated and, at the first order in n and for $z > d$ one has:

$$\psi_t(z) = Ae^{iKz} \qquad \text{with} \qquad A = 1 + i\frac{2\pi nd}{k} f(k) \approx e^{i\frac{2\pi nd}{k} f(k,0)}. \tag{2.7}$$

We can interpret this phase shift as a modification δK of the wave vector of the incident particle when the particle is inside the cloud slice:

$$\delta K = \frac{2\pi n}{k} \mathrm{Re}[f(k)]. \tag{2.8}$$

This corresponds to a change of the kinetic energy of the particle equal to $\frac{2\pi\hbar^2 n}{m_r}\mathrm{Re}[f(k)]$. That is, the incident particle sees a potential energy created by the cloud slice equal

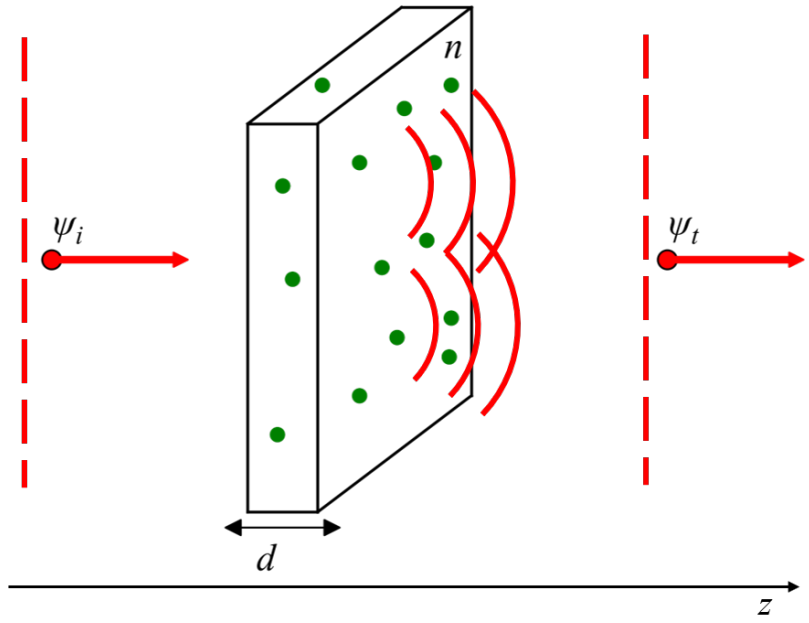

Figure 2.1: **Refractive index approach explanation of the mean field shift**. A particle of mass M and momentum K crosses a thin slice of a cloud of atoms of mass m and density n. The transmitted wave ψ_t is dephased with respect to the incident one, ψ_i, by a phase shift proportional to the scattering length a between the particle and the atoms in the slice, which can be interpreted as resulting from a potential energy exerted by the cloud slice onto the incident particle. Adapted from Ref. [Dal89].

to

$$U = -\frac{2\pi\hbar^2 n}{m_r}\mathrm{Re}[f(k)]. \tag{2.9}$$

We can now use the assumption of s-wave scattering to write $f(k) \xrightarrow{k\to 0} (-a^{-1} - ik)^{-1}$, and recover the familiar expression for the mean field potential in the case in which the incident particle is *distinguishable* from the cloud atoms:

$$U = \frac{2\pi\hbar^2 n}{m_r}a. \tag{2.10}$$

In the case of a *indistinguishable* particle, the initial state given by Eq. (2.6) has to be symmetrized, but the derivation is identical, leading to a mean field potential

$$U = \frac{4\pi\hbar^2 n}{m_r} a. \tag{2.11}$$

From these results we see that while the particle travels through the cloud, its energy is changed proportional to na, that is, the particle will experience a positive (negative) shift in case of repulsive (attractive) interactions, and the magnitude of this shift will be proportional to the density of atoms in the cloud.

2.1.3 Scattering length and Feshbach resonances

Feshbach resonances are an inestimable tool that allows control on the scattering length, and thus on the interactions, between particles. While I refer the reader to Refs. [Chi10; Kok15] for a detail explanation of FRs in ultracold gases, in this Section I will briefly review the main concepts, mostly following Ref. [Chi10].

The basic idea can be pictured with a two-channel model for the scattering process between two particles, and is depicted in Fig. 2.2. We consider two molecular potentials, $V_{\mathrm{bg}}(R)$ and $V_{\mathrm{C}}(R)$, as functions of the interparticle distance R. $V_{\mathrm{bg}}(R)$ asymptotically connects to the two free particles and, for small collisional energy E, represents the open (or entrance) channel. $V_{\mathrm{C}}(R)$ represents the energetically forbidden closed channel, and can support bound molecular states with energy $E_{\mathrm{C}}(R)$ close to the threshold of the open channel. If the bound state in the closed channel energetically approaches the scattering state in the open channel, the colliding atoms resonantly couple to this bound state and their scattering length diverges. This is the mechanism behind the occurrence of FR. If there is no coupling between the two channels, the existence of the bound state in the closed channel has no effect on the scattering in the open channel. On the other hand, in the presence of small coupling,

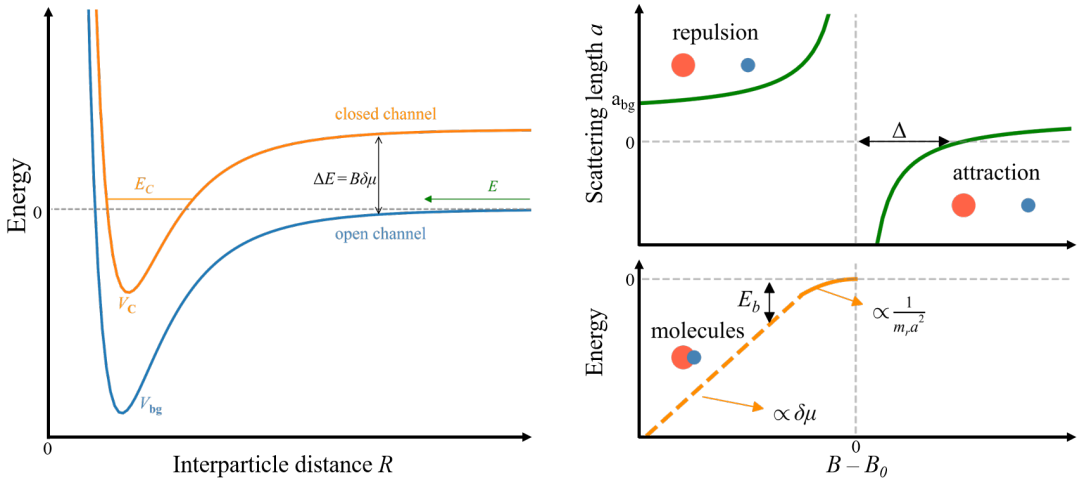

Figure 2.2: **Sketch of a Feshbach resonance. Left:** Two-channel model for a Feshbach resonance. When two atoms collide at energy E in the open channel they resonantly couple to a molecular bound state of energy E_c in the closed channel. In magnetic FR the energy difference ΔE between the two channels can be tuned thanks to an external applied magnetic field B. **Right:** scattering length a (upper panel) and molecular state energy (lower panel) *vs* the applied external magnetic field in the vicinity of a FR. Adapted from [Chi10].

the scattering length will be large and positive if the bound state in the closed channel is just below the threshold of the continuum spectrum in the open channel, and large and negative if it is above such threshold. Note that a weak coupling can be enough to lead to a strong mixing between the two channels. If the two channels have different magnetic moments ($\delta\mu \neq 0$), the energy difference between them can be tuned by applying an external magnetic field B, according to $\Delta E = B\delta\mu$. This tunability is what makes FR particularly appealing: Simply applying an external field we are able to tune the interactions between two atoms at will. Note that magnetic tunability is not the only way in which the energy difference between the two channels can be varied: Another powerful way is to use optical methods, which lead to optical FRs

[Fed96]. Ref. [Moe95] introduced a simple dependence between the scattering length of the two colliding particles and the applied magnetic field:

$$a = a_{\mathrm{bg}} \left(1 - \frac{\Delta}{B - B_0} \right), \tag{2.12}$$

where a_{bg} is the off-resonant value of the scattering length associated with $V_{\mathrm{bg}}(R)$, B_0 the center of the resonance, and Δ its width. Note that for $B = B_0$ the scattering length diverges and we reach the unitarity limit.

When the two channel resonantly mix, an avoid crossing between the scattering and the molecular states occurs, giving rise to two separated branches: A repulsive branch in which the scattering atoms repel each other, and an energetically lower attractive branch, in which the atoms are attracted between each other. This interaction grows with approaching the center B_0 of the FR, where the scattering length diverges and a *dressed* molecular state occurs. For large positive values of the scattering length, the binding energy of this dressed molecular state is given by

$$E_b = \frac{\hbar^2}{2m_r a^2} \tag{2.13}$$

and depends quadratically on the magnetic detuning $B - B_0$, because of the strong influence of the mixing of the channels. Away from the resonance center, in the region where $a > 0$, the energy of the weak bound molecular state varies linearly with the applied magnetic field with a slope given by $\delta\mu$ (see Fig. 2.2).

An important distinction between FRs is the one between *broad*, or open-channel dominated, and *narrow*, or closed-channel dominated, FR. In the first case, the universal range persists for a large fraction of the resonance width, while in the second only for a small fraction of it. This classification is not strict and different criteria can be applied. As a rough categorization one can use the width Δ of the resonance as

discriminating parameter, identifying broad resonances in case $\Delta \gg 1$ G and narrow ones in case $\Delta \ll 1$ G. Since Δ is not the only relevant parameter describing a FR, but also a_{bg} and $\delta\mu$ play an important role, one can introduce a dimensionless parameter that contains this quantities to describe the resonance strength. In literature there are different choices of such parameter [Bru04; Köh06; Chi10], and here we opt for the range parameter R^*, defined as [Pet04; Bru05]

$$R^* = \frac{\hbar^2}{2m_r \delta\mu a_{\mathrm{bg}} \Delta}. \tag{2.14}$$

If R^* is small compared to r_{vdW}, the resonance is called broad, vice versa, if R^* is larger than r_{vdW}, the resonance is called narrow. Since in general $|a|$ is of the same order of r_{vdW}, at a broad resonance the physics is universal, meaning that R^* plays a negligible role. If we go now in the specific of ultracold Fermions, since particles collide with typical momenta of the order of the Fermi momentum k_F, a new length scale emerges in the system, $1/k_F \sim n^{-1/3}$, to which we can compare R^*. In this case we have a broad resonance if $k_F R^* \ll 1$, and a narrow one if $k_F R^* \gg 1$ [Mas14]. With this definition, broad and narrow FR are distinguished by how their widths compares with the typical atomic kinetic energy, the Fermi energy. From another point of you, we can see that, approaching the resonance center, the scattering length a first reaches the effective range in the case of a broad FR, while the atom spacing in a narrow FR [Gur07].

In the case in which the scattering process involves fermions, a useful way of quantifying the interspecies interaction strength is by mean of the dimensionless *interaction parameter* X, defined as

$$X = -\frac{1}{\kappa_{\mathrm{F}} a}. \tag{2.15}$$

2.2 ATOM-FIELD INTERACTIONS

In ultracold atoms experiments, we manipulate the internal atomic states mostly via light and radio frequency (RF) fields. In order to understand how this is possible, in this Section, I will review the basic principles of the interactions between an atom and an electromagnetic field.

2.2.1 Two-level atom

Let's start by developing the theory for a two-level atom coupled to a classical light field. In the following, I will present the derivation presented in Refs. [Coh98a; Lou00]. The two-level atom energy structure is illustrated in the left panel of Fig. 2.3. The atom has a ground state $|0\rangle$ and an excited state $|1\rangle$, the two being coupled by an electric dipole transition of frequency ω_0. The atom interacts with a monochromatic radiation field of frequency ω, which can be detuned by an amount $\Delta = \omega - \omega_0$ from the atomic transition. The goal is to know how the populations of the states $|0\rangle$ and $|1\rangle$ vary with time due to the presence of the radiation field.

Before proceeding, I would like to point out that the two-level atom is not just a mere abstraction used to simplify the problem, but it is indeed a very good approximation when considering two adjacent hyperfine levels in alkali atoms. For example, the two lowest hyperfine states of ^{41}K at a field of 335 G are separated by $E/h \approx 57$ MHz, that is in the RF regime. Since in this case the momentum transferred to an atom due to absorption is negligible, this RF transition can be modelled as a pure spin-flip process. Moreover, since the lowest hyperfine state is the ground state we can assume that this transition involves only these two levels, and we can treat this problem as a non-interacting two-level system in presence of an external radiation field.

Getting back to our derivation, the evolution of the system is described by the

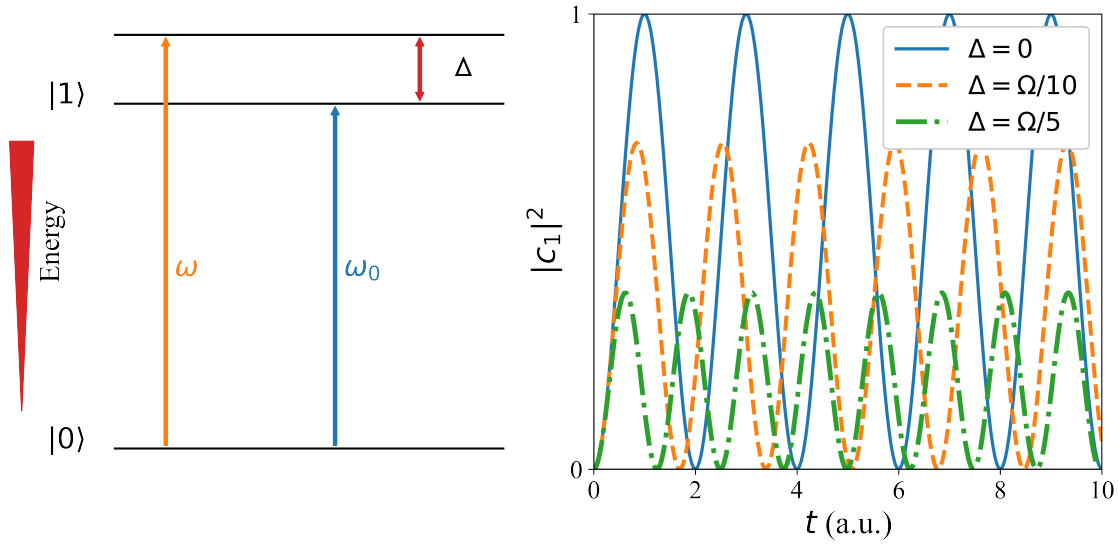

Figure 2.3: **Two-level system. Left:** sketch of the energy of the two levels separated by the bare atomic transition ω_0 and coupled by a field of frequency ω detuned from the bare transition by an amount Δ. **Right:** Rabi oscillations of the population of the $|1\rangle$ state as a function of time for different values of the detuning Δ.

time-dependent Schrödinger equation

$$i\hbar\frac{\partial}{\partial t}\Psi = \hat{H}\Psi, \tag{2.16}$$

with

$$\Psi(\mathbf{r},t) = c_0(t)\,|0\rangle + c_1(t)\,|1\rangle\,e^{-i\omega_0 t} \tag{2.17}$$

the atomic wave function and

$$\hat{H} = \hat{H}_0 + \hat{V} \tag{2.18}$$

the Hamiltonian of the system. Here $\hat{H}_0$ is the unperturbed atom Hamiltonian, and $\hat{V} = \hat{d}\cdot\hat{E}$ describes the atom-light interaction, with $\hat{d}$ being the dipole moment and $\hat{E}$ the external electric field, which for a plane wave can be written as $\hat{E} = \hat{\epsilon}E_0\cos(k\mathbf{r}-\omega t)$. With these assumptions, and using the rotating wave approximation

($\Delta \ll \omega$ and $\Omega \ll \omega$), we can write two couple equations for the coefficients c_0 and c_1:

$$\begin{aligned} i\hbar\frac{dc_0(t)}{dt} &= c_1\hbar\Omega^*\frac{e^{i\Delta t}}{2} \\ i\hbar\frac{dc_1(t)}{dt} &= c_0\hbar\Omega\frac{e^{-i\Delta t}}{2}, \end{aligned} \tag{2.19}$$

where we have introduced the *Rabi frequency*

$$\Omega = \frac{E_0}{\hbar}\langle 1|\,\hat{d}\cdot\hat{\epsilon}\,|0\rangle\,, \tag{2.20}$$

describing the strength of the coupling between the atom and the electric field. It depends on the polarization via the dipole matrix element between the two states, and its value increases by increasing the intensity of the field. If we now assume that the system was initially prepared in the state $|0\rangle$, we find that the probability of finding the atom in the state $|1\rangle$ at a time t is given by

$$|c_1(t)|^2 = \frac{\Omega^2}{\Omega_{\text{eff}^2}}\sin^2\left(\frac{\Omega_{\text{eff}}t}{2}\right), \tag{2.21}$$

where $\Omega_{\text{eff}} = \sqrt{\Omega^2+\Delta^2}$ is the *effective Rabi frequency*.

In the right panel of Fig. 2.3, examples of the oscillations of the population in the state $|1\rangle$ are reported for different values of the detuning Δ. We can see that only in the resonant case, $\Delta = 0$, we can have full transfer from one state to the other. The shortest time at which this happens is at $t = \pi/\Omega$, and a pulse with this duration is called a π-pulse. Analogously, we can define as $\pi/2$-pulse the shortest pulse that transfers the atom initially prepared in $|0\rangle$ into an equal linear superposition of $|0\rangle$ and $|1\rangle$.

In the presence of an oscillating electric field, the strongly coupled bare atom en-

ergy eigenstates are shifted. In order to understand how, we can rewrite Eqs. (2.19) removing the explicit time dependence on the right hand side. In doing so, we define the new coefficients $\tilde{c}_0 = c_0$ and $\tilde{c}_1 = c_1 e^{i\Delta t}$, in terms of which Eqs. (2.19) become

$$\begin{aligned} i\hbar \frac{d\tilde{c}_0(t)}{dt} &= \tilde{c}_1 \hbar \frac{\Omega}{2} \\ i\hbar \frac{d\tilde{c}_1(t)}{dt} &= \tilde{c}_0 \hbar \frac{\Omega}{2} - \tilde{c}_1 \hbar \Delta. \end{aligned} \tag{2.22}$$

The Hamiltonian thus reads

$$\hat{H} = \frac{\hbar}{2} \begin{bmatrix} 0 & \Omega \\ \Omega & -2\Delta \end{bmatrix} \tag{2.23}$$

and, by diagonalise it, we can find that the eigenvalues are

$$\begin{aligned} E_0 &= \frac{\hbar}{2} \left(-\Delta + \sqrt{\Omega^2 + \Delta^2} \right) \\ E_1 &= \frac{\hbar}{2} \left(-\Delta - \sqrt{\Omega^2 + \Delta^2} \right), \end{aligned} \tag{2.24}$$

and the new eigenstates are

$$\begin{aligned} |\tilde{0}\rangle &= \sin\theta \, |0\rangle + \cos\theta \, |1\rangle \\ |\tilde{1}\rangle &= \cos\theta \, |0\rangle - \sin\theta \, |1\rangle, \end{aligned} \tag{2.25}$$

with $\cos 2\theta = -\Delta/\Omega_{\text{eff}}$. We can interpret these states, each of them being a superposition of the $|0\rangle$ and $|1\rangle$ bare eigenstates, as if the bare atom would be *dressed* by the radiation field.

From these results, we can see that the $|0\rangle$ and $|1\rangle$ states experience a shift that depends on the detuning Δ, and has opposite sign for the two states, as depicted in

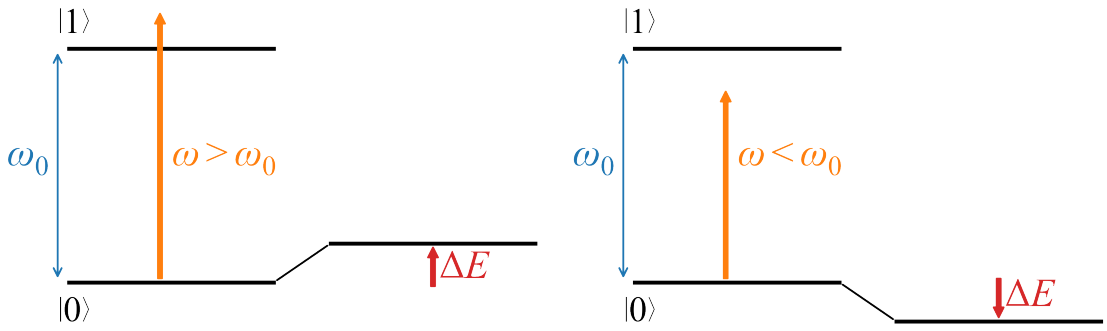

Figure 2.4: **Light shift of the ground state.** When coupled with non resonant light, the atomic states experience an up shift when the detuning is on the red side of the atomic resonance (left panel), or a down shift for blue detuned light (right panel). Adapted from Ref. [Coh98b].

Fig. 2.4. This is known as the *light* (or *AC Stark*) *shift*. Far from resonance, where $\Omega \ll |\Delta|$, each state experiences a shift $\Delta E = \frac{\hbar\Omega^2}{4\Delta}$, proportional to the field intensity.

I conclude this Section by underlining that here we didn't consider a very important part of the problem that is always present in the real world: spontaneous emission. An elegant way to take this effect (and others) into account is to exploit a *density matrix* formalism, which allows to write the evolution of the system in terms of *Bloch equations*. Discussing such formalism is beyond the purpose of this introduction and I refer the reader to Refs. [Coh98a; Lou00] for further information.

2.2.2 Radio frequency spectroscopy

We can now use what we have learnt in Section 2.2 to describe a vary powerful tool used in order to record the energy spectrum of a sample: *spectroscopy* [1].

From energy conservation law, we know that the only possible frequencies emitted or absorbed by an atom are the ones corresponding to the energy difference between

[1] Hybrid word composed by the Latin word *spectrum*, *image*, and the Greek word *skopeo*, *I observe*.

pairs of the atom energy levels, that is $\hbar\omega = E_{n+1} - E_n$. This implies that we can use light as a tool to investigate atomic energies: This is at the base of spectroscopy.

In a many-body system we are mainly interested in the single particle excitation spectrum, characterized by the spectral function $A(\mathbf{k}, \omega)$ which gives information on the existence of single-particle excitations with frequency ω and momentum $\mathbf{k}$, and can thus provide insight on possible quantum effects in the system. The spectral function can be probed via different spectroscopies. In this Section, I will focus in particular on RF spectroscopy, since this is a core technique for the experiments presented in this Thesis, and I refer the reader to literature for discussion of other types, such as Raman [Dao07; Dao09; Hu22], Bragg [Tör15], and lattice modulation [Tör15] spectroscopies. The first proposal of applying this technique to ultracold atoms came in 2000 from Ref. [Tör00] as a method to observe Cooper pairs in ultracold fermionic gases. The idea is that, since the energy splitting between two hyperfine levels in most of the species used in ultracold atoms experiments are of the order of tens of MHz, RF fields can be used to drive transition between two levels in such systems. RF spectroscopy is based on the fact that we can have maximum transfer only at resonance. By scanning the frequency of the RF field, the energy spectrum of the system can be probed recording the transferred fraction of atoms from one level to the other. If there are no interactions, the transferred fraction will exhibit a strong enhancement close to the bare transition frequency between the two levels. If interactions are present, they will broaden and shift the resonance peak, giving rise to a more complicated RF spectrum, which therefore provides information on interaction effects. There are some properties of RF spectroscopy that are worth to be noticed [Ket08]: Since RF fields have long wavelengths ($\lambda \sim 3$m), the momentum transferred to the atoms is negligible, moreover, since the RF fields are usually generated by antenna of dimensions $\sim$ cm, they are approximately constant over the size of the atomic sample, usually of the order of hundreds of μm, so that the full cloud is fully addressed at the same time.

Theoretical details on spectroscopies in general, and RF spectroscopy in particular, applied to ultracold Fermi gases are reviewed in [Tör15; Tör16].

Here I will discuss the general features of this tool, focusing on the problem, relevant for this Thesis, of an impurity immersed in a bath with which it can interact. As often is the case in ultracold atoms experiments, we can approximate such impurity as a two-level system: one level, which we name $|0\rangle$, does not interact with the bath, while the other, named $|1\rangle$, does. We can study this system via RF spectroscopy in two different ways: We can start with the impurity in $|0\rangle$ and transfer it to $|1\rangle$, or, vice versa, we can start with the impurity in $|1\rangle$ and transfer it to $|0\rangle$. These two methods are depicted in Fig. 2.5. The first is called *ejection* (sometimes *direct* [Mas14]

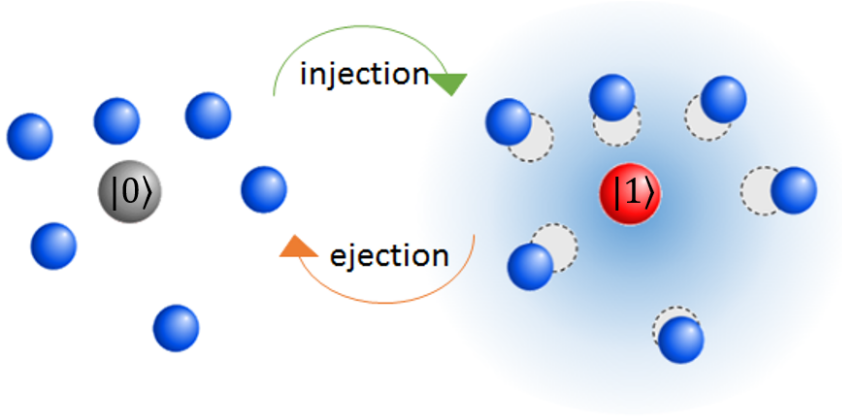

Figure 2.5: **Injection and ejection spectroscopy.** In *injection* spectroscopy, an impurity, initially in a state $|0\rangle$, non interacting with the bath, is brought in a state $|1\rangle$, which is strongly interacting. In *ejection* spectroscopy, an impurity in the interacting state $|1\rangle$, is driven to the not interacting state $|0\rangle$.

or *standard* [Sch18]) spectroscopy, and it used mainly to investigate the ground state of the interacting system. This technique was used to study pairing phenomena in the BCS-BEC crossover [Chi04; Shi07; Ste08], and the emergence of the attractive polaron in an equal masses mixture [Sch09]. Moreover, in our laboratory, we exploit this scheme to measure the center of the FRs, as described in Chapter 4.4.2. The

second method is called *injection* (sometimes *indirect* [Mas14] or *reversed* [Sch18]) spectroscopy, and it is particularly suitable to study states that are not the ground state of the system, since the particles are transferred into a strongly interacting state, probing the whole spectral function of the system [Mas14]. Thanks to this technique, the repulsive polaron was observed and characterized in both mass imbalanced and mass balanced systems [Koh12; Sca17]. Moreover, we applied this scheme in the measurements presented in this Thesis. We investigated the properties of polarons across a FR, and since they are not the ground state for a wide range of interactions (see Chap. 3), the choice of the *injection* method was natural [Fri21; Bar23]. Theoretically, if the initial system is in thermal equilibrium, these two schemes are related to each other by a function of the free energies of the system with and without interactions between the impurity and the bath [Liu20b; Liu20a].

CHAPTER

POLARONS 3

Most of the problems in Physics lie in determining the behavior of bodies when they interact among each others. While we are able to give a general solution for the one- or two- body problems, the scenario becomes more and more complex the more bodies are involved. For example, in condensed matter the number of interacting particles considered is of the order of the Avogadro number, $N \sim 10^{23}$. The problem of understanding how several particles behave when interacting among each others is known as the *many-body problem*. While there is no general solution to this problem, a plethora of approximation has been applied in different fields in order to address specific issues. One of these is the renown Landau's *Fermi liquid theory*, aimed to handle the problem of many interacting fermions. The basic idea is to reduce the behavior of one particle interacting with many (let's call them the "bath"), to the one of a free noninteracting particle, which we are able to solve. With this aim, we can describe a particle interacting with all the particles of the bath as a free *quasi-particle* made of the bare particle *dressed* by the excitations that it creates in its surrounding. This new *quasi-particle* absorbs into itself the fact that the bare particle plus the excitations of the surrounding has different properties with respect to the non interacting one, for example a different effective mass m^*. This concept, introduced by L. Landau in the '30s [Lan33], had and has an invaluable role in the developing of our understanding of many physical systems.

An important example of quasi-particle in solid state physics is the exciton, a bound state between an excited electron and a hole propagating in a semiconductor. But the most famous quasi-particle is the polaron, originally introduced to describe an electron moving in a metal: The interaction between the electron and the ions of the lattice generates a displacement of the ions, resulting in a polarization cloud that dresses the electron [Lan33]. In this case the impurity, the electron, is dressed by phonos, that are bosonic excitations, and we call this a Bose polaron. Indeed the polaron its named after the environment the impurity is embedded in, so Bose polaron if the environment is bosonic, Fermi polaron if the environment is fermionic. While the first has a direct comparison with solid state systems, the second can be viewed as a paradigmatic realization of Landau's quasi-particle concept, and it has historically attracted more and more interest in understanding the BCS-BEC crossover and the normal state of a polarized Fermi gas [Che06b; Lob06; Com07; Com08]. Moreover the Fermi polaron plays a role, e.g, in the physics of semiconductors [Sid17; Mui22], and in the study of neutron matter [For14; Vid21; Nak20].

The Fermi polaron is the object of this Thesis and this Chapter is devoted to summarize its main properties and how to observe them.

In Section 3.1 I will give a general introduction to the Fermi polaron studies, in Section 3.2 the properties of an isolated polaron are derived in a $T-$matrix framework, Section 3.3 is dedicated to the theoretical description of the mediated polaron-polaron interactions emerging from Landau's Fermi liquid theory, and finally, in Section 3.4, I will explain the main experimental techniques exploited to study polarons.

3.1 FERMI POLARONS

Seminal experiments and theory works on polarized Fermi gases show that a trapped polarized fermionic cloud forms a shell structure with a superfluid core where the two spin densities are equal, and an outer shell composed by a normal gas with imbalanced spin densities [Lob06; Che06a; Che06b; Sch09; Com08]. The Fermi polaron was then introduced as a limit to describe the normal component occupying the outer shell of the cloud: one impurity in a bath composed by polarized normal Fermi gas. So the problem reduces to the study of the $N + 1$ system composed by $N \uparrow$ particles from the Fermi sea (FS) and one $\downarrow$ impurity.

In order to understand how this problem has been tackled, let's consider $N \uparrow$ particles of mass $m_\uparrow$ forming a FS with Fermi momentum k_F and density $n_\uparrow = k_\mathrm{F}^3/(6\pi^2)$, in which an impurity $\downarrow$ of mass $m_\downarrow$ is embedded. To keep the description simple, let's assume that a mass ratio $m_\uparrow/m_\downarrow < 8.17$, so that trimers, tetramers, and Efimovian states are not present [Lan14] . Moreover, let's assume that the two species interact via a broad Feshbach resonance (FR), where the scattering length a and the interatomic distance between the $\uparrow$ particles are much greater than the effective range characterising the $\uparrow - \downarrow$ interspecies interaction[1]. We can start to investigate this system summarizing what we know about its ground state in vacuum, that is for $n_\uparrow \to 0$, for different values of the scattering length a between the impurity and the FS. If $a < 0$ the only state is the single impurity; if $a > 0$ there can be two states: a single impurity and a dimer formed by the impurity and a particle from the FS.

[1] A discussion on broad and narrow resonances is presented in Chapter 2.1.3. Here we just note that the main effect of having a narrow FR in the regime $k_F R^* \gg 1$ is to shift the polaron-to-molecule transition to negative values of the scattering length, whereas it is located at positive scattering lengths in the zero-range limit $k_F R^* \to 0$. The mass ratio and the effective range of the resonance play an important role in determine the polaron-to-molecule transition. I refer the reader to Refs. [Tre12; Mas14] for further theoretical details, and to Ref. [Nes20] for an experimental observation.

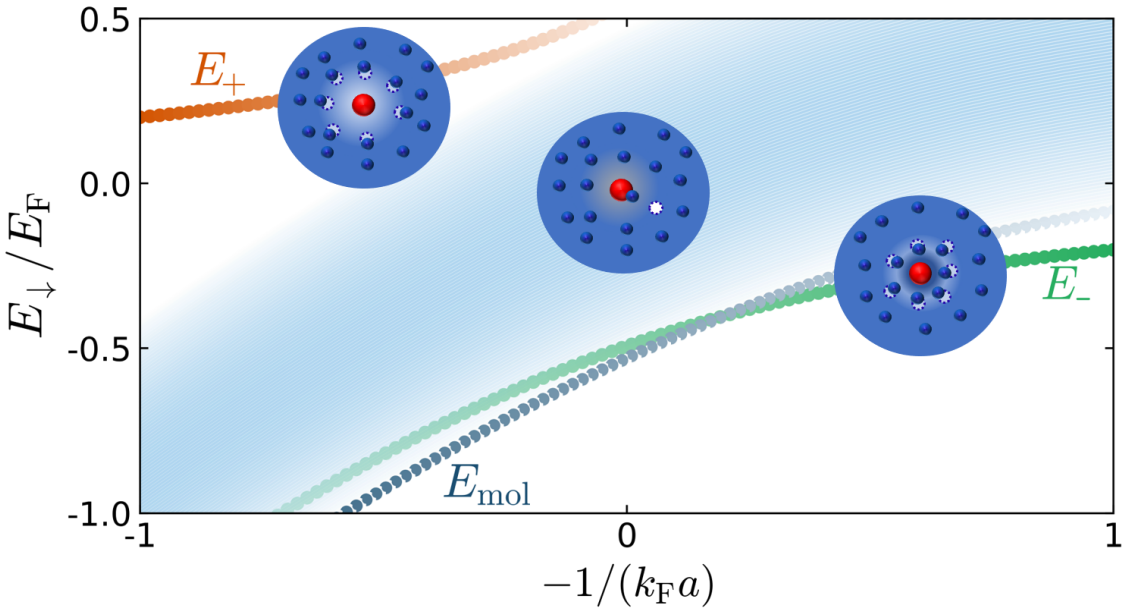

Figure 3.1: **Energy spectrum of an impurity in a Fermi sea**. The green line represents the energy of the attractive polaron, E_-, which is the ground state on the BCS side of the resonance. For strong attraction ($-1/(k_\mathrm{F}a) \approx 0.2$), the ground state becomes the molecule, described by the blue dotted line, E_mol. The metastable repulsive polaron in depicted by the orange line, E_+. The shaded area corresponds to the molecule-hole continuum, which arises from the fact that a $\uparrow$ particle with an energy between 0 and E_F can be removed from the FS and form a molecule. The theory data, from Ref. [Mas20], correspond to the ^{6}Li-^{41}K mixture at the 335-G FR.

Let's now increase the density $n_\uparrow$ of the FS. For weak interactions the energy of the considered states will be modified from its vacuum value by the mean field energy due to the presence of the FS (see Chapter 2.1.2): In the BCS limit, for $a < 0$ and small, the energy of the single impurity will be reduced, while in the BEC limit, for small $a > 0$, both the single impurity and the dimer energy will be increased. Since these states are well defined in vacuum, we expect their adiabatic continuations to remain the ground state of the system (except for the unstable single impurity for $a > 0$).

Let's do a step further and consider what happens if we now increase the interspecies interactions beyond the mean field limit. In this strongly interacting regime the single

impurity and the dimer will interact with the surrounding FS, creating particle-hole fluctuations. We will call the resulting few-body system dressed by fluctuations a *polaron* or a *molecule* (a more proper term will be *dressed dimeron* and both can be found in literature). In particular, the dressed state connecting to the single impurity state in vacuum is called the *attractive polaron* on the BCS side of the resonance, formed by the impurity attracting particles of the FS, or the *repulsive polaron* on the BEC side of the resonance, formed by the impurity repelling particles of the FS. These states, together with the molecule-hole continuum arising from the fact that a molecule can be formed by removing an $\uparrow$ particle with any energy between 0 and E_{F}, are depicted in Fig. 3.1 for the ^{6}Li$-^{41}$K mixture in the proximity of a FR centered around ~ 335 G. In addition of being a source of particle-hole pairs, the FS blocks the momentum of the $\uparrow$ particles from going below $\hbar k_{\mathrm{F}}$. These effects lead to the fact that the energy of the impurity becomes a nonlinear function of $k_{\mathrm{F}}a$ and the effective mass is shifted from its bare value. In summary, we can treat the impurity in a FS as a few-body state with particle-hole fluctuations whose vacuum nature is generally preserved, but whose properties are quantitatively shifted from the vacuum values [Lan14].

An elegant description of the ground state of the $N+1$ system was proposed by Chevy in Ref. [Che06b] using a variational approach. Inspired by first order perturbation theory, he assumed the variational wave function for the system of a single impurity with momentum $\mathbf{p}$ immersed in a homogeneous FS to be of the form

$$|\psi\rangle = \left(\phi c^\dagger_{\mathbf{p}\downarrow} + \sum_{q<k_F}^{k>k_F} \phi_{\mathbf{kq}} c^\dagger_{\mathbf{p+q-k}\downarrow} c^\dagger_{\mathbf{k}\uparrow} c_{\mathbf{q}\uparrow}\right)|\mathrm{FS}\rangle, \tag{3.1}$$

where $c^\dagger_{\mathbf{p}\sigma}$ creates an impurity ($\sigma = \downarrow$) or an atom of the FS ($\sigma = \uparrow$) with momentum $\mathbf{p}$, and $|\mathrm{FS}\rangle$ denotes the unperturbed FS. The ϕs coefficients are varied in order to min-

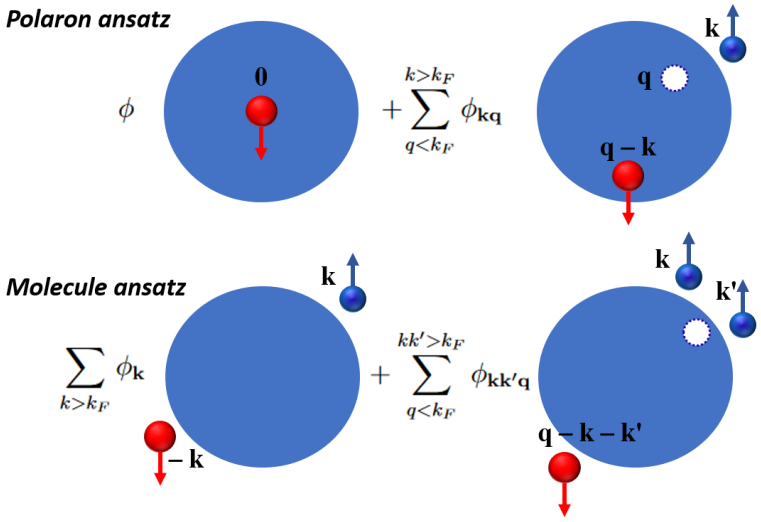

Figure 3.2: **Polaron and molecule ansätze**. Here we consider one particle-hole fluctuation and total momentum $\mathbf{p} = 0$. Adapted from Ref. [Lan14].

imize the energy in a gran canonical ensemble. Eq. (3.1) describes the modification of the unperturbed FS wave function due to the inclusion of one particle-hole fluctuation. Even though this model is fairly simple, considering only one particle-hole excitation, its results fit pretty nicely with experimental observations [Sch09; Koh12; Fri21] due to the almost exact cancellation of a large set of high-order Feynman diagrams [Com08; Lan14]. I want to note here that Eq. (3.1) was obtained requiring a constant number of $\uparrow$ particles, and has the limit of not properly describing the molecular state. This can be solved by adding more particle-holes pairs with some specific constrains [Mor09; Lan14], but this approach is rather cumbersome and one can obviate to this by writing an analogous ansatz for the molecular state, allowing for the number of particles in the FS to change [Pun09; Lan14]:

$$|\psi\rangle = \left(\sum_{k>k_F} \phi_{\mathbf{k}} c^\dagger_{-\mathbf{k}\downarrow} c^\dagger_{\mathbf{k}\uparrow} + \sum_{q<k_F}^{kk'>k_F} \phi_{\mathbf{kk'q}} c^\dagger_{\mathbf{q-k-k'}\downarrow} c^\dagger_{\mathbf{k'}\uparrow} c^\dagger_{\mathbf{k}\uparrow} c_{\mathbf{q}\uparrow} \right) |\mathrm{FS}_{N-1}\rangle. \tag{3.2}$$

These two ansätze, graphically summarized in Fig. 3.2, if allowed to be expanded to an arbitrary number of particle-hole pairs, are equivalent in describing the ground state of the system, as explained in Ref. [Lan14].

What discussed until now is valid for the ground state of the system (the attractive polaron or the molecule) and in the case of a broad FR. An extension of this model describing the metastable repulsive polaron is presented in Ref. [Mas11], and an extension to narrow resonances can be found in Refs. [Tre12; Qi12]. Some of these results are summarized in Section 3.2.

3.2 PROPERTIES OF ISOLATED POLARONS

In this Section, I will derive the properties of a single impurity $\downarrow$ forming a polaron in FS sea of $\uparrow$ particles. In such derivation I will follow a diagrammatic approach, as presented in Ref. [Fri21].

3.2.1 Energy, effective mass and polaron residue

The minimization of the energy based on the variational ansatz (3.1) yields an identical result to the diagrammatic calculation within the "ladder" (or "forward-scattering") approximation [Com07], but the latter, once properly analytically continued [Mas11], allows also to investigate the properties of the repulsive branch, and eventually the effects of non-zero temperature, in a straightforward way. The retarded self-energy of a single impurity of mass $m_\downarrow$, with momentum $\mathbf{p}$ and energy ω in a Fermi sea of particles with mass $m_\uparrow$ reads (here and in the following, if not

otherwise specified, we set $\hbar = k_B = 1$)

$$\Sigma(\mathbf{p},\omega) = \sum_{\mathbf{q}} f(\xi_{\mathbf{q}\uparrow}) T(\mathbf{p}+\mathbf{q}, \omega+\xi_{\mathbf{q}\uparrow}) \tag{3.3}$$

$$= \sum_{\mathbf{q}} \frac{f(\xi_{\mathbf{q}\uparrow})}{\frac{m_r}{2\pi\tilde{a}} - \sum_{\mathbf{k}} \left[\frac{1-f(\xi_{\mathbf{k}\uparrow})}{\omega-(\epsilon_{\mathbf{p}+\mathbf{q}-\mathbf{k}\downarrow}+\epsilon_{k\uparrow}-\epsilon_{q\uparrow})+i0_+} + \frac{2m_r}{k^2} \right]}, \tag{3.4}$$

where $f(x) = 1/[\exp(\beta x)+1]$ is the Fermi function at inverse temperature β, and $T(\mathbf{P},\Omega)$ is the T-matrix describing the scattering of an $\uparrow\downarrow$ pair of atoms with total momentum $\mathbf{P}$ and total energy Ω. Here we have introduced the kinetic energy of a σ atom measured with respect to the chemical potential $\xi_{\mathbf{k}\sigma} = \epsilon_{\mathbf{k}\sigma} - \mu_\sigma = k^2/2m_\sigma - \mu_\sigma$, the reduced mass $m_r = m_\uparrow m_\downarrow/(m_\uparrow + m_\downarrow)$, and the energy-dependent quantity

$$\frac{1}{\tilde{a}(\omega,K)} = \frac{1}{a} + R^* k_r^2, \tag{3.5}$$

where $k_r = \sqrt{2m_r[\omega - K^2/(2M) + E_F]}$ (with $K = |\mathbf{p}+\mathbf{q}|$ and $M = m_\uparrow + m_\downarrow$) is the relative momentum of the colliding pair, and E_F is the Fermi energy of the homogeneous FS. Since we consider the properties of a single $\downarrow$ particle, we have set its chemical potential to zero.

The Green's function of the impurity reads

$$G_\downarrow(\mathbf{p},\omega) = \frac{1}{\omega - \epsilon_{\mathbf{p}\downarrow} - \Sigma(\mathbf{p},\omega) + i0_+}. \tag{3.6}$$

Its spectral function $A = -2\mathrm{I}m[G_\downarrow]$ features two branches of excitations, one at negative and one at positive energies. In the vicinity of these sharp excitations, the Green's function at small momenta may be approximated as

$$G_\downarrow(\mathbf{p},\omega) \approx \frac{Z_\pm}{\omega - E_\pm - \frac{p^2}{2m_\pm^*} - iZ_\pm \mathrm{I}m[\Sigma(\mathbf{p},E_\pm)]}. \tag{3.7}$$

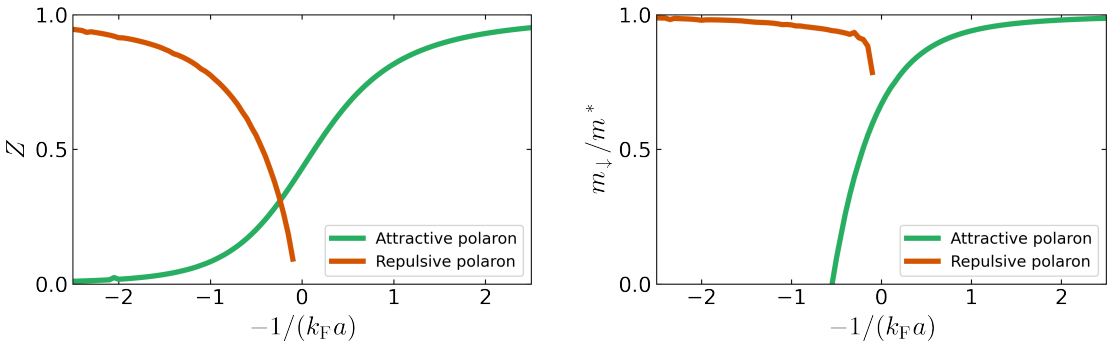

Figure 3.3: **Polaron residue and effective mass**. Theory data, from Ref. [Mas20], are for the ^{6}Li-^{41}K mixture at the 335-G FR.

The energy of an attractive $(-)$ polaron at zero momentum, $\mathbf{p} = 0$, is the purely real solution at negative energies of

$$E_- = \Sigma(0, E_-), \tag{3.8}$$

while the energy of the repulsive $(+)$ zero momentum polaron is the positive energy solution of

$$E_+ = \mathrm{Re}[\Sigma(0, E_+)]. \tag{3.9}$$

The energies of the attractive and repulsive polaron are reported in Fig. 3.1 for the case of the ^{6}Li-^{41}K mixture close to a FR centered around 335 G.

An important quantity describing the polaron is its *residue*, Z, which represents the overlap between the quasi-particle and the bare particle states. In the ansatz (3.1), Z corresponds to $|\phi|^2$, and in terms of the self energy it can be defined as

$$Z_\pm = \frac{1}{1 - \mathrm{Re}[\partial_\omega \Sigma(0, \omega = E_\pm)]}. \tag{3.10}$$

As we previously pointed out, the polaron can be described by a free particle with

a different, effective mass. This is given by

$$m_{\pm}^{*} = \frac{m_{\downarrow}/Z_{\pm}}{1 + \mathrm{Re}[\partial_{\epsilon_{\downarrow\mathbf{p}}}\Sigma(0, E_{\pm})]}. \tag{3.11}$$

These quantities are reported in Fig. 3.3 in the case of the ^{6}Li-^{41}K mixture at 335 G. The energy, residue, and effective mass obtained from this theory compare very well with both MC simulations and experiments [Pro08; Sch09; Nas09; Koh12; Kos12; Sca17].

Turning now to the properties of the molecules, their energies can be computed from the Ansatz (3.2), describing a bare molecule dressed by particle-hole excitations in the bath [Mor09; Pun09; Com10; Mas12; Tre12; Qi12].

3.2.2 Polaron decay

The repulsive polaron is unstable towards decay into lower-lying excitations, but it remains a well-defined quasi-particle as long as its decay rate Γ is small [Bru10; Mas11; Koh12; Sca17]. The population decay rate for the two-body process, leading a polaron to decay into free particles (pf), is given by

$$\Gamma_{pf} = -2Z_{+}\mathrm{I}m[\tilde{\Sigma}(0, E_{+})], \tag{3.12}$$

where $\tilde{\Sigma}$ is defined in Eq. (S.16) of Ref. [Sca17]. The competing process, leading a polaron to decay onto a dressed molecule, is instead given by [Koh12]

$$\begin{aligned}\Gamma_{pm} =& \frac{64 k_F a}{45\pi^3}(Z_{+}^{3} Z_M)\left(\frac{m_{\uparrow}}{m_{+}^{*}}\right)^{2}\left(1 + \frac{m_{\uparrow}}{m_{\uparrow} + m_{\downarrow}}\right)^{3/2} \\ &\times \left(\frac{E_F}{E_{+} - E_M}\right)^{5/2} \frac{a}{a^{*}\sqrt{1 + 4R^{*}/a^{*}}} E_F,\end{aligned} \tag{3.13}$$

where E_M is the energy of a dressed molecule, and $a^* = \sqrt{2m_r E_b}$ is the typical size of a vacuum dimer at a narrow resonance.

In the extreme BEC limit, where bath effects become negligible, and in presence of a broad resonance, the three-body recombination proceeds at a rate [Pet03]

$$\Gamma_3 = \left(\frac{\bar{\epsilon}_\uparrow}{\epsilon}\right) \alpha n_\uparrow^2. \tag{3.14}$$

Here, $\bar{\epsilon}_\uparrow$ is the average kinetic energy of majority atoms, ϵ is the binding energy of the $\uparrow\downarrow$ dimer, and α is a constant which for mass ratio between Li and K takes the value

$$\alpha_\uparrow = 2.57 \frac{\hbar^5}{m_\uparrow^3 \epsilon^2}. \tag{3.15}$$

3.3 MEDIATED POLARON-POLARON INTERACTION

Now that we have learnt about the properties of an isolated polaron, we can turn our attention to what happens in the case of a finite density of polarons. This section is dedicated to the theoretical description of the mediated interaction between two polarons. We use the term "mediated" to describe an interaction between two particles, in our case two polarons, due to the two-body interaction of these with a third particle, in our case one particle of the FS. On a general ground, mediated interactions between particles are always attractive, regardless the interparticle interactions being attractive or repulsive. In a trap, this can be understood with an intuitive picture involving three particles: let's assume that we have two particles, A1 and A2, which don't interact between each others but they do, equally, with a third particle, B. If A1 and A2 experience the same attraction towards B, they will end up both closer to B and then closer to each other, effectively experiencing an attractive interaction. On the other hand, if they experience the same repulsion away from B,

they will try to repel B and will end up closer to each other, thus experiencing again an effectively attractive interaction. For quantum particles this argument is true in the case of A1 and A2 being bosonic particles. Mathematically this effect results from an exchange term in the interaction energy. Thus one can then see that for fermionic particles there is a sign inversion due to Pauli principle, leading to the opposite result: In this case the mediated interaction is always repulsive [Yu12]. In the following, I will summarize the main results concerning the mediated polaron-polaron interaction as it emerges from Landau's Fermi liquid theory. Note, however, that the theoretical landscape brims with works that go beyond this (e.g., Refs. [Gir12; Taj18; Hu18]). I decided to limit the discussion to this description because of its simplicity and because it can explain, to a large extent, our experimental observations, as we will see in Chapter 6.

Before discussing in more detail the theory underling the mediated polaron-polaron interaction in the next Section, here the main result of the Landau's Fermi liquid theory concerning this problem is reported. By adding impurities to the system, the polaron energy shift per impurity depends on the interaction strength between the impurities and the bath, described by the dimensionless interaction parameter X (defined in Eq. (2.15)), and the impurity concentration $\mathcal{C}$, defined as the ratio between the impurity and the bath number densities $n_\downarrow/n_\uparrow$, and can be written as [Fri21; Yu12; Sca22]

$$\Delta E(X,\mathcal{C}) = E_\downarrow(X) \mp \frac{1}{3}(\Delta N(X))^2\,\mathcal{C}\,E_\mathrm{F} + MF \tag{3.16}$$

The first term, $E_\downarrow$, is the single impurity polaron energy and depends only on the interaction strength between the impurities and the bath. The second term accounts for interactions between two polarons mediated by particles of the bath. It is linear in the impurity concentration and depends on X via ΔN, the number of

bath particles in the dressing cloud of the impurity (defined in Eq. (3.19) later in the text). The last term, MF, stands for the mean field shift generated by the presence of the other impurities. The $-$ $(+)$ sign corresponds to bosonic (fermionic) impurities [Mor10; Yu12], and highlights the fact that mediated interactions are always attractive (repulsive).

3.3.1 Landau Fermi liquid theory for polaron-polaron interactions

In this Section, a formal derivation of Eq. (3.16), as presented in Ref. [Fri21], is given. Since the derivation in the case of thermal bosonic and fermionic impurities is equivalent apart for an overall sign change [Yu12], for readability, in the following only the case of bosonic impurities is treated.

Within Fermi liquid theory [Mor10; Yu10; Yu12], the total energy density of a gas containing $N_\downarrow \ll N_\uparrow$ impurities in a large sea of $N_\uparrow$ ideal fermions may be written as

$$\mathcal{E}(n_\uparrow, n_\downarrow) = \frac{3}{5} E_F n_\uparrow + E_\downarrow n_\downarrow + \frac{1}{2} f n_\downarrow^2. \tag{3.17}$$

The first term in this expression represents the energy of the unperturbed FS, the second is the contribution of isolated polarons, and the third is the polaron-polaron interaction.

The effective interaction f between Landau quasi-particles contains two contributions: $f = g_\downarrow + f_\mathrm{x}$. The first one is the direct (or mean-field) interaction, $g_\downarrow = 4\pi\hbar^2 a_{\downarrow\downarrow}/m_\downarrow$, where $a_{\downarrow\downarrow}$ is the scattering length between bare impurities. The second term, instead, describes an exchange contribution, mediated by particle-hole excitations in the FS. At $T = 0$, this induced interaction between bosonic impurities is given by [Yu12]

$$f_\mathrm{x} = -\frac{(\Delta N)^2}{\mathcal{N}}. \tag{3.18}$$

Here $\mathcal{N} = \frac{3n_\uparrow}{2E_F}$ is the density of states at the Fermi energy, and ΔN is the number of particles in the dressing cloud of a polaron, given by [Mas11]

$$\Delta N \equiv \left.\frac{\partial n_\uparrow}{\partial n_\downarrow}\right|_{\mu_\uparrow} = -\left(\frac{\partial \mu_\downarrow}{\partial n_\uparrow}\right)_{n_\downarrow} \Big/ \left(\frac{\partial \mu_\uparrow}{\partial n_\uparrow}\right)_{n_\downarrow} \approx -\frac{\partial \mu_\downarrow}{\partial E_F}. \tag{3.19}$$

In the last step, we have exploided the fact that $\mu_\uparrow \approx E_F$. ΔN is obtained from a thermodynamical argument requiring that the density of the FS far from the impurity does not change when adding the impurity [Mas11]. We see that less than one particle of the bath is dressing the impurity, and that this number is positive for the attractive branch, indicating that particles from the bath are attracted to the impurity, and negative for the repulsive branch, indicating repulsion, as depicted in Fig. 3.4.

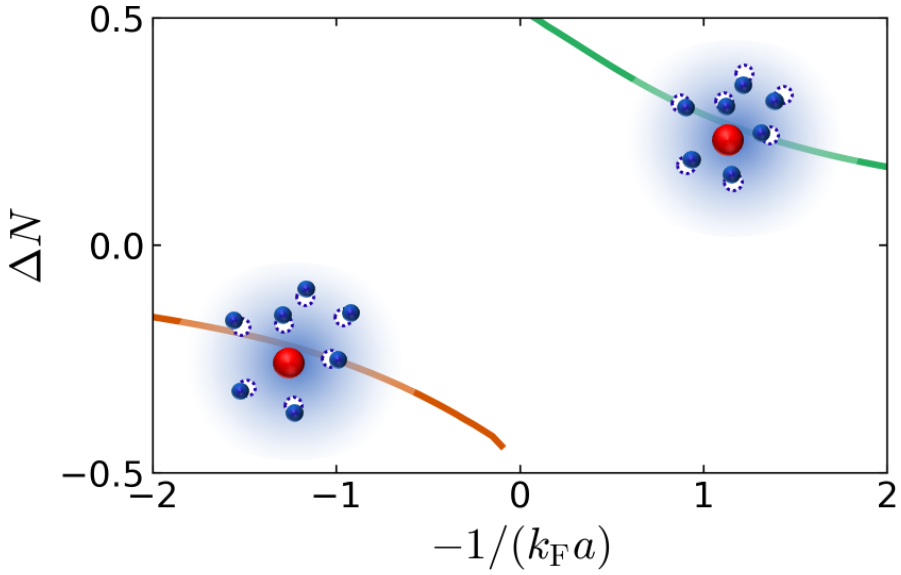

Figure 3.4: **Number of particles in the dressing cloud,** ΔN. The data are obtained from numerical calculation in the case of the ^{6}Li- ^{41}K mixture at the 335-G FR [Mas20].

We can derive Eq. (3.18), following the lines of Ref. [Yu12]. Within Landau theory,

a $\uparrow$ particle and a $\downarrow$ polaron interact with a coupling constant g_{x} given by

$$g_{\mathrm{x}} = \frac{\partial^2 \mathcal{E}}{\partial n_\uparrow \partial n_\downarrow} = \frac{\partial \mu_\uparrow}{\partial n_\downarrow}. \tag{3.20}$$

To second order in g_{x}, the polaron-polaron interaction is then given by

$$\mathcal{E}^{(2)} = -\frac{g_{\mathrm{x}}^2}{V^3} \sum_{\mathbf{p}_\uparrow, \mathbf{p}_\downarrow, \mathbf{q}} \frac{(1 - f_{\mathbf{p}_\uparrow + \mathbf{q}})(1 + f^{(b)}_{\mathbf{p}_\downarrow - \mathbf{q}}) f^{(b)}_{\mathbf{p}_\downarrow} f_{\mathbf{p}_\uparrow}}{\frac{(\mathbf{p}_\uparrow + \mathbf{q})^2}{2m_\uparrow} + \frac{(\mathbf{p}_\downarrow - \mathbf{q})^2}{2m^*_\downarrow} - \frac{p_\downarrow^2}{2m^*_\downarrow} - \frac{p_\uparrow^2}{2m_\uparrow}}, \tag{3.21}$$

where $f^{(b)}$ indicates Bose functions since we are assuming a bosonic impurity. The exchange contribution to Landau's polaron-polaron interaction can be calculated from this as

$$f_{\mathrm{x}} = \frac{\delta^2 \mathcal{E}^{(2)}}{\delta f^{(b)}_{\mathbf{p}_\downarrow} \delta f^{(b)}_{\mathbf{p}_\downarrow - \mathbf{q}}}, \tag{3.22}$$

where both $\mathbf{p}_\downarrow$ and $\mathbf{q}$ are vanishingly small. This gives

$$f_{\mathrm{x}} = -\frac{g^2}{V} \left(\sum_{\mathbf{p}_\uparrow} \frac{f_{\mathbf{p}_\uparrow} - f_{\mathbf{p}_\uparrow + \mathbf{q}}}{\frac{(\mathbf{p}_\uparrow + \mathbf{q})^2}{2m_\uparrow} - \frac{p_\uparrow^2}{2m_{\uparrow -}}} \right)_{q \to 0} = g_{\mathrm{x}}^2 \chi, \tag{3.23}$$

where χ is the so-called Lindhard function. At zero temperature, χ equals the density of states at the Fermi surface $\mathcal{N} = \frac{\partial n_\uparrow}{\partial \mu_\uparrow} = \frac{3 n_\uparrow}{2 E_F}$ and we obtain

$$\begin{aligned} f_{\mathrm{x}} = -g_{\mathrm{x}}^2 \mathcal{N} &= -\left(\frac{\partial \mu_\uparrow}{\partial n_\downarrow} \right)^2 \frac{\partial n_\uparrow}{\partial \mu_\uparrow} = -\left[-\frac{\left(\frac{\partial \mu_\uparrow}{\partial n_\downarrow} \right)}{\left(\frac{\partial \mu_\uparrow}{\partial n_\uparrow} \right)} \right]^2 \frac{\partial \mu_\uparrow}{\partial n_\uparrow} \\ &= -\frac{(\Delta N)^2}{\mathcal{N}}. \end{aligned} \tag{3.24}$$

In the last step we have used $\left(\frac{\partial x}{\partial y} \right)_z \left(\frac{\partial y}{\partial z} \right)_x \left(\frac{\partial z}{\partial x} \right)_y = -1$.

When the impurities are fermionic, an almost identical calculation leads to $f_{\mathrm{x}}^{(f)} =$

$-f_x$. Physically, this can be understood in terms of the Pauli repulsion between identical fermions or, alternatively, considering that the effective interaction involves the exchange of the impurities, which leads to a sign change for fermions as compared to bosons [Mor10; Yu10; Yu12; Cam18a]. The Landau interaction f between impurities is finally given by

$$f = \mp \frac{(\Delta N)^2}{\mathcal{N}} + g_\downarrow, \tag{3.25}$$

where the different sign, as already mentioned, corresponds to different impurity statistics: $-$ in case of bosonic, and $+$ in the case of fermionic impurities. Note that the Landau polaron-polaron induced interaction (which is the first term in the latter expression) is always attractive for bosonic impurities (and repulsive for fermionic ones), irrespective of whether the impurity-bath interaction is attractive or repulsive.

Introducing the impurity concentration $\mathcal{C} = n_\downarrow/n_\uparrow$, the increase of the energy of the gas when adding one impurity can be written as

$$\mu_\downarrow = \frac{\partial \mathcal{E}}{\partial n_\downarrow} = E_\downarrow \mp \frac{2}{3}(\Delta N)^2 \, \mathcal{C} \, E_F + g_1 n_\downarrow. \tag{3.26}$$

In RF injection, we are gradually increasing the number of impurities, and therefore the polaron-polaron interactions. Taking a simple average, one gets

$$\bar{\mu}_\downarrow = \frac{1}{N_\downarrow} \int_0^{N_\downarrow} \mu_\downarrow(N'_\downarrow) \, dN'_\downarrow = \Delta E, \tag{3.27}$$

where ΔE is the energy shift per impurity

$$\Delta E = \frac{\mathcal{E} - \frac{3}{5} E_F n_\uparrow}{n_\downarrow} = E_\downarrow \mp \frac{1}{3}(\Delta N)^2 \, \mathcal{C} \, E_F + \frac{g_\downarrow n_\downarrow}{2}. \tag{3.28}$$

As an additional note, I want to point out that in case of degenerate fermionic

impurities, there are additional terms coming from the fact that the impurities will form their own FS [Gir12], and that their kinetic energy will not be negligible. These terms can be sizable enough to mask the effect of mediated polaron-polaron interactions. In Ref. [Sca17] one of these effects was exploited for measuring the effective mass of the polaron in a RF spectroscopy experiment.

3.4 PROBING THE POLARON

In this Section, I want to summarize the theoretical results for the main quantities describing the Fermi polaron, and give a list of some experimental observation of them. In Table 3.1, I summarize the main property of the Fermi polaron, their theoretical description, the main experimental techniques exploited to study them, and a (not exhaustive) list of references where such techniques were used. Here I focus only on the Fermi polaron in three dimension. The role of dimensionality is very interesting but beyond the scope of this summary, and I refer the reader to Ref. [Taj21] for further details. In addiction to the quantities discussed in Section 3.2 and Section 3.3, the reader can find information about the Tan contact [Sca22]. Moreover, the experimental observation of the fast dynamics of the polaron is reported.

Table 3.1: **Polaron proprieties, their relation to the self energy and some experimental observations**. In the experimental technique column, "spect." stays for spectroscopy, "osci." for oscillations, "*in situ*" for *in situ* density measurements, and "interf." for interferometry.

Polaron property	Relation to self energy	Exp. technique	Refs
Energy (zero momentum)	$E_\pm = Re\left[\Sigma(0, E_\pm)\right]$	RF spect.	[Sch09; Koh12; Sca17; Yan19; Fri21; Bar23]
Energy (momentum resolved)	$E_\pm = Re\left[\Sigma(\mathbf{p}, E_\pm)\right]$	Raman spect.	[Nes20]
Residue	$Z_\pm = \frac{1}{1-\mathrm{Re}[\partial_\omega \Sigma(0,\omega=E_\pm)]}$	RF spect. Rabi osci. Raman spec.	[Sch09] [Koh12; Sca17; Adl20] [Nes20]
Effective mass	$m^*_\pm = \frac{m_\downarrow/Z_\pm}{1+\mathrm{Re}[\partial_{\epsilon_{\downarrow\mathbf{p}}} \Sigma(0,E_\pm)]}$	collective osci. RF spect. *in situ*	[Nas09] [Sca17] [Nav10]
Decay	$\Gamma = -2Z\mathrm{Im}[\Sigma(0, E)]$	RF spect. Rabi osci. Ramsey interf.	[Koh12; Sca17; Yan19; Fri21] [Koh12; Adl20] [Cet15]
Particles in dressing cloud	$\Delta N \equiv \frac{\partial n_\uparrow}{\partial n_\downarrow}\Big\vert_{\mu_\uparrow} \approx -\frac{\partial \mu_\downarrow}{\partial E_F}$	*in situ*	[Yan19]
Polaron-polaron mediated interaction	$f_x = \mp\frac{2}{3}\frac{\Delta N^2}{n_\uparrow} E_F$	RF spect. (Ramsey interf.)	[Fri21; Bar23] ([Cet16])
Contact	$C = 8\pi m_r \frac{\partial E}{\partial(-1/a)}$	RF spect. Raman spect.	[Yan19] [Nes20]
Fast dynamics		Ramsey interf.	[Cet16]

CHAPTER

FeLi(Bo)Kx 4

In this Chapter, I want to introduce FeLi(Bo)Kx, the laboratory in which I spent my PhD years. Moreover, I will give some technical details that will be useful for the discussion of the main experimental results presented in Chapter 5 and Chapter 6. As most of the experimentalists know pretty well, a laboratory is more than just a room with fancy devices you exploit to make your own research. A lab is an ecosystem of tools, instruments, appliances, etc., all interconnected to create an efficient organism, together with which you investigate Nature. This organism needs attention and care, and at the end you will perceive it as a living entity. All the people that worked with it during the years left a deep sign that you can feel, so that the actual working team is much bigger than the couple of PhD students present in the room at the moment. For these reasons, in the following I will refer to this laboratory as if it was a sentient creature, FeLi(Bo)Kx, and in discussing the work in the laboratory I will use "we".

I will start with a short historical overview in Section 4.1. I will then introduce the atomic species we work with in Section 4.2. In Section 4.3, I will give a succinct presentation of the experimental apparatus, and describe how we create radio frequency fields, the most important tool with which we address and investigate our systems. Finally, in Section 4.4, I will describe the preparation and characterization of the two heteronuclear mixtures with which the experiments presented in this Thesis

were performed.

4.1 FeLi(Bo)Kx DURING THE YEARS

FeLi(Bo)Kx stands for **Fe**rmionic **Li**thium, **K**alium (potassium)[1], that can be either fermionic or **Bo**sonic, and another additional species, **x**. The last term arises from the possibility to add another species to our experiment thanks to the presence of a three-species oven [Wil09], but the physics of two-species mixture is rich enough that this feature was never exploited. This experiment, built in the first decade of 2000, was one of the first creating a heteronuclear Fermi-Fermi (FF) mixture. At the time of its design, homonuclear fermionic spin mixtures of both lithium and potassium were an established tool for exploring strongly interacting Fermi gases [Ing08], and Feshbach resonances (FR) in heteronuclear mixtures of fermions and bosons were observed in ^{6}Li–^{23}Na [Sta04] and ^{87}Rb–^{40}K [Ino04]. In this context, the purpose of FeLiKx was to create an environment for exploring a strongly interacting mass-imbalanced heteronuclear Fermi-Fermi system. After the characterization of this system and its FRs [Wil08; Spi09; Nai11; Spi10; Tre11], FeLiKx started to study the problem of a fermionic impurity in a Fermi sea (FS). This line of research led to the first observation of the repulsive Fermi polaron [Koh12], the study of the decoherence of the impurity in the FS [Cet15], and the investigation of the dynamics of the polaron formation [Cet16]. The next goal was then to observe mediated polaron-polaron interaction. Since such interaction depends on the concentration of the impurities, FeLiKx thought of becoming FeLi**(Bo)**Kx, adding the possibility to switch between fermionic and bosonic impurities. Indeed the concentration of bosonic impurities is easier to

[1] The English name for the element potassium comes from the word potash, which refers to an early method of extracting various potassium salts: placing in a pot the ash of burnt wood or tree leaves, adding water, heating, and evaporating the solution. The symbol K stems from kali, itself from the root word alkali, which in turn comes from Arabic: *al-qalyah* 'plant ashes'. (from `https://en.wikipedia.org/wiki/Potassium`).

increase, not being constrained by the Pauli principle. The existing setup was thus modified in order to be able to trap the bosonic isotope of potassium ^{41}K. The details of such modification can be found in Rianne S. Lous' PhD thesis [Lou18a]. During the characterization of this new Fermi-Bose (FB) mixture, FeLi(Bo)Kx exploited the most striking feature of bosonic particles, Bose-Einstein condensation, developing a new technique for measuring the temperature of a degenerate FS in which a BEC is embedded [Lou17], observing how the BEC phase-separate from the FS [Lou18b] and probing its breathing mode [Hua19]. Then FeLi(Bo)Kx started to feel its age. This is the point at which I joined the team. It took almost two years of constant repairing in order to rejuvenate FeLi(Bo)Kx. Those were really dark and frustrating days, but after all the struggling we finally got our first results on the characterization of the polaron in a FB mixture of ^{6}Li and ^{41}K [Fri21], presented in Chapter 5, and the first observation of mediated polaron-polaron interactions in both a FB and a FF mixture [Bar23], presented in Chapter 6.

4.2 WHY Li AND K

In our system, we use the fermionic isotope of lithium, ^{6}Li, and either the bosonic ^{41}K, or the fermionic ^{40}K isotope of potassium, obtaining either a FB or a FF mixture, respectively. Li and K are of particular interest because they are the only alkali metals presenting both natural fermionic and bosonic isotopes. Their mass imbalance is such that it allows to investigate interesting physics, e.g. polarons [Koh12; Cet16; Fri21; Bar23], (Feshbach) molecules [Voi09; Rid11; Jag16; Yan20b], the BCS-BEC crossover [Yi06; Mac05], and exotic superfluid phases [Baa13]. Another peculiar feature is the relatively different optical polarizabilities at 1064 nm: In our optical dipole trap, their ratio is $\alpha_{\mathrm{K}}/\alpha_{\mathrm{Li}} \approx 2$ [Tan10; Saf13]. This leads to a roughly two times deeper optical potential for K with respect to Li. Combining this trapping effect with the mass

imbalance, we can see that the two species can be cooled to a point where either both K and Li, or only Li atoms are degenerate, allowing for investigating the effect of the degeneracy of the impurities in a FS. The similar features of the FRs for our FB and FF mixtures (see Sec. 4.4.2) allows for a direct comparison of the effects of the impurity statistics. For the FRs considered, all the unwanted scattering length are negligible (see Tab. 4.4 and Tab. 4.5). Last but not least, as already mentioned, at the time of the designing of the experiment, the techniques for trapping, cooling (to degeneracy), and manipulating the fermionic isotopes of Li and K were already well established.

Apart from FeLi(Bo)Kx, up to my knowledge, there are five other experiments that work, or have worked, with Li-K mixtures. In the group of K. Dieckmann, previously in Munich and now in Singapore, they successfully brought a ^{6}Li-^{40}K mixture to degeneracy thanks to sympathetically cooling with ^{87}Rb [Tag08], and they are now creating rotovibrational ground state molecules to study the resulting dipolar gas [Voi09; Yan20b; Bot22]. In Amsterdam, the group of J. Walraven, now not operating anymore, characterized some of the ^{6}Li-^{40}K FR resonances [Tie10]. M. Zwierlein and collaborators, in Boston, cooled down to degeneracy a ^{6}Li-^{40}K-^{41}K mixture, where ^{41}K was the coolant, and observed FRs between ^{6}Li and ^{41}K, and between ^{40}K and ^{41}K [Wu11]. In the laboratory of F. Chevy and C. Salomon in Paris, they simultaneous sub-Doppler laser cooled ^{6}Li and ^{40}K using D1 optical transitions [Sie15], they observed the formation of electronically excited heteronuclear ^{6}Li^{40}K* molecules [Rid11], they investigated the quasi-thermalization of the mixture in absence of interactions, and proposed a novel approach to analogically simulate Weyl particles [Suc16]. In Hefei, J. Pan and coworkers created a mixture of ^{6}Li and ^{41}K [Wu17], studied its s- and p- interspecies FRs and the intraspecies d- FRs in ^{41}K [Liu18], and investigated the double superfluidity of the Bose-Fermi mixture [Yao16; Wu18]. Up to now, FeLi(Bo)Kx is the only experiment that allows to switch between the two

potassium isotopes ^{40}K and ^{41}K, allowing the investigation of the effect of quantum statistics in two different, yet very similar, systems.

4.3 EXPERIMENTAL SETUP

We use an all-optical approach [Spi10] to prepare our system in a 1064-nm crossed-beam optical dipole trap (CODT), where atoms are trapped, cooled and manipulated thanks to magnetic field coils and radio frequency (RF) antennas. Thanks to a dual-species oven[2], we are able to prepare either FB or FF mixtures of lithium and potassium. Details on the preparation of such mixtures are presented in Sec. 4.4. While I refer to the PhD theses of Erich Wille [Wil09], for a description of the general experimental setup, and of Rianne S. Lous [Lou18a], for the technical implementation of the ^{41}K isotope, I would like to stress here that in our setup we can switch between the two potassium isotopes, ^{41}K and ^{40}K, in a few minutes, allowing for a handy investigation of the two different systems.

4.3.1 Li and K spin states

In this section I present the ^{6}Li, ^{41}K and ^{40}K hyperfine spin states used in the experiment. These are listed in Tab. 4.1 and depicted in Fig. 4.1. In describing the experiments, in order to have a unified wording while describing the FB and FF experiments, I will refer to $^{6}\mathrm{Li}|1\rangle$ simply as Li, and use the notation K0 and K1 for the non interacting and interacting state of K, regardless the isotope involved. A third spin state of K is used in the preparation of the sample, as discussed later in Section 4.4.1, and I will refer to this as $\mathrm{K}_{\mathrm{anc}}$, again regardless the K isotope involved.

[2] As already mentioned, designed for three species but used for two.

Table 4.1: **^{6}Li, ^{41}K, and ^{40}K hyperfine states used in the experiments**. The labeling is done counting from the lowest hyperfine (HF) state. *Conv.* refers to the conventional nomenclature used in this Thesis.

Conv.	HF state	F	m_F	Conv.	HF state	F	m_F	Conv.	HF state	F	m_F
Li	^{6}Li $\|1\rangle$	1/2	1/2	K1	^{41}K $\|1\rangle$	1	1	K_{anc}	^{40}K $\|1\rangle$	9/2	−9/2
	^{6}Li $\|2\rangle$	1/2	−1/2	K0	^{41}K $\|2\rangle$	1	0	K0	^{40}K $\|2\rangle$	9/2	−7/2
	^{6}Li $\|3\rangle$	3/2	−3/2	K_{anc}	^{41}K $\|3\rangle$	1	−1	K1	^{40}K $\|3\rangle$	9/2	−5/2

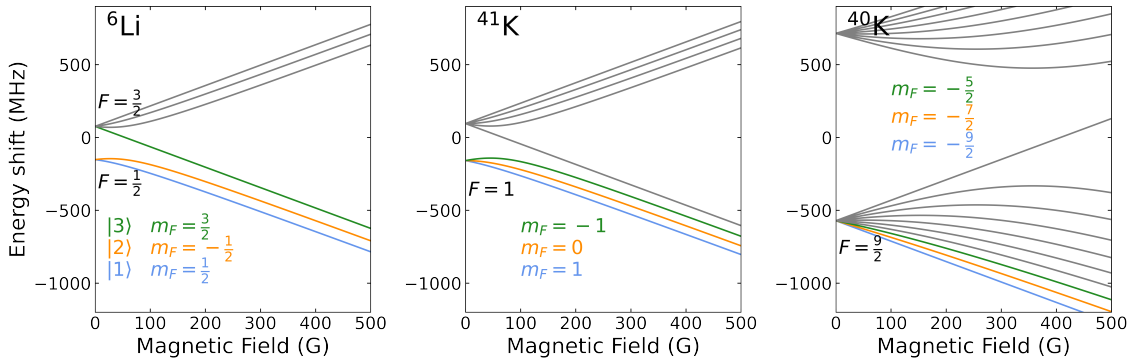

Figure 4.1: **Magnetic field dependence of the ground states of ^{6}Li, ^{41}K, and ^{40}K.**

4.3.2 Radio frequency control in FeLi(Bo)Kx

In our experiment, the separation between two consecutive hyperfine states of interest is of tens of MHz (Fig. 4.1), which can be easily covered by a RF field. Because of this, RF fields are the main tool that we exploit to address different spin states. Moreover, RF spectroscopy is the principal technique used in the measurements described in this Thesis. For these reasons, I want to dedicate this Section to a brief discussion of how we generate RF fields in FeLi(Bo)Kx. For a general introduction, I refer the reader to Chapter 2.2 for a discussion about atom-light interaction and RF spectroscopy.

We create RF fields with antennas consisting of copper wires soldered to BNC con-

Table 4.2: **Antennas used in FeLi(Bo)Kx**. The corresponding frequencies, state transitions, magnetic fields at which they are exploited, and their applications in the experiment are summarized.

Antenna	Frequency (MHz)	Transition	Field (G)	Application
Li switchable	83.8	Li $\|2\rangle \rightarrow$ Li $\|3\rangle$	585	zero crossing of Li $\|2\rangle -$ Li $\|3\rangle$ FR
	74.3	Li $\|1\rangle \rightarrow$ Li $\|2\rangle$	335	Li-K FR
	65.8	^{41}K $\|3\rangle \rightarrow^{41}$ K $\|2\rangle$	335	prepare K in ^{41}K $\|2\rangle$
^{41}K	57.9	^{41}K $\|2\rangle \rightarrow^{41}$ K $\|1\rangle$	335	Li-K FR
	57.9	Li $\|1\rangle \rightarrow$ Li $\|2\rangle$	92.2	change Li spin ratio
^{40}K	36.9	^{40}K $\|1\rangle \rightarrow^{40}$ K $\|2\rangle$	155	prepare K in ^{40}K $\|2\rangle$
	38.6	^{40}K $\|2\rangle \rightarrow^{40}$ K $\|3\rangle$	155	Li-K FR

nectors, furthermore capacitors are added in order to tune the resonance frequency of the antennas and match their impedance. The antennas transmit the signal supplied from an RF generator, and this signal can be amplified at need. In Table 4.2, the possible frequencies available in our system, and the hyperfine transitions they correspond to are listed. In our setup there is a fixed antenna, called here *Li switchable antenna*, which mainly addresses different Li hyperfine states. The name *switchable* comes from the fact that a relay is used to switch between two pairs of capacitors, in order to obtain two different resonant frequencies. In addition to this, there is either a ^{41}K or a ^{40}K *antenna*, which mainly addresses the ^{41}K or ^{40}K states at magnetic fields close to the respective FR with Li.

We can generated two different types of pulses: a rectangular or a Blackman shaped pulse, as depicted in Fig. 4.2. The first is the simplest form of RF pulse, and it is generated by applying a sinusoidal signal $A_{\mathrm{R}}(t) = A\sin(2\pi\nu_{\mathrm{RF}}t)$, for a duration τ_{RF}. If we consider its power spectrum, obtained from its Fourier transformation, we notice that this signal is not monochromatic, presenting two distinct side lobes typical of a sinc function. If used in RF spectroscopy, this pulse could thus excite multiple states, leading to a misinterpretation of the resulting spectroscopic signal. To obviate to this issue, we use instead a Blackman pulse, defined as

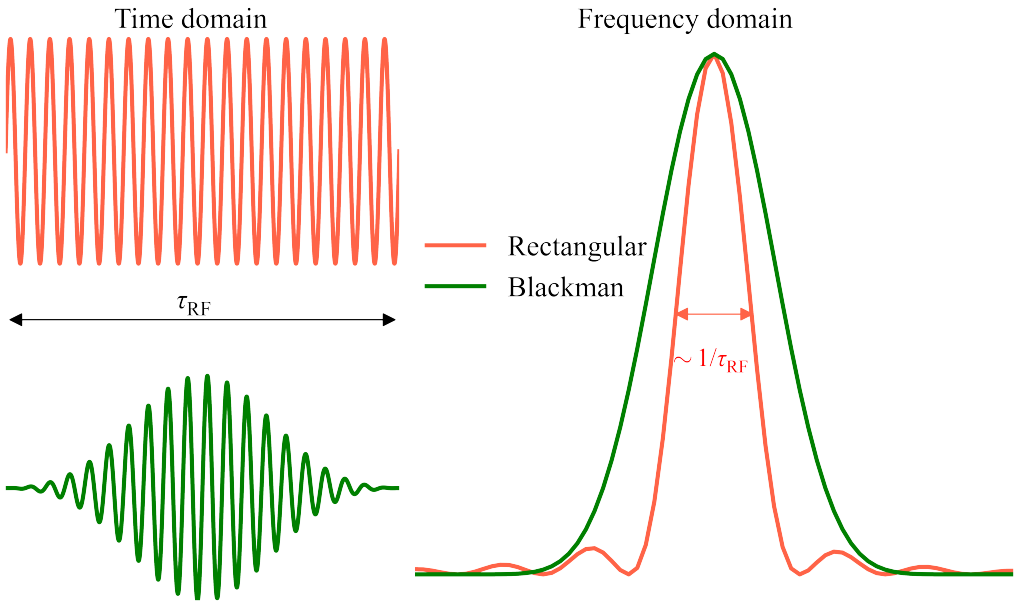

Figure 4.2: **Rectangular vs Blackman pulse.** Comparison between the two pulse shapes exploited in our experiment. **Left:** Pulses in the time domain. **Right:** Power spectrum of the pulses in the frequency domain, obtained from a Fourier transformation. The power spectrum of the BM pulse results in a monochromatic but broader signal with respect to the rectangular pulse.

$$A_{\mathrm{BM}}(t) = \left[0.42 - 0.5\cos\left(2\pi\frac{t}{\tau_{\mathrm{RF}}}\right) + 0.08\cos\left(4\pi\frac{t}{\tau_{\mathrm{RF}}}\right)\right]\sin\left(2\pi\nu_{\mathrm{RF}}t\right). \tag{4.1}$$

From Fig. 4.2 we can see that, while this pulse shape results in a monochromatic signal in the frequency domain, its width is larger than the one obtained from the rectangular pulse. This means that for the same pulse length the BM pulse will provide a worse spectral resolution. Apart from spectral resolution, it is sometimes important to transfer atoms from one state to an other in the shortest possible time. This time is limited by the power of the RF generator, and we can see that, for the same power, the rectangular pulse is faster than the BM pulse. For example, to drive

the bare 57 MHz K0 $\rightarrow$ K1 transition for the ^{41}K isotope, we use a 100 W RF amplifier, and we obtain a minimum duration for a $\pi-$pulse of $\tau_\pi \approx 52\,\mu$s for a rectangular, and $\tau_\pi \approx 78\,\mu$s for a BM pulse. To summarise, we exploit the monochromaticity of the BM pulse to investigate unknown systems via RF spectroscopy, while we take advantage of the fastness of the rectangular pulse when we need to interrogate the system in a short time, for example because of fast loss processes.

4.4 FF AND FB MIXTURES IN FeLi(Bo)Kx

In this Section, I will give some technical details on the FB and FF mixtures with which we performed the experiments presented in Chapter 5 and Chapter 6. I will discuss how we prepare and characterize the samples, and how we determine the center of the FRs exploited.

4.4.1 Preparation, detection and characterization of the samples

The preparation of our sample is very similar for the two cases of the FB and the FF mixtures, thus, I will present here a unified description of the two. The Li and K atoms are first loaded from a Zeeman-slowed atomic beam into a dual-species magneto-optical trap and then transferred into a single-beam optical dipole trap (SODT), which is derived from a 200-W fiber laser at a wavelength of 1070 nm. During the transfer process we apply grey-molasses cooling on the D1 line of Li, which reduces the temperature to about 50 μK and polarizes the majority of Li atoms into the lowest hyperfine spin state ^{6}Li $|1\rangle$ [Bur14; Fri15]. Mixing the lowest two spin states with a resonant RF, we then produce a 50/50 mixture of Li atoms in the lowest two states ^{6}Li $|1\rangle$ and ^{6}Li $|2\rangle$. We keep the sample for a time of typically 0.5 s (3 s) in the FB (FF) case, in which spin relaxation induced by interspecies collisions polarizes the K atoms into the state $\mathrm{K}_{\mathrm{anc}}$ [Spi10; Lou17]. This spin relaxation process is optimized

at a magnetic field of ∼200 G for ^{41}K and ∼15 G for ^{40}K.

Evaporative cooling is then implemented by ramping the power of the SODT down to zero while ramping down the power of a crossed optical dipole trap (CODT), which is turned on at maximum power together with the SODT at the loading stage. The ramp is performed in ∼ 5 s and a wait time of 1 s is added to reach thermal equilibrium between the two species. During the evaporation stage the K atom are sympathetically cooled by the Li atoms, which are in a mixture of ^{6}Li $|1\rangle$ and ^{6}Li $|3\rangle$ states (obtained after a further RF transfer of atoms from ^{6}Li $|2\rangle$ to ^{6}Li $|3\rangle$) at 485 G for the FB case, and in a mixture of ^{6}Li $|1\rangle$ and ^{6}Li $|2\rangle$ states at 923 G for the FF case.

The power of the CODT is adjustable in order to reach the desired temperature of the atomic clouds, and we rise it in the final stage of the preparation process to reach the same trapping frequencies for each experimental run, minimizing the effect of optical shifts of the FR induced by the trap light (see Supplemental Material of [Cet15; Lou18b]). The trap frequencies for the FB and FF case are listed in in Tab. 4.3. The CODT features an aspect ratio of about seven, with the weak axis oriented horizontally. The differential gravitational sag of both species amounts to about 3 μm and can be neglected since the Fermi sea is much larger.

Table 4.3: **Trap frequencies in the FB and FF mixtures**

mixture	$\omega_{\mathrm{Li_{ax}}}$ (Hz)	$\omega_{\mathrm{Li_{rad}}}$ (Hz)	$\omega_{\mathrm{K_{ax}}}$ (Hz)	$\omega_{\mathrm{K_{rad}}}$ (Hz)
FB	$2\pi \times 49.5(5)$	$2\pi \times 382(3)$	$2\pi \times 31.0(5)$	$2\pi \times 227(3)$
FF	$2\pi \times 67(1)$	$2\pi \times 544(8)$	$2\pi \times 41(1)$	$2\pi \times 308(5)$

After evaporative cooling, in order to obtain a fully polarized sample of Li in the ^{6}Li $|1\rangle$ state, we remove the atoms in the second spin state of Li by applying a resonant 10-μs light pulse at 567 G (1180 G) in the FB (FF) case.

Then the magnetic field is ramped close to the FR of interest near 335 G for the

FB mixture and 155 G for the FF mixture. At this point, we switch to a different set of coils, which facilitates precise magnetic field control to the level below a few mG. The trap contains a thermalized sample of roughly 10^5 Li atoms in the lowest hyperfine spin state and 10^4 L atoms in the K_{anc} state[3]. The temperature T is 102 – 137 nK in the FB case, and 190 – 285 nK in the FF case. At these temperatures, the Fermi sea is deeply degenerate, with $T/T_F \approx 0.15$ (FB) and $T/T_F \approx 0.25$ (FF). And the K impurities can be either in the thermal regime, or form a partial BEC.

At the end of each experimental cycle, we switch off the CODT, let the atoms expand for an adjustable time, and detect them using state-selective absorption imaging. This allows us to image the atoms in two spin states per species for each experimental cycle. Details on the imaging technique and on how to obtain the atom number are provided in the Supplemental Material of Ref. [Cet15].

We measure the temperature of our samples with two different methods, depending if a BEC is present or not. For thermal impurities, we determine the temperature by ballistic expansion of the K atoms after releasing them from the trap, both in the FB and in the FF case. In the FB case, if a BEC is present, we follow the approach described in Ref. [Lou17], and we release the atoms from the trap to determine the condensate fraction of the K atoms. From this and the known atom numbers and trap frequencies, we calculate the temperature.

The density profiles of both the degenerate Li Fermi gas and the bosonic K cloud are calculated using standard textbook relations [Pit16]. We neglect small finite-size or interaction corrections for the condensate [Lou18b]. Since the Fermi pressure acts on the Li atoms, and the optical potential is about two times deeper for K, K sample is much smaller than the spatial extent of the Li cloud, and this allows us to treat the

[3]Note that, even though we repaired big part of the experimental set up, our oven was not providing the same atom flux as in the past, and this flux was constantly diminishing during the measurements presented in this Thesis.

latter as an essentially homogeneous environment [Koh12]. Since in the experiments described in this Thesis we obtain our spectroscopic signal from the K component, we introduce the K-averaged atom number densities, $\bar{n}_{\mathrm{Li}}$ and $\bar{n}_{\mathrm{K}}$, for both species, namely

$$\bar{n}_{\mathrm{Li,K}} = \frac{1}{N_{\mathrm{K}}} \int n_{\mathrm{Li,K}}(\mathbf{r}) n_{\mathrm{K}}(\mathbf{r}) d^3\mathbf{r}, \tag{4.2}$$

with $n_{\mathrm{Li,K}}(\mathbf{r})$ being the local number density at position $\mathbf{r}$ of Li and K, respectively. Similarly we define the effective Fermi energy as

$$\epsilon_{\mathrm{F}} = \frac{1}{N_{\mathrm{K}}} \int E_{\mathrm{F}}(\mathbf{r}) n_{\mathrm{K}}(\mathbf{r}) d^3\mathbf{r}, \tag{4.3}$$

where the local Fermi energy at position $\mathbf{r}$ is given by

$$E_{\mathrm{F}}(\mathbf{r}) = \frac{\hbar^2 (6\pi^2 n_{\mathrm{Li}}(\mathbf{r}))^{2/3}}{2m_{\mathrm{Li}}}. \tag{4.4}$$

Finally, we define the effective Fermi wave number as $\kappa_{\mathrm{F}} = \sqrt{2m_{\mathrm{Li}}\epsilon_{\mathrm{F}}}/\hbar$. We emphasize that, owing to the much smaller size of the K cloud, the effect of inhomogeneity in n_{Li} (and thus in E_{F}) is small and accounts for about 10%.

4.4.2 Characterization of the FRs

In this Section, the measurements done in order to characterise the FRs in the FB and FF mixtures in FeLi(Bo)Kx are described. I refer the reader to Chapter 2.1.3 for a short overview on the basic concepts of FRs. The main features of the FRs for our FB and FF mixtures are listed in Tab. 4.4. We emphasize that the close similarity of these parameters allows for a direct comparison of the two mixtures. Morover, although these FRs are both closed-channel dominated [Chi10], their width

is large enough to stay in a near-universal interaction regime ($\kappa_F R^* < 1$) with the FS. In Tab. 4.5 we report the value of the intraparticle scattering lengths for K: Their values are small and similar for the two isotopes, allowing to neglect them in our experiments.

Table 4.4: **Comparison between FB and FF Feshbach resonances.** The center of the resonance B_0, its width Δ, the differential magnetic moment $\delta\mu$, the range parameter R^*, the scattering length a_{init} relative to Li-K0, and the background scattering length a_{bg} relative to Li-K1 are summarized for the FRs relative to the two mixtures used in our experiment.

Parameter	FB	FF
B_0 (G)	335.080(1) [Fri21]	154.7126(5) [Bar23]
Δ (G)	0.9487 [Lou18b]	0.92(5) [Nai11]
$\delta\mu/h$ (MHz/G)	2.660(8) [Lou18b]	2.3 [Nai11]
R^*/a_0	2241(7) [Lou18b]	2405(63) [Bar23]
a_{init}/a_0	63 [Han10]	62.5 [Nai11]
a_{bg}/a_0	60.865 [Lou18b]	63.0 [Nai11]

Table 4.5: **Theoretical values of K intraspecies scattering lengths**. **Left**: ^{41}K scattering lengths at a magnetic field $B \approx 335\,\text{G}$ extracted from Ref. [Lys10]. **Right**: ^{40}K background scattering lengths for the FRs located at 174.3 G, 224.2 G, and 202.1 G, between K1 and K0, K1 and K_{anc}, and K0 and K_{anc}, respectively, as in Ref. [Lud12]. Note that for ^{a} an experimental value of 174 can be found in Ref.[Reg03], and for ^{b} the value of 174 was found in Ref.[Lof02]. All values are in units of a_0.

^{41}K	K1	K0	K_{anc}
K1	60.7		
K0	60.8	60.9	
K_{anc}	60.8	61.3	60.9

^{40}K	K1	K0	K_{anc}
K1	-		
K0	183.5	-	
K_{anc}	163.7^a	167^b	-

The knowledge of the center B_0 of the FRs exploited in our experiments is crucial for having a good understanding of the observed phenomena. In the following, I present how we determine this value. In particular, I report the measurement, presented in Ref. [Fri21], for the determination of B_0 for the FR close to 335 G between Li and K1 for the FB mixture. An analogous measurement was carried out during the

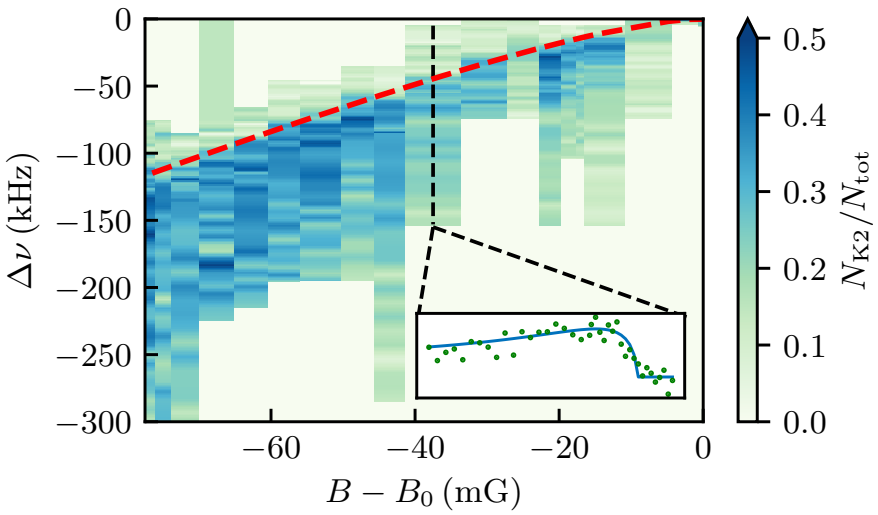

Figure 4.3: **Molecule dissociation measurement for B_0 determination in the FB case**. The transferred fraction to K0 (color scale) is shown in dependence of magnetic field and RF detuning for various magnetic fields around the center of the FR. The inset shows an example spectrum, taken at $B - B_0 \approx -37\,\mathrm{mG}$. After determining the binding energy of the molecules as a function of the interaction strength, we fit the resulting data with Eq. (4.5), shown by the red dashed line, with B_0 as the only fitting parameter.

experiments reported in Ref. [Bar23] and presented in Chapter 6, for characterizing the FR at 155 G for the FF mixture.

As shown in Fig. 4.3, we determine the molecular binding energy E_b, in vacuum, at different interaction strengths and we fit it with the function

$$E_b = \frac{\hbar^2}{8(R^*)^2 m_r}\left(\sqrt{1 - \frac{4R^*(B-B_0)}{a_{bg}\Delta}} - 1\right)^2, \tag{4.5}$$

derived in [Pet04; Lev11]. The reduced mass $m_r = m_{Li}m_K/(m_{Li}+m_K)$, the resonance width Δ, the range parameter R^*, and the background scattering length a_{bg} are known, which leaves B_0 as the only fitting parameter in this model[4]. The resulting

[4]During the characterization of the FF resonance, we found a better fit by considering R^* a free

values for the center of the FRs are reported in Tab. 4.4. Note that the center of the resonances suffers from a light shift due to the trapping potential (see Supplemental Material of [Cet15; Lou18b]). In order to take this shift into account, the calibration of the FRs and the actual experiments are performed with the same trapping settings.

Eq. (4.5) describes the binding energy of molecules in vacuum. Since interactions with the remaining FS, which can lead to a systematic shift on the order of 5 mG, are not included, we experimentally determine B_0 by molecule dissociation *in vacuum* via ejection spectroscopy, in contrast to our previous method (see Appendix of [Lou18b]).

The measurement consisted in the creation of molecules with thermal impurities on the repulsive side of the resonance ($X \approx -0.8$ for the FB case, where X is the interaction paramenter defined in Eq. (2.15)) by applying an RF pulse to the K0 atoms at a frequency corresponding to the binding energy $\nu \approx E_b/h$, which we optimized roughly on maximum molecule association efficiency. Then, we ramped the magnetic field to lower X values, therefore increasing the binding energy. This procedure prevented the molecules from dissociating as we applied an RF pulse to transfer the remaining unbound Li$|1\rangle$ atoms into Li$|2\rangle$. To be sure that no particles, except the molecules, were present, we applied a 10 μs resonant cleaning pulse to ^{6}Li$|2\rangle$ and another one to K0. Then we ramped back the magnetic field to reach the final interaction strength X for which we wanted to determine the binding energy. At this field, we applied another RF pulse to transfer the K1 atoms into K0, and consequently dissociate the molecules. By varying the detuning $\Delta\nu = \nu_0 - \nu$ of this last pulse with respect to the bare K0→K1 transition, we obtained the dissociation spectrum with a line shape determined by the frequency-dependence of the Franck-Condon factor, as described in Ref. [Chi05]. The inset of Fig. 4.3 shows a sample spectrum for the FB

parameter as well, this gives a $\sim$ 10% difference on the value used in previous experiments [Koh12; Cet15; Cet16].

case at a magnetic detuning $B - B_0 \approx -37\,\mathrm{mG}$, and the corresponding fit to extract the binding energy. We recorded dissociation spectra in a range of about 80 mG, where we expected molecules to exist.

CHAPTER

CHARACTERIZATION OF POLARONS IN A FERMI-BOSE MIXTURE 5

In this Chapter, I present the results published in Ref. [Fri21]. In this work we investigated the properties of a strongly interacting imbalanced Fermi-Bose (FB) mixture of bosonic ^{41}K impurities immersed in a Fermi sea (FS) of ultracold ^{6}Li atoms. The presence of bosonic impurities enabled us to explore the Fermi polaron for large impurity concentrations, including the extreme case in which the impurities form a Bose-Einstein condensate (BEC). The system was characterized by means of radio-frequency (RF) injection spectroscopy for tunable interactions using an interspecies Feshbach resonance (FR). We found that the energy of the Fermi polarons formed by particles in the thermal fraction of the impurity cloud remains rather insensitive to the impurity concentration, even as we approach equal densities for both species. The apparent insensitivity to high concentration is consistent with the Landau's quasi-particle theoretical prediction of a weak effective interaction between the polarons (see Chapter. 3.3.1), which was not detectable within the precision of the reported measurements (Chapter 6 will present a new set of measurements in which such interaction was unambiguously observed). The condensed fraction of the bosonic ^{41}K

gas, much denser than its thermal component, leads to a breakdown of the Fermi polaron description. Indeed, we observed a new branch in the RF spectrum characterized by a small energy shift, consistent with the presence of Bose polarons formed by ^{6}Li fermions inside the ^{41}K BEC. A closer investigation of the behavior of the condensate by means of Rabi oscillation measurements supported this observation, indicating that we could realize both Fermi and Bose polarons, two fundamentally different quasi-particles, in the same cloud.

This Chapter is organised as follows. After introducing the experiment in Section 5.1, I will introduce technical details in Section 5.2. In particular the preparation of the samples and their detection, the interspecies interactions between the impurity and the bath in our system, the explanation of our spectroscopic procedure, and the relevant quantities for our experiment are explained. After this technical introduction, the main results are presented. In Section 5.3 the impurity energy spectra in the two regimes in which the impurities are thermal, and in which they form a partial BEC are presented and commented. While for the thermal case, and for the thermal part of the cloud in the partial BEC case, the observed spectra are well described by the theory of a single impurity forming a polaron, in the partial BEC case we observed the emergency of an additional feature in the spectra. Section 5.4 discusses this new feature, which can be understood in the frame of the Bose polaron physics, considering that the condensed part of cloud has a higher density than the FS, leading to an inversion of the roles of the impurity and the bath. Thus, what we observed was the energy shift of the bosonic K bath due to the presence of Bose polarons formed by the fermionic Li impurities. In Section 5.5, Rabi oscillations measurements in the partial BEC regime are presented. We observed inhibition of Rabi oscillations of an RF-coupled BEC in the environment of a FS. While this is an interesting many-body phenomenon, its nature is still not completely understood and needs further investig-

ation. In Section 5.6, the observations regarding the lifetime of the repulsive polaron in the thermal regime are presented. For strong interactions two-body decay into the attractive polaron seems to be the main loss channel. For weaker interactions, considering that the attractive polaron is ill-defined, due to the smallness of its residue, and decays into the molecular states, three-body decay processes become dominant. Finally, in Section 5.7, the first attempt to observe the polaron-polaron mediated interaction is presented. The results were encouraging but not conclusive, and the final observation of this effect [Bar23] will be the topic of Chapter 6.

5.1 INTRODUCTION

Our main motivation was to characterize the Fermi polaron formed by bosonic impurities, and investigate how a high concentration of impurities affects its properties. We performed the measurements with bosonic ^{41}K impurities, forming either a thermal cloud (ThC), or a partial BEC (pBEC). We can identify three different regimes of impurity densities in our FB mixture, as illustrated in Fig. 5.1. The blue background and the red dots represent the Li FS and the K impurities, respectively. As in our previous work on the FF system [Koh12], we used RF injection spectroscopy to transfer the K impurities from a non-interacting spin state K0, into a state K1 which interacts with the fermionic bath.

In the case of a single impurity (left column), the K atom is dressed by particle-hole excitations of the FS, which lead to local density modulations in the bath, and to the formation of the Fermi polaron. In this low concentration regime, the quantum statistics of the impurity does not matter. The situation is accurately described in terms of the variational ansatz presented in Chapter 3.2. As we add more K atoms, we expect to introduce polaron-polaron interactions into our system, as depicted in the middle column of Fig. 5.1. In this density regime, the spatial overlap of the dens-

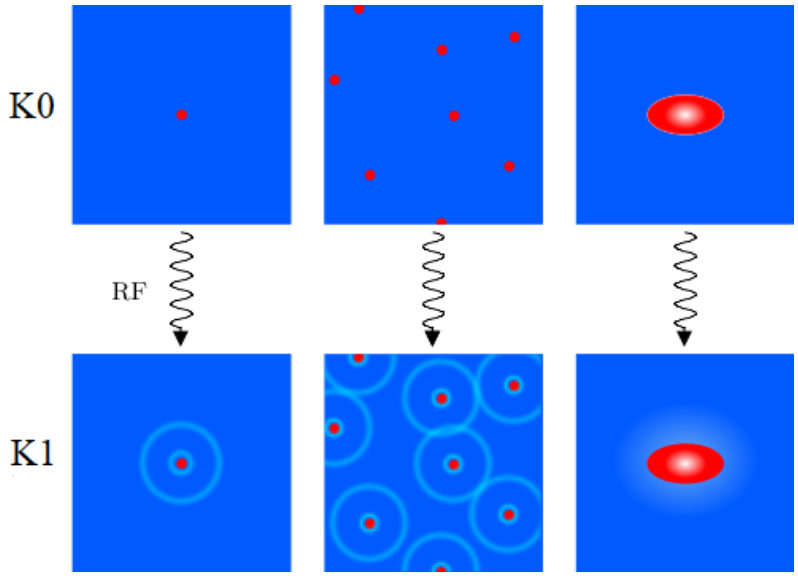

Figure 5.1: **Fermi-Bose mixture in three different impurity density regimes explored in our experiment**. The upper (lower) row shows the non-interacting (interacting) impurities immersed in a FS, which is represented by the blue background. The interaction between the impurities and the FS gives rise to density modulations in the latter, as illustrated by the light-blue rings around the K atoms. An RF pulse brings the system from a non-interacting (K0) to a strongly interacting (K1) state. The three columns illustrate three different regimes. From left to right the impurity density is increased and we go from a single impurity to a high density sample, finally reaching a mixed phase containing a large BEC component. Adapted from Ref. [Fri21].

ity modulations around the impurities will result in an effective interaction between the quasi-particles mediated by the fermions of the bath, which is attractive due to the bosonic nature of the ^{41}K atoms [Mor10; Yu10; Yu12; Cam18a; San08; Hu18; Cam18b; Taj18; DeS19; Edr20], as discussed in Chapter 3.3. This effective interaction plays a key role in Landau's quasi-particle theory, and its unambiguous experimental observation in quantum-degenerate gases will be the subject of Chapter 6. In the high-density regime (right column), the impurities in the center of the trap form a BEC, the density of which can exceed the one of the FS (for example, by a large factor

of ~ 36 in our experiment). In this case, the two species interchange their roles and, locally, the Li atoms can be considered as impurities in the K BEC. Such a scenario is commonly described in terms of Bose polarons [Hu16; Jør16]. Therefore, as we vary the K density from a thermal cloud to a BEC, we can realize the transition from a system of Fermi polarons to a system of Bose polarons.

5.2 TECHNICAL DETAILS

For the measurements presented in this Chapter, we used the bosonic ^{41}K isotope of potassium as impurity embedded in a FS of ^{6}Li atoms. The interparticle interactions between the two species are tuned thanks to a FR centered at $B_0 = 335.080(1)\,\mathrm{G}$. For the details on the characterization of this FR, the reader can look back at Chapter 4.4.2.

5.2.1 Spin states

In the following we use the convention on naming the spin states introduced in Chapter 4.2. For the main RF spectroscopic measurements, the ^{6}Li atoms forming the spin-polarized FS were always kept in the lowest hyperfine spin state $F, m_F = (1/2, +1/2)$, simply named Li. In our spectroscopic injection scheme, the initial state K0 was represented by the state (1, 0), and the final Feshbach-resonant state K1 corresponded to $(1, +1)$.

5.2.2 Sample preparation

After the preparation described in detail in Chapter 4.4.1, we obtained a mixture of roughly 10^5 Li and 10^4 K0 atoms in thermal equilibrium between each other, with temperatures of $T \approx 100\,\mathrm{nK}$ at a magnetic field of $B \approx 335\,\mathrm{G}$. The atoms were trapped in a 1064 nm crossed optical dipole trap (CODT) with radial trap

frequencies $\omega_{\mathrm{rad,K}} = 2\pi \times 227\,\mathrm{s}^{-1}$ and $\omega_{\mathrm{rad,Li}} = 2\pi \times 382\,\mathrm{s}^{-1}$, and axial frequencies $\omega_{\mathrm{ax,K}} = 2\pi \times 31\,\mathrm{s}^{-1}$ and $\omega_{\mathrm{ax,Li}} = 2\pi \times 49.5\,\mathrm{s}^{-1}$ for K and Li, respectively.

We conducted our measurements in two different regimes, in which we either a ThC, or a pBEC of K atoms is immersed in a degenerate FS of Li atoms. In order to achieve the pBEC, while maintaing the same trap settings in the two regimes in order to avoid a light shift of the FR (see Chapter 4.4.1), we altered the preparation stage for the pBEC with respect to the ThC in two ways. First, we increased the initially loaded atom numbers by varying the loading time, and secondly we applied an additional evaporation step, in which we further ramped down the power of our CODT, and slowly (within 1s) recompressed it to the initial values at the end of the preparation stage. With this procedure, we ensured a two-fold increase in the number of K atoms and thus an increase of the critical temperature for condensation by about 30%. The condensed fraction was typically of the order of $\beta \approx 0.5$.

5.2.3 Interaction tuning

Since our experiment was based on the interactions between the impurities and the FS, a precise knowledge of them was of crucial importance. Most of the measurements presented in this Chapter were conducted in the strongly interacting regime ($-1 \lesssim X \lesssim 1$), where X is the dimensionless interaction parameter defined in Eq. (2.15). This required good accuracy and precision in our knowledge of the magnetic field strength. Therefore, we experimentally determined the residual fluctuations around the target value, resulting in a statistical uncertainty of $\sigma_B = 0.5\,\mathrm{mG}$, which translated to a corresponding uncertainty $\sigma_X < 0.035$ of the interaction parameter X. Furthermore, we observed a slow drift of the magnetic field strength, which we took into account by taking the average value of the magnetic field determined before and after each measurement. We disregarded all measurements exceeding a magnetic

field drift of 3 mG. The uncertainty in the B field, and the fact that the strongly interacting regime given by the Feshbach resonance is only ~ 30 mG broad, set the resolution that we could achieve for X. For this reason, we discretized the variation of the interaction parameter, and divided the region between $-1.5 < X < 1.5$ into 12 bins, each having a width of ~ 0.25.

5.2.4 Radio-frequency excitation scheme

In order to probe the energy spectrum of our K atoms across the Feshbach resonance, we exploited injection RF spectroscopy. While an introduction to this technique is given in Chapter 2.2.2, we recall here that with such method the impurity atoms are transferred from a non-interacting into an interacting state. One advantage of this procedure is that the system can be transferred to a strongly interacting state that is not necessarily the ground state of the system. It therefore enables us to study the repulsive polaron as a metastable state [Mas11; Koh12], along with its non-equilibrium evolution.

Our system was excited by an RF pulse that transferred atoms from the non-interacting K0 to the interacting K1 state in the presence of Li. In order to avoid side lobes in the spectrum we used a Blackman-shaped pulse (see Chapter 4.3 for details). We adjusted it to be a resonant π-pulse for a bare K cloud, i.e. in the absence of the Li atoms. The power of this pulse was chosen such that at the resonance frequency ν_0, where the maximum transfer occurs, we obtained a pulse duration of $\tau_{\mathrm{RF}} = 1$ ms. This duration was chosen as a compromise between spectral resolution and lifetime. The former is set by the spectral width of the RF pulse $\sigma_{\mathrm{RF}} = 0.7$ kHz, which, depending on the specific sample preparation, was around $\sigma_{\mathrm{RF}} \approx 0.04\,\epsilon_{\mathrm{F}}/\hbar$. The latter is given by the shortest lifetime of the polaron, which we estimated to be around 1 ms. In most of our measurements we varied the frequency detuning $\Delta\nu = \nu_0 - \nu$ with

respect to the bare K0 $\rightarrow$ K1 transition, keeping the pulse power unchanged. Our spectroscopy signal is the transferred fraction of potassium atoms $N_{\mathrm{K1}}/N_{\mathrm{tot}}$, where N_{K1} is the atom number in the K1 state, and $N_{\mathrm{tot}} = N_{\mathrm{K1}} + N_{\mathrm{K0}}$ is the total atom number in both states. The dependence of the spectroscopic signal $N_{\mathrm{K1}}/N_{\mathrm{tot}}$ on $\Delta\nu$ reflects the energy spectrum of our strongly interacting system of K1 atoms immersed in a Li FS. We determined the uncertainty of the atom numbers from the standard deviation of repeated measurements.

5.2.5 Relevant parameters

In Table 5.1, we present an overview of typical values for the most relevant experimental parameters for the experiments presented in this Chapter. The given uncertainties reflect the standard deviation for all measurements.

Table 5.1: **Experimental parameters.** We report several relevant experimental parameters values for measurements in the ThC and pBEC regime. Adapted from Ref. [Fri21].

Parameter	ThC	pBEC
ϵ_{F}	$k_B \times 930(60)\,\mathrm{nK}$	$k_B \times 620(50)\,\mathrm{nK}$
$1/\kappa_{\mathrm{F}}$	$4000(130)\,a_0$	$4800(200)\,a_0$
$\kappa_{\mathrm{F}} R^*$	0.57(2)	0.47(2)
T	130(13) nK	118(21) nK
T/T_{F}	0.14(1)	0.19(3)
N_{Li}	$2.8(2) \times 10^5$	$1.2(1) \times 10^5$
N_{K0}	$1.2(1) \times 10^4$	$2.7(3) \times 10^4$
$\bar{n}_{\mathrm{Li}}$	$1.9(2) \times 10^{12}\mathrm{cm}^{-3}$	$1.0(1) \times 10^{12}\mathrm{cm}^{-3}$
$\bar{n}_{\mathrm{K0}}$	$0.92(7) \times 10^{12}\mathrm{cm}^{-3}$	$1.4(1) \times 10^{12}\mathrm{cm}^{-3}$
$\bar{n}_{\mathrm{K0,BEC}}$	–	$3.8(1) \times 10^{13}\mathrm{cm}^{-3}$
β	–	0.46(7)
$\mathcal{C}_{\mathrm{K0}}$	0.61(7)	1.5(5)
$\mathcal{C}_{\mathrm{K0,BEC}}$	–	36(6)

In particular, the total atom numbers of Li, N_{Li}, and K, N_{K}, and the condensate

fraction β in the pBEC regime are listed, and we give the concentrations $\mathcal{C}_{\mathrm{K0}} = \bar{n}_{\mathrm{K0}}/\bar{n}_{\mathrm{Li}}$ and $\mathcal{C}_{\mathrm{K0,BEC}} = \bar{n}_{\mathrm{K0,BEC}}/\bar{n}_{\mathrm{Li}}$ for the thermal and the condensed part of the non-interacting sample, respectively. Note that in the majority of our measurements, we stated the concentration of the non-interacting sample. The value for the interacting case $\mathcal{C}_{\mathrm{K1}} = \bar{n}_{\mathrm{K1}}/\bar{n}_{\mathrm{Li}}$ was experimentally not directly accessible because of interaction effects on the spatial distribution, and could thus only be estimated, as discussed later in Sec. 5.7.

5.3 THERMAL SAMPLE VS PARTIAL BEC

In order to investigate the full spectral response of the system across the strongly interacting regime, we combined RF spectra taken at different values of X. The spectra, recorded in the ThC and pBEC regime, are depicted in Figs. 5.2(a) and (b), respectively. The x-axis represents the discretized dimensionless interaction parameter X, individual bins containing an average of 1 to 4 measurements. Each bin shows the transferred fraction $N_{\mathrm{K1}}/N_{\mathrm{tot}}$ as a function of the energy detuning of the RF pulse $h\Delta\nu$ (defined in Sec. 5.2.4), normalized to the effective Fermi energy, ϵ_{F}.

The theoretical predictions, red dashed and orange dash-dotted lines, denote a variational calculation describing a single impurity interacting with a FS using a two-channel model, as discussed in Chapter 3.2.

In Fig. 5.2a [1], we show the full spectral response in the ThC regime, consisting of the repulsive and the attractive polaron branches exhibiting a positive and negative energy shift, respectively. Moreover, we observed a decrease of contrast as the interac-

[1] A small non-zero background in our spectra, especially in the pBEC regime, may be attributed to imaging artefacts. Our absorption pictures show a residual signal in K1 when imaging a BEC in K0. We explain this by scattering of off-resonant light from a very dense atomic sample, and subtract the resulting signal from the real atom number.

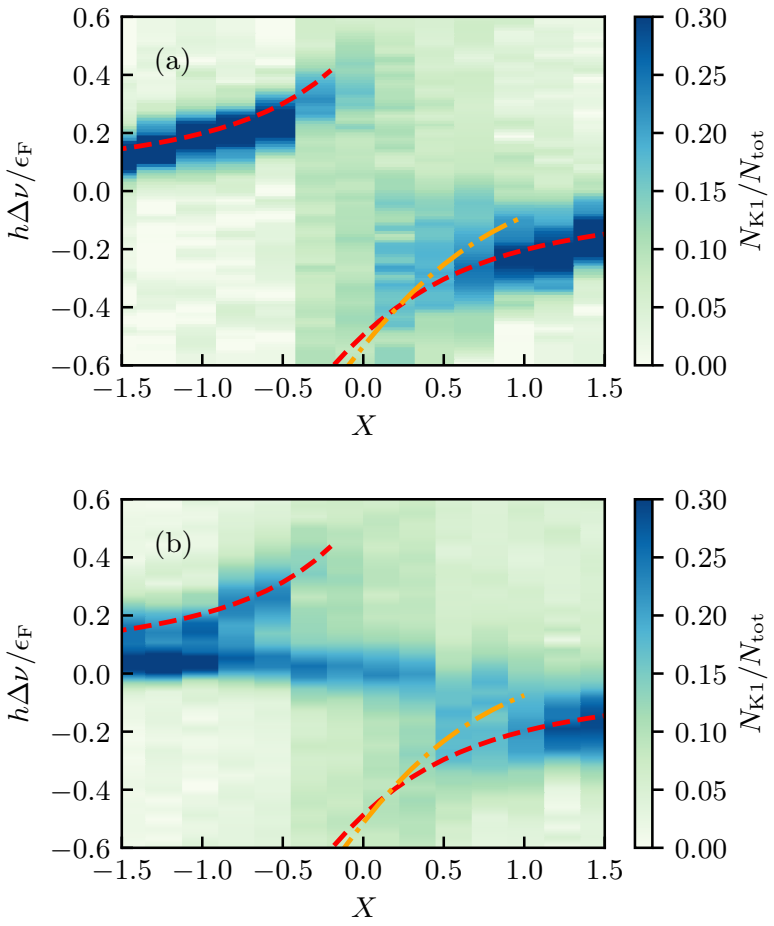

Figure 5.2: **Spectral response of a bosonic ^{41}K sample immersed in a ^{6}Li Fermi sea**. **(a)** and **(b)** show the measured excitation spectra in the ThC and in pBEC regime, respectively. The spectra are shown as a function of the interaction parameter X and the dimensionless RF detuning $h\Delta\nu/\epsilon_F$. The color map refers to the transferred fraction of atoms from K0 to K1. Red dashed and orange dash-dotted lines illustrate our theoretical predictions for the polaron and molecule energies in the single-impurity limit, respectively. Individual bins contain averages of 1 to 4 measurements. From Ref. [Fri21].

tion was tuned close to $X = 0$. The obtained polaron energies are in good agreement with the theoretical predictions for the single impurity scenario, represented by the red dashed lines, although the fairly high impurity concentration, $\mathcal{C}_{K0} = 0.61(7)$.

In Figure 5.2b, we present the recorded spectrum in the pBEC regime. A striking difference between the ThC and pBEC spectra is that, in the latter, a new branch, which shows a small energy shift, emerges in the spectrum. The bimodal spectral response is a consequence of different resonance frequencies of the transfer to the K1 state for the two components of the gas. The response of the thermal part of the K cloud is still well described by the single impurity theory, even though the K density is similar to the Li density (see Tab. 5.1). In stark contrast to this, the condensed part is transferred at a frequency close to the non-interacting value $\Delta\nu = 0$, with a small but consistent upshift, corresponding to a few percent of the Fermi energy. As we will discuss in Sec. 5.4, this shift can be attributed to the formation of Bose polarons, with the Li atoms playing the role of the impurities in a bath formed by the K BEC.

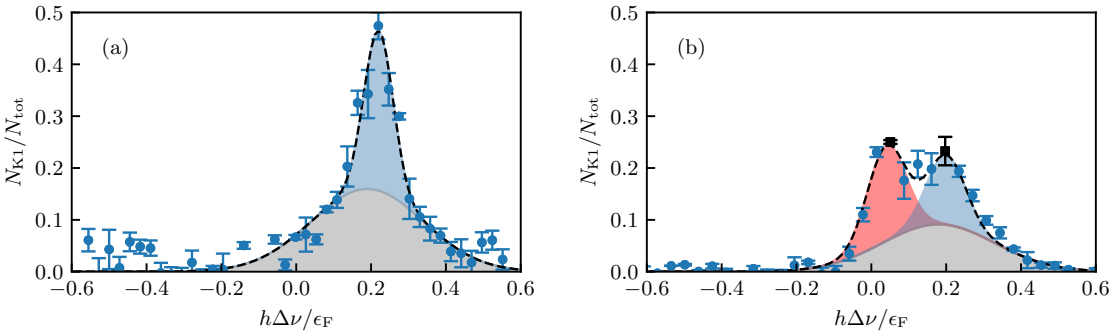

Figure 5.3: **Typical polaron spectra in the ThC (a) and pBEC (b) regime**. We show the fraction of transferred atoms as a function of the frequency detuning $\Delta\nu$ of the applied RF pulse at an interaction strength of $X \approx -0.7$. The shaded areas under the curves illustrate the contributions resulting from a fit by a double-Gaussian (ThC, left) and triple-Gaussian (pBEC, right) function. Black dashed lines depict their sum. The width of the narrow peaks was fixed to the Fourier width of the applied pulse. The measurement points marked by black squares in (b) are further discussed in Fig. 5.4. From Ref. [Fri21].

In order to further investigate the differences between the ThC and pBEC regimes,

in Figs. 5.3a and Figs. 5.3b we compare two sample spectra taken in the two regimes at an interaction strength of $X \approx -0.7$. In the ThC regime we find a single narrow peak, which we attribute to the Fermi polaron, along with a broader background, which we interpret as a many-body continuum of states. The observed spectrum can be well fitted with a double Gaussian,

$$G(\Delta\nu) = G_{\mathrm{p}}(\Delta\nu) + G_{\mathrm{bg}}(\Delta\nu), \tag{5.1}$$

as also used in our previous work [Koh12]. Each Gaussian takes the form

$$G_{\alpha}(\Delta\nu) = A_{\alpha} e^{-(\Delta\nu-\Delta\nu_{\alpha})^2/(2{\sigma_{\alpha}}^2)}, \tag{5.2}$$

with A_{α}, $\Delta\nu_{\alpha}$, σ_{α} representing the amplitude, center and width of the Gaussian for $\alpha = \mathrm{p}$, bg. The polaron peak, $\alpha = \mathrm{p}$, was fixed to a spectral pulse width of $\sigma_p = 0.7\,\mathrm{kHz} \approx 0.04\,\epsilon_{\mathrm{F}}/h$, which corresponds to the Fourier width resulting from the finite duration of the 1-ms RF pulse. The background, $\alpha = \mathrm{bg}$, is marked by the gray, broad Gaussian in Fig. 5.3. In the sample spectrum in Fig. 5.3a, we transferred about 50% of the atoms into the interacting state at a frequency detuning corresponding to $h\Delta\nu \approx 0.2\epsilon_F$.

In the pBEC regime, depicted in Fig. 5.3b, we identify a maximum transfer at two well-defined frequencies. We approximated the lineshape of the whole spectrum by a triple Gaussian function

$$\tilde{G}(\Delta\nu) = \tilde{G}_{\mathrm{p}}(\Delta\nu) + \tilde{G}_{\mathrm{bg}}(\Delta\nu) + \tilde{G}_{\mathrm{BEC}}(\Delta\nu). \tag{5.3}$$

The first two terms stem from the polaron and the many-body continuum background, $\tilde{G}_{\mathrm{p}}(\Delta\nu)$, $\tilde{G}_{\mathrm{bg}}(\Delta\nu)$, respectively. We assumed that the ratio of the two amplitudes stays the same as determined in Fig. 5.3a, but their absolute values are reduced

corresponding to the fraction of non-condensed atoms, as

$$\tilde{G}_{\mathrm{p,bg}}(\Delta\nu) = G_{\mathrm{p,bg}}(\Delta\nu) \times (1-\beta). \tag{5.4}$$

The third term describes the transfer of the condensed fraction as

$$\tilde{G}_{\mathrm{BEC}}(\Delta\nu) = G_{\mathrm{BEC}}(\Delta\nu) \times \beta, \tag{5.5}$$

where $G_{\mathrm{BEC}}(\Delta\nu)$ is defined in the same way as Eq. 5.2.

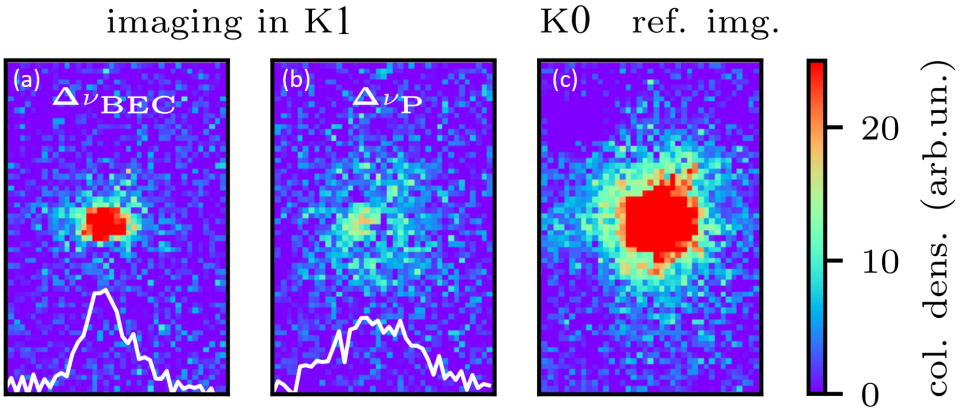

Figure 5.4: **Absorption images of K in the pBEC regime**. **(a)** and **(b)** were taken after a short time of flight of 6 ms and correspond to the two measurements marked by black squares in Fig. 5.3b. They show the atoms at the transfer frequencies $\Delta\nu_{\mathrm{BEC}}$ and $\Delta\nu_{\mathrm{p}}$, respectively. **(c)** is a reference picture of the K0 cloud, before the transfer, with $\beta \approx 0.5$, taken after a time of flight of 4 ms. The color map depicts the column density in arbitrary units. The field-of-view of all images is about $(150 \times 230)\,\mu$m. The white solid lines show the corresponding projected line-density profiles. Adapted from Ref. [Fri21].

To have a better insight on the nature of the double peak feature in the pBEC regime, in Fig. 5.4a and Fig. 5.4b, we show absorption images of atoms in K1 after 6 ms from being released from the trap, within 6 μs after the RF pulse. The two

pictures correspond to the measurements for the two frequency detunings $\Delta\nu_{\mathrm{BEC}}$ and $\Delta\nu_{\mathrm{p}}$, for which we observed maximum transfer of the BEC and the thermal cloud , respectively. These two detunings are marked by black squares in Fig 5.3b. The atomic clouds in the images have the same atom number, but very different spatial distributions. Fig. 5.4a shows a dense cloud that only extends over about $40\,\mu$m, whereas Fig. 5.4b shows dilute atoms that are distributed over the whole picture. In Fig. 5.4c, we present a reference picture of a K0 cloud before transfer, with a BEC fraction of $\beta \approx 0.5$. The comparison of these images strongly supports our interpretation that the two different frequencies correspond to the resonance frequencies of the two components of the partial BEC.

In summary, our observations showed that the spectra for the ThC and the non-condensed part of the pBEC sample are consistent with a theoretical description of the Fermi polaron and with our previous measurements on the Fermi polaron with fermionic impurities [Koh12]. In contrast, the condensed part of the partial BEC, which has a very large concentration of K atoms, with $\mathcal{C}_{\mathrm{K0}} \approx 36$, showed a much smaller energy shift that seems unrelated to the Fermi polaron. In the next Section a closer look to the behavior of the condensate part is presented.

5.4 BOSE POLARONS

In this Section, the additional energy branch emerging in the polaron spectrum in the pBEC regime is investigated.

In order to explore this, we took a set of spectra for impurity concentration values in the range $0 < \mathcal{C}_{\mathrm{K0}} < 45$ in the pBEC regime, at an interaction strength $X = -0.6(1)$[2]. We varied this concentration by changing various parameters, such as the loading time and the evaporation endpoint in our preparation sequence, as described

[2]The uncertainty denotes the standard deviation that characterizes typical experimental fluctuations.

in Section 5.2.2. Since only a fraction of the atoms in K0 is transferred, and only atoms in K1 interact with the FS, the interacting impurity concentration $\mathcal{C}_{\mathrm{K1}}$ is the relevant parameter. This, however, could not be directly inferred because of our incomplete knowledge of interaction effects on the spatial distribution during the RF pulse. We therefore introduce estimated concentrations, obtained by multiplying the concentration of the non interacting impurities, K0, by the estimated transferred fraction at the resonance frequency. In this way we define two concentrations:

$$\tilde{\mathcal{C}}_{\mathrm{K1,p}} = \mathcal{C}_{\mathrm{K0}} \times \frac{\tilde{A}_{\mathrm{p}} + \tilde{A}_{\mathrm{bg}}}{1-\beta} \qquad \text{and} \qquad \tilde{\mathcal{C}}_{\mathrm{K1,BEC}} = \mathcal{C}_{\mathrm{K0}} \times \frac{\tilde{A}_{\mathrm{BEC}}}{\beta}, \tag{5.6}$$

for the non-condensed and the condensed component of the K atoms, respectively. The amplitudes $\tilde{A}_\alpha$ correspond to the fitting amplitudes, as discussed in Sec. 5.3.

The analysis of the density dependence of the thermal part will be the subject of Section 5.7. Here we use the results relative to the condensed part to discuss the additional energy branch that comes from the condensed fraction of the K atoms.

In Fig. 5.5, the position of the spectroscopic peak relative to this branch is shown as a function of the interacting impurity concentration $\tilde{\mathcal{C}}_{\mathrm{K1,BEC}}$. We observed a small but consistent energy shift of $\sim 0.04\epsilon_F$.

An estimation of this energy shift may be obtained in the framework of the Bose polaron physics considering the following arguments. First, since the three scattering lengths between the K atoms in the two spin states (a_{11}, a_{00} and a_{01}) differ by less than 0.3% (see Tab. 4.5), the energy shift must be attributed mostly to K-Li interactions. Second, since the density of the condensed part of the K atoms is much higher than the one of the Li atoms in the center of the trap (see x-axis of Fig. 5.5), the situation is reversed in the sense that one can now regard the Li atoms as impurities embedded in a BEC of K atoms. A suitable framework to analyze this is therefore the one

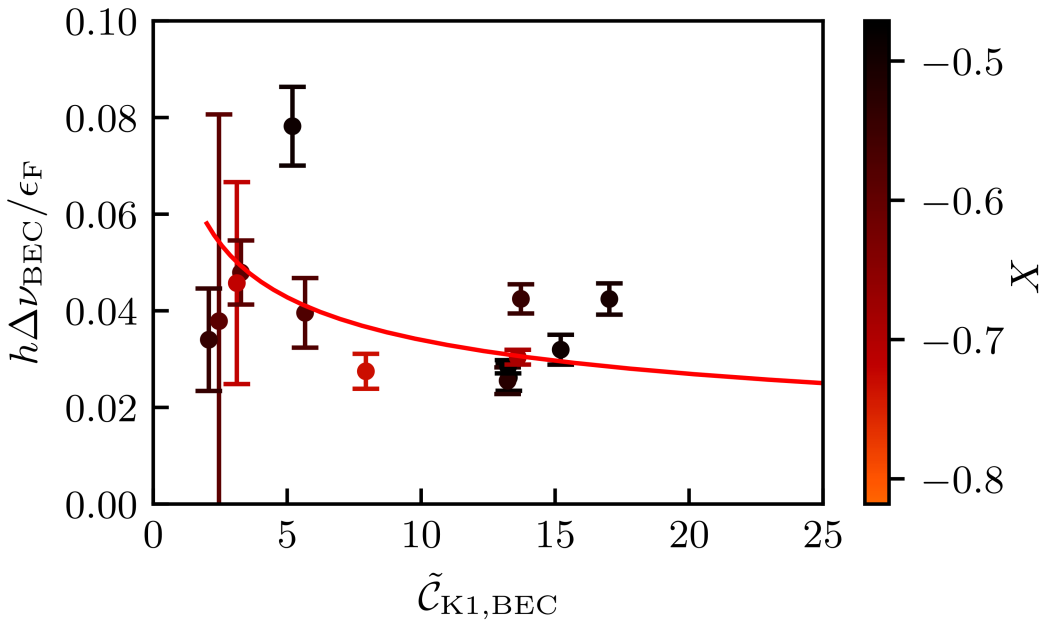

Figure 5.5: **Concentration dependence of the observed BEC peak position**. The color code refers to the interaction parameter X. A fit to the data of the theoretical prediction according to Eq. (5.11) is shown as the red solid line. The error bars of the data points represent the uncertainties of the fits. Adapted from Ref. [Fri21].

of Bose polarons formed by Li atoms in the K1 BEC, rather than the one of Fermi polarons. The total energy shift can therefore be estimated as

$$\Delta E_{tot} = N_{\mathrm{Li}} E_{\mathrm{Li}}, \tag{5.7}$$

where N_{Li} is the number of Li atoms inside the K1 BEC, and E_{Li} is the energy of a single Bose polaron. In the strongly interacting region on the BEC side of the resonance, a repulsive Bose polaron has a typical energy

$$E_{\mathrm{Li}} = \xi \epsilon_n, \tag{5.8}$$

where ξ is a constant of order unity [Hu16; Jør16; Peñ19; Yan20a; Sko21]. The energy

of the Bose gas, ϵ_n, is defined in analogy with the Fermi energy as

$$\epsilon_n = \hbar^2 \kappa_n^2 / (2m_{\mathrm{K}}), \tag{5.9}$$

with $\kappa_n = (6\pi \bar{n}_{\mathrm{K1,BEC}})^{1/3}$, so that

$$\epsilon_n / \epsilon_{\mathrm{F}} = (m_{\mathrm{Li}}/m_{\mathrm{K}})(\mathcal{C}_{\mathrm{K1,BEC}})^{2/3}. \tag{5.10}$$

The relevant concentration is the one of the K1 BEC that interacts with the Li atoms, which we approximated as $\mathcal{C}_{\mathrm{K1,BEC}} \approx \tilde{\mathcal{C}}_{\mathrm{K1,BEC}}$. Since via RF spectroscopy we measure the energy shift per atom transferred from K0 to K1, the relevant quantity is the energy shift per K atom in the K1 BEC, which is given by

$$\Delta E_{tot}/N_{\mathrm{K1,BEC}} = (6/41)(\tilde{\mathcal{C}}_{\mathrm{K1,BEC}})^{-1/3} \xi \epsilon_{\mathrm{F}}. \tag{5.11}$$

With ξ as the only free parameter, this equation can then be fitted to the experimental data, as reported in Fig. 5.5, yielding $\xi \approx 0.5$. The resulting curve, shown by the solid line, reasonably agrees with the experimental data. We should however mention a few caveats. First, the K1 BEC is only formed above a certain critical concentration, but the RF probe transfers the atoms gradually into the K1 state. This effect is further explored in Sec. 5.5. It follows that the observed behavior is presumably a result of an average BEC density experienced by the Li atoms during the RF probe. Second, the bosons and the fermions will eventually phase separate for the given interaction strength [Lou18b; Hua19], which also complicates the interpretation of the experiment. Nevertheless, the agreement between theory and experiment for a reasonable value of the fit parameter, $\xi \approx 0.5$, suggests that the observed shift of the BEC energy is, indeed, due to the formation of Bose polarons in the center of trap.

5.5 RABI OSCILLATIONS MEASUREMENTS

We further investigated the nature of the thermal and condensed parts of the K cloud by performing Rabi oscillation measurements, the results of which are shown in Fig. 5.6.

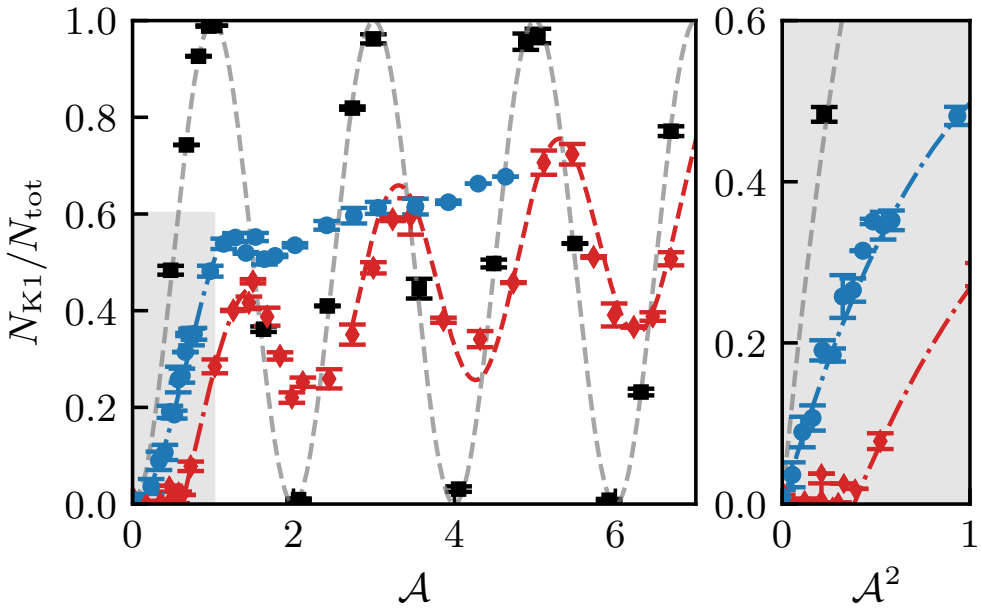

Figure 5.6: **Rabi oscillations measurements. Left:** We show the dependence of the transferred fraction on the pulse area, normalized to a 1-ms RF π-pulse in the non-interacting case $\mathcal{A} = \sqrt{P/P_\pi}$ (see text for details). The black squares show the Rabi oscillations of a non-interacting sample. The blue circles and red diamonds show the measurements conducted in the ThC and the pBEC regime at ν_p and ν_{BEC}, respectively. The gray and red dashed lines depict a $\sin^2$ oscillation at the non-interacting Rabi frequency, where the latter has a reduced amplitude by the factor β, corresponding to the BEC fraction. The blue and red dash-dotted curve show the initial transient of a $\sin^2$ oscillation with Rabi frequencies reduced by the interaction. **Right:** the region of weaker RF pulses, marked by the shaded area in the left panel, is plotted against the square of the pulse area $\mathcal{A}^2$. From Ref. [Fri21].

A 1-ms RF pulse was applied to transfer atoms from K0 into K1. The transferred

fraction of atoms was then measured as a function of the pulse area $\mathcal{A} = \sqrt{P/P_\pi}$, where the peak RF power P of our Blackman pulse was the experimentally controlled variable, and P_π was the corresponding power to achieve a π-pulse in the non-interacting case. First, we took a reference measurement without the presence of Li, that is for the bare K0 $\rightarrow$ K1 transitions. As we varied the RF power, we observed Rabi oscillations of the non-interacting sample (black squares in Fig. 5.6), which were well fitted with a $\sin^2$ function, as illustrated by the black dashed line.

After this, we prepared our atoms in the ThC at $X \approx -0.5$, and tuned the radio frequency to the polaron peak at ν_p (blue circles). We observed an initial increase in the signal that follows a $\sin^2$ behavior (dash-dotted blue line). For $\mathcal{A} \gtrsim 1$, this changed into a steady increase in the transferred fraction with no clear oscillations. We can explain this effect by the decay of the polaron to other states, such as molecules [Mas12]. Such states have a reduced overlap with the non-interacting state, and therefore the transfer probability from K0 to K1 is higher than the back transfer from the dressed molecular state to K0. This results in a growing population in K1 with increasing RF power.

When we prepared a pBEC sample and tuned the frequency of the RF pulse to ν_BEC (red diamonds), the system behaved in a very different way. In the region $\mathcal{A} \gtrsim 1$ of Fig. 5.6, we observed a clear oscillating behavior, depicted by the red dashed line. The frequency is the same as for the non-interacting case, but the amplitude is reduced by a factor that is close to the BEC fraction β. This is consistent with a BEC of K atoms oscillating between the K1 and K0 states, largely unaffected by the small concentration of Li atoms. The increasing background can be attributed to an off-resonant contribution originated from the non-condensed component.

A remarkable feature shows up in the behavior of the condensate for weak RF pulses. For $0 < \mathcal{A} \lesssim 1$, we found that the atom transfer is inhibited. In order to highlight this striking effect, in the right panel of Fig. 5.6 we plot the transferred

fraction in this region, marked by the shaded area in the left panel, as a function of $\mathcal{A}^2$. This representation turns an initial quadratic dependence on $\mathcal{A}$, typical for the coherent evolution of a quantum system, into a linear dependence on $\mathcal{A}^2$. Such a behavior is nicely visible in all three data sets. However the red diamonds show a transfer of the BEC only after a critical value of $\mathcal{A}^2 \approx 0.4$ is reached. This peculiar effect likely arises from a density-dependent shift of the resonance frequency. In the regime of low concentration, $\mathcal{C}_{\mathrm{K1}}$, the final state of the system is the Fermi polaron. This results in almost no transfer for small $\mathcal{A}$ in Fig. 5.6, since the detuning of the RF pulse to the polaron energy is about $4\Gamma_p$, where Γ_p is the spectral width of the polaron peak and the Fourier width of the RF pulse is $1/\tau_{\mathrm{RF}} \approx \Gamma_p$. On the other hand, when the RF pulse transfers enough atoms to create a K1 BEC, the resonance frequency shifts to the one determined by the Bose polarons and permits the transfer to start.

On top of this effect, as the BEC density increases in K1, phase separation may occur and fermions can be expelled from the spatial region occupied by the bosons [Lou18b; Hua19]. We estimated this effect to take place while the RF pulse is applied, since in our experiment there is no clear separation of the corresponding timescales. In this scenario, the two species will separate at an RF power that is high enough for a significant fraction of the BEC to be transferred. After this, the K cloud will exhibit Rabi oscillations similar to the non-interacting case.

The origin of the observed inhibition of Rabi oscillations of an RF-coupled BEC in the environment of a FS is an interesting many-body phenomenon and needs further investigation in future work.

5.6 LIFETIME OF REPULSIVE POLARON

The repulsive Fermi polaron is a metastable quasi-particle, which can decay via two- or three-body processes into lower energy states [Mas11; Mas14], as discussed in Chapter 3.2. In order to determine its lifetime, we performed measurements in the ThC regime for $X < 0$. The repulsive polaron was populated by applying a π-pulse with a duration $\tau = 0.3\,\mathrm{ms}$ (instead of the 1 ms used in all measurements shown before) and frequency detuning $\Delta\nu_\mathrm{p}$. In this way, we resonantly excited the quasi-particle with a short pulse in order to maximize the number of transferred atoms. After this excitation, about $\sim 50\%$ of the atoms were found to remain in K0. We therefore applied a $10\,\mu$s resonant "cleaning" light pulse to remove them from the trap, thus creating a pure sample of strongly interacting K1 and Li atoms. At this point, we waited for a variable time before applying another RF pulse, identical to the first one, which only addresses the polarons that have not yet decayed. In contrast to all measurements presented so far, the measured signal was now the fraction of atoms transferred back into the non-interacting state K0.

We fitted an exponential decay to the data sets obtained for various values of X, and extracted the $1/e$ decay time, τ_p, which represents the lifetime of the polaron. The blue circles in Fig. 5.7 show the repulsive polaron decay rate $\Gamma = 1/\tau_\mathrm{p}$ as a function of the interaction strength. Approaching the resonance, the decay rate rises from $10^{-3}\,\epsilon_\mathrm{F}/\hbar$, at $X \approx -1.5$, to about $10^{-2}\,\epsilon_\mathrm{F}/\hbar$, at $X \approx -0.2$. This corresponds to polaron lifetimes between $\sim 10\,\mathrm{ms}$ and $\sim 1\,\mathrm{ms}$, and is in excellent agreement with our previous experiments on Fermi polarons with fermionic impurities [Koh12].

The solid orange line in Fig. 5.7 is a theoretical prediction based on the assumption that the repulsive polaron decays via a two-body process into the attractive polaron, which due to its high kinetic energy can be approximated by a free particle. The dashed orange line gives, on the other hand, the three-body decay rate into the

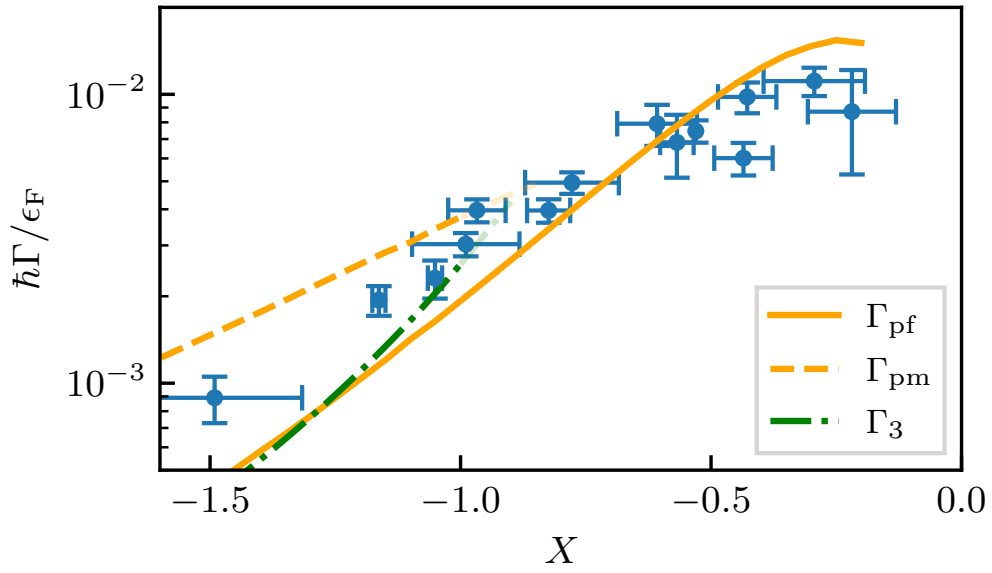

Figure 5.7: **Decay rate of the polaron for different interaction strengths X.** Blue circles depict the measured lifetimes of the polaron. The orange solid and dashed lines show theoretical calculations of the two- and three-body decay, respectively. The three-body recombination rate in vacuum is depicted by the green dash-dotted line. See Chapter. 3.2 for details. From Ref. [Fri21].

molecule, taking into account bath effects in the perturbative regime. Finally, the green dash-dotted line shows the three-body decay rate in a vacuum for a broad resonance [Pet03], adapted here to describe a narrow resonance. For details on the calculations of these rates, see Chapter 3.2.2. By comparing these theory lines with the experimental data, we see that two-body decay into the attractive polaron seems to be the main loss channel for strong interactions. However, for weaker interactions the attractive polaron is ill-defined, due to the smallness of its residue, and decays into the molecular states. In this regime, three-body decay processes become dominant. This is consistent with the observations for the case of fermionic impurities [Koh12; Sca17].

In addition we observed a residual signal remaining in K1 after the second RF

pulse, which transfers the repulsive polarons into K0. It consists of remaining polarons and their decay products. In order to investigate the nature of the residual component, we let the polaron decay for a variable time t, and then we performed ejection spectroscopy. In contrast to the measurement described so far, we varied the frequency of the second RF pulse, which transfers K1 atoms back to K0.

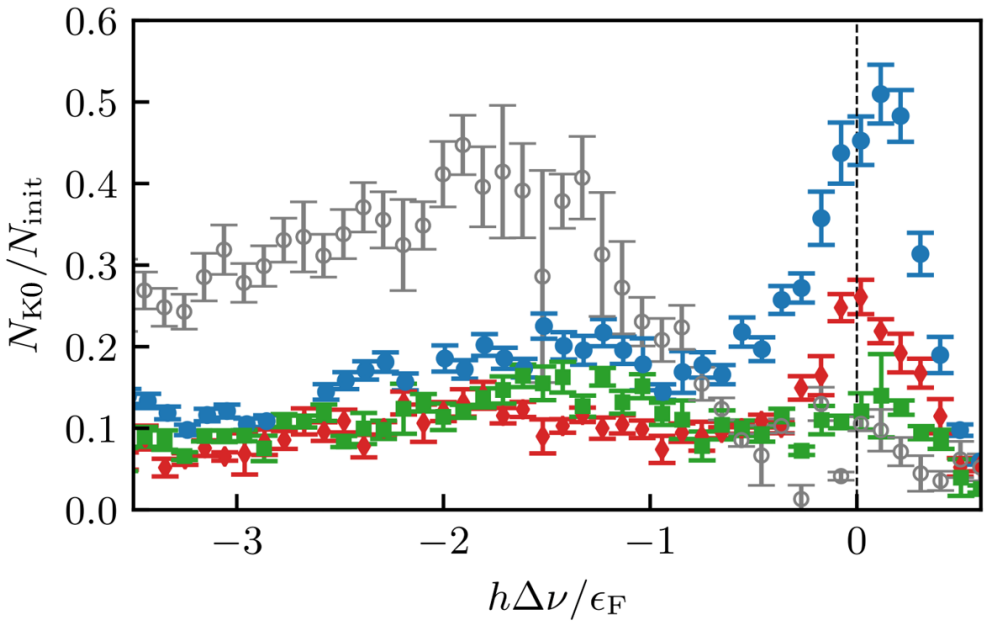

Figure 5.8: **Ejection spectra of the repulsive polaron and its decay products.** We show the fraction of atoms transferred from K1 to K0 as a function of the applied RF signal at $X = -0.80(2)$. The blue circles, red diamonds, and green squares show the spectrum after a waiting time of 1.2 ms, 2.2 ms, 5.2 ms. These three measurements are normalized to the total atom number of the measurements with the shortest wait time (blue circles). As a comparison, a molecule dissociation spectrum (gray empty circles) is also presented. Adapted from Ref. [Fri21].

In Fig. 5.8, we show such measurements for three waiting times, $t_1 = 1.2\,\mathrm{ms}$, $t_2 = 2.2\,\mathrm{ms}$, and $t_3 = 5.2\,\mathrm{ms}$, all taken at the same interaction strength $X = -0.80(2)$. We show the transferred fraction N_{K0}/N_{init} relative to the total atom number $N_{\mathrm{init}} = N_{\mathrm{K1}}(t_1) + N_{\mathrm{K0}}(t_1)$ after a wait time of t_1. The blue circles, red dia-

monds, and green squares represent the ejection spectra recorded after waiting times of t_1, t_2, and t_3, respectively. We expected the decay product consisting of molecules, since this is the predicted ground state for $X = -0.80$. In order to check this, we compared the ejection spectra with a molecule dissociation spectrum, shown by the gray open circles in Fig. 5.8. To obtain this spectrum, we started with a ThC sample in the non-interacting state K0. Then we associated molecules by applying a 3π pulse bringing the atoms in K0 to K1 at a frequency adjusted such that it corresponds to the binding energy of the molecule at $X = -0.80$. Since we did not transfer all K0 atoms into the molecular state, we applied a resonant "cleaning" light pulse, which removes the remaining atoms from the trap. Therefore we obtained a mixed sample of Li-K1 molecules and bare Li atoms. Then we performed ejection spectroscopy to probe the molecular spectrum. This was achieved by applying another 3π pulse, at different frequencies, to dissociate the molecules. Note that this particular spectrum is normalized to its own total atom number $N_{\mathrm{init}} = N_{\mathrm{tot}}$.

Let us now compare the four ejection spectra presented in Fig. 5.8. In the measurement relative to the shortest waiting time (blue circles), we recognize a narrow peak at positive energies, which we identify as the repulsive polaron. The broad pedestal at negative energies, on the other hand, reflects the response of the molecules, as we can infer from the similarity with the bare molecular spectrum. By increasing the waiting time from t_1 to t_2, and then to t_3, we observe a decrease of transferred atoms at the repulsive polaron frequency, as a consequence of its decay.

Given that the polarons decay into molecules, we would have expected a corresponding increase in their spectral signal, i.e. the broad pedestal, as reported in the Supplemental Material of [Koh12] for the Li-K FF mixture. This was however not observed. Instead, as the waiting time of the measurements in Fig. 5.8 is increased from t_1 to t_3, we saw a reduction of K atoms in the trap by a factor of ~ 2, while the broad pedestal was unchanged. From this, and the measurements presented in Fig. 5.7,

we speculated that the repulsive polarons decay into molecules, which themselves undergo relatively fast collisional decay into lower lying molecular states, where the excess energy of the latter is sufficient to remove the atoms from the trap. We believe that Fermi-Bose dimers are less robust against collisions, as compared to Fermi-Fermi dimers, for which we have demonstrated a Pauli suppression effect in Ref. [Jag16].

5.7 FIRST ATTEMPT TO OBSERVE THE MEDIATED POLARON-POLARON INTERACTION

On a general ground, by increasing the concentration of the impurities, these can start to interact, and such interactions should manifest themselves as a change in the polaron energy as a function of the impurity concentration, as discussed in see Chapter 3.3. Here we present our first attempt of observing such phenomena. In particular, we discuss the behavior of the thermal part of the K cloud in the pBEC regime, for different interacting impurity concentration $\tilde{\mathcal{C}}_{\mathrm{K1,p}}$, as defined in Eq. (5.6). The data were taken from the same measurements presented in Section 5.4.

In Fig. 5.9, we show our results regarding the density variation of the energy of the repulsive polaron. The color scale indicates the particular values of the interaction parameter X for each data point. In Chapter 3.3, we discussed how the Fermi liquid theory leads to an effective interaction between the polarons mediated by the Fermi gas. Here we recall the main results, which we will use to understand our experimental observations. According to this theory, the energy shift per impurity, taking into account the concentration average due to the RF transfer, is given by Eq. (3.28):

$$\Delta E = E_{\downarrow} - \frac{1}{3}(\Delta N)^2\,\mathcal{C}_{\mathrm{K1}}\,E_F + \frac{g_1 n_1}{2}, \tag{3.28}$$

The theory lines in Fig. 5.9 were obtained from this equation: The solid and dashed lines correspond to an interaction strength of $X = -0.6$ and $\pm$ its standard exper-

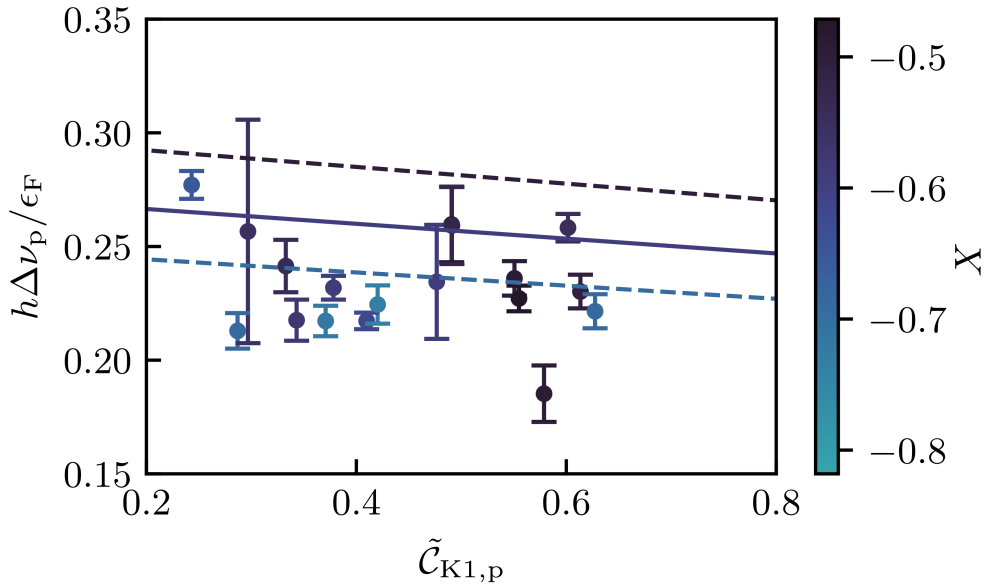

Figure 5.9: **Concentration dependence of the energy of the repulsive Fermi polaron.** The color code refers to the interaction strength X. The solid and dashed lines show the theoretical predictions including polaron-polaron interactions, according to Eq. (3.28), for the mean value and its standard deviation of $X = -0.6 \pm 0.1$. Adapted from Ref. [Fri21].

imental deviation of 0.1. We note that, due to the small value of the scattering length a_{11} between the atoms in K1 (see Tab. 4.5), the negative slope of these lines is essentially only due to the mediated interaction. From Fig. 5.9, we see that our experimental observations are consistent with the predicted concentration dependence of the polaron energy. In particular, the polaron energy extracted from our measurements is smaller than the predicted energy in the single impurity case. The mean temperature of the measurements presented is $T/T_\mathrm{F} = 0.17(2)$, so that we expected the result to be fairly close to the zero-temperature limit assumed by the theory.

Given the large fluctuations in the data, and the theoretical predicted small influence of the effective interaction, we could not provide conclusive evidence of presence of this effect from the measurements presented in this Chapter. However, these gave

a hint that such effect is observable in our experiment, and in Chapter 6 more systematic measurements leading to its observation are discussed.

5.8 CONCLUSIONS

In this Chapter, we presented the first observations concerning the Fermi polaron with bosonic impurities. We explored the case of high densities below and above the threshold for Bose-Einstein condensation of the impurity cloud, and found very different behaviors. For a thermal impurity cloud, we probed the energy of the attractive and the repulsive quasi-particle branches across the strongly interacting regime, and found properties similar to those of the previously investigated FF system. Our observations are, within the experimental uncertainties, fully consistent with the single-impurity theoretical predictions, despite the fact that the impurity concentration is near unity.

We investigated the spectral response of a partially condensed cloud of impurities, and observed a drastic change on its energy spectrum. We found that, in addition to the signature of the repulsive and attractive polaron, a new branch, the BEC branch, emerges in the spectrum, which shows no sign of the Fermi polaron anymore. Instead, we found a small positive shift in energy over a wide range of interactions. We speculated that, since the impurity concentration far exceeds unity, this effect may be explained by an interchange of the role of the two atomic species, where the BEC and the FS represent now the environment and the impurities, respectively. Such a scenario is usually described in terms of Bose polarons [Hu16; Jør16]. This suggests that the Fermi and the Bose polaron appear as different branches of one spectrum.

We dedicated particular attention to the region of positive scattering lengths, where the repulsive Fermi polaron is realized. As we varied the concentration, the energy shift of the condensed component of the partial BEC remained small and positive.

We found good qualitative agreement with a Bose polaron description, where the back action of the Bose polarons on the bath results in a small, but clearly observable energy shift.

In order to gain further insight into the transitional behavior from low to high concentration, we varied the strength of the spectroscopy pulse that transfers the partial BEC into a state which is strongly interacting with the fermionic bath. For low pulse strengths, we observed a peculiar interaction-induced inhibition of the transfer, whereas for high pulse strengths we essentially recovered the behavior of a non-interacting cloud. This striking result suggests a shift of the resonance frequency with varying concentration, which supports our interpretation of a transition of our mixture between regimes governed by two fundamental quasi-particles, the Fermi and the Bose polaron.

In order to further characterize the metastable repulsive Fermi polaron, we measured its decay rate, and compared it to theoretical predictions of different decay channels. Our observations close to the center of the FR are in very good agreement with two-body scattering processes, in which the repulsive polaron decays into a bare particle. Furthermore, we found qualitative agreement between the measured decay rates for moderate interactions and our theoretical calculations of three-body decay.

As we closer investigated the concentration dependence of the thermal component of the partial BEC at strong repulsive interactions, our results indicate a slightly smaller energy of the Fermi polaron with respect to what expected from a single-impurity prediction. The experimental uncertainty in the determination of the interaction strength, which is very sensitive to magnetic field fluctuations, rendered a qualitative analysis impossible. However, theoretical calculations, including polaron-polaron interaction, predict a decreasing energy shift with increasing concentration, which is consistent with our experimental data. This suggests that interaction effects amongst polarons could be observed in more precise measurements, which we have conducted

and will be the subject of Chapter 6.

Our capability of creating a partial BEC, which strongly interacts with a surrounding FS, allows us to investigate the behavior of vastly different concentration regimes in the same setup. Future measurements focused on the transition between the two fundamentally different polarons could shed light on the largely unknown physics beyond the single quasi-particle picture, where polaron-polaron interactions play a significant role.

CHAPTER

OBSERVATION OF THE MEDIATED POLARON-POLARON INTERACTION 6

Motivated by the preliminary results on the mediated polaron-polaron interaction presented in Chapter 5.7, we further investigated this phenomenon. The results of this work led to the publication manuscript (in the final stage of preparation at time of submission of the present Thesis) in Ref. [Bar23].

Convinced that the main limitation to this observation was the fluctuation in the interaction parameter X (defined in Eq. 2.15), we put effort in knowing with better accuracy and precision our magnetic field. Moreover we put additional care in keeping all the other experimental parameter, such as temperature and Fermi energy of the Fermi sea (FS), as constant as possible, in order to be able to consider the impurity concentration as the only varied parameter for each set of measurements relative to the value of a given interaction parameter. These efforts, summarized later in Tab. 6.1 and Tab. 6.2, brought to the first observation of the mediated polaron-polaron interaction, and of its sign inversion due to the impurity statistics, in an ultracold atoms system.

In this Chapter, I will describe the radio frequency spectroscopy measurements that we performed in order to observe the mediated polaron-polaron interaction. In these measurements we exploited the strictly similarity of the two different ultracold mixtures of Li and K realisable in our experiment: the Fermi-Bose (FB) mixture of ^{6}Li and ^{41}K, and the Fermi-Fermi (FF) mixture of ^{6}Li and ^{40}K.

This Chapter is organized as follows. After an introduction, in which I will quickly revise the Landau theory for the mediated polaron-polaron interaction, in Section 6.1, I will introduce some technical details, in Section 6.2. In particular I will describe the preparation of the samples, their detection and their characterization, and I will list some relevant quantities for our experiments. After this technical introduction, in Section 6.3 I will describe our experiments, and compare our results with both Landau's Fermi liquid theory and a new model, developed by our theory collaborators in the context of the work presented in this Chapter.

6.1 INTRODUCTION

The main motivation of our experimental work was to test the validity of Landau's Fermi liquid prediction of the mediated polaron-polaron interaction for increasing impurity concentration C, and variable interaction strength X (see Chapter 3.3.1). Indeed, for large impurity concentrations the underlying physics changes in the regime $\mathcal{C} \approx 1$ to nearly balanced FB [Fra10; Lud11; Yu11] and FF [Gub13; Pin21] mixtures, and in the extreme limit $\mathcal{C} \to \infty$ the roles of the impurity and the bath are reversed [Fri21]. Furthermore, in the strongly interacting regime, the approach of considering interacting polarons becomes questionable as their particle character, quantified by the quasi-particle residue, vanishes (see Chapter 3.2), and incoherent excitations dominate.

In particular we were aimed to determine the magnitude of the challenging weak predicted polaron energy shift due to the mediated polaron-polaron interaction and its linearity with increasing impurity concentration. On a qualitative level, we tested the predicted independence of the sign of the energy shift for attractive and repulsive interspecies interaction, and its sign reversal with impurity quantum statistics. The confirmation of the predicted behaviour of the sign is an essential test for the validity of the Fermi-liquid approach, as discussed in Ref. [Yu12].

As described in Chapter 3, when an impurity is immersed in a bath with which it interacts, it forms a quasi-particle named polaron. In the case of several impurities, the created polarons can interact between each others, and the physics become richer and more complicated. A textbook example of the novelty that such interactions can bring is the phenomenon of superconductivity, generated by the attractive polaron-polaron interaction. Despite the large range of control that ultracold gases experiments provide, the mediated polaron-polaron interaction was not yet observed in such systems: In Refs. [Sch09; Sca17], this effect was masked by the fact that the impurities were degenerate [Gir12], while in our previous work Refs. [Cet16; Fri21], only hints of such effect were visible.

In the framework of Landau Fermi liquid theory, a $\downarrow$ impurity interacting with a degenerate FS of $\uparrow$ particles forms a Fermi polaron. The energy of such a quasi-particle is proportional to the Fermi energy E_F of the FS, and depends on the strength of the interaction between the impurity and the particles in the fermionic bath. The normalized energy $E_\downarrow/E_\mathrm{F}$ of a single polaron can then be expressed by a universal function $\mathcal{E}_\downarrow(X)$ [Che06b; Lob06; Com07; Com08; Pro08; Mas11; Tre12; Sch18], which has been widely studied in previous experiments [Sch09; Koh12; Sca17; Yan19; Fri21].

By increasing the concentration of the impurities, more polarons are formed and they can interact with each other via the bath. This mediated polaron-polaron interaction leads to a shift in the polaron energy with respect to the single impur-

ity case, which depends on the impurity concentration $\mathcal{C} = n_\downarrow/n_\uparrow$, as discussed in Chapter 3.3.1.

Taking these two energy contributions into account, and restricting the consideration to low concentrations $\mathcal{C} \ll 1$, the energy to add an impurity atom to the system, which we define as ΔE_p, can be expressed, after normalization to E_F, in terms of two universal functions [Fri21; Yu12; Sca22][1]:

$$\frac{\Delta E_\mathrm{p}(X, \mathcal{C})}{E_\mathrm{F}} = \mathcal{E}_\downarrow(X) + \mathcal{E}'_{\downarrow\downarrow}(X)\,\mathcal{C}. \tag{6.1}$$

While the first term represents the single-impurity limit, the second term accounts for interactions between polarons mediated by particles of the FS. This term is linear in the impurity concentration $\mathcal{C}$, and depends on X via an *interaction coefficient*, represented by the function

$$\mathcal{E}'_{\downarrow\downarrow}(X) = \mp\frac{2}{3}\Delta N^2(X), \tag{6.2}$$

where $\Delta N(X)$ is the number of bath particles in the dressing cloud of the impurity, as defined in Chapter 3.3.1. The $-$ $(+)$ sign corresponds to bosonic (fermionic) impurities: Ref. [Yu12] predicts the mediated polaron-polaron interaction to be attractive for bosonic and repulsive for fermionic impurities, the latter arising from an effective repulsion resulting from Pauli blocking effects.

In Fig. 6.1 we illustrate the interaction dependence of the polaron energy according to Eq. (6.1) for three exemplary cases: single impurity (dashed black line), and finite concentration for bosonic (green solid line) and fermionic (orange solid line) impurities

[1] Note that this is equivalent to Eq. (3.28), normalized to the Fermi energy. There is however a slight difference in describing the mediated interaction term Eq. (6.2). As it will be clear later in the text, this difference arises because here we consider the effect of the RF transfer in defining the experimental obtained concentration, while, in Eq. (3.28), this effect was taken into account into the theory.

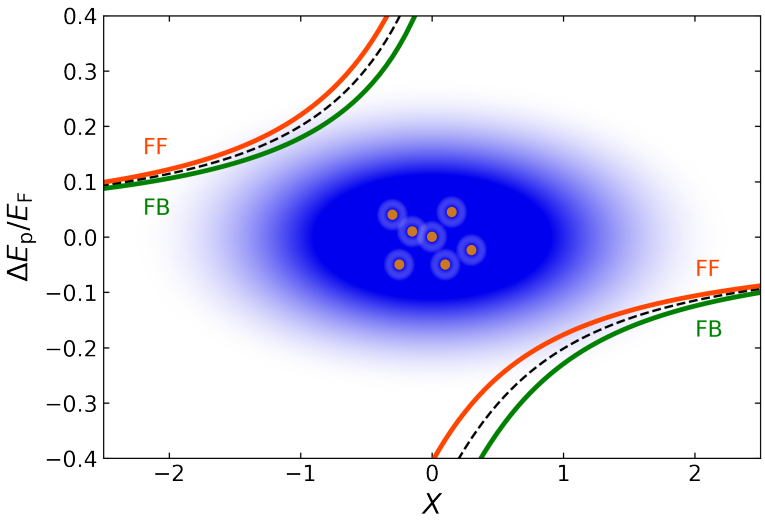

Figure 6.1: **Polaron energy shift including mediated interactions**. Polaron energy branches as a function of the dimensionless interaction parameter X, according to Eq. (6.1) in the limit of a single impurity (black dashed lines), and for finite concentration for Fermi-Bose (FB, solid green lines) and Fermi-Fermi (FF, solid orange lines) Li-K mixture. Note that, for illustrating the weak mediated interaction, we have exaggerated the effect by choosing $\mathcal{C} = 0.5$, while the underlying model is strictly valid only for $\mathcal{C} \ll 1$.

in a FS. The figure also highlights that the mediated interaction effect (exaggerated by choosing a large concentration of $\mathcal{C} = 0.5$) is rather weak, which makes its observation very challenging in a real experiment.

6.2 TECHNICAL DETAILS

For the measurements presented in this Chapter, we use either a FB mixure of ^{6}Li and ^{41}K, or a FF mixture of ^{6}Li and ^{40}K. The interparticle interactions between the two species are tuned thanks to a FR centered at $B_0 = 335.080(1)$ G in the FB case, and at $B_0 = 154.7126(5)$ G in the FF case. For the details on these FRs, the reader can look back at Chapter 4.4.2.

The possibility to change the impurity from bosonic to fermionic, while keeping all the other features almost identical, was a key ingredient in our system, allowing for a direct observation of the effect of the impurity statistics in the polaron problem. Moreover, we benefited from the Li-K mass imbalance, which allowed to prepare a system with high impurity concentration where the fermionic bath was degenerate, while the impurities were kept in the thermal regime. Indeed, we think that the fact that the impurities were thermal was a major feature in observing the mediated polaron-polaron interaction, allowing to neglect the effects due to the impurity degeneracy [Gir12; Sch09; Sca17]. Another advantage of mixed-species system was that the FS represented a nearly homogeneous environment for the impurities. This was due to the fact that the K cloud was located at the center of the trap and its size was much smaller than the spatial extent of the Li cloud because of the Fermi pressure acting on the Li atoms and the optical potential being about two times deeper for K [Koh12]. This allowed to treat our impurities as embedded in a FS with nearly constant chemical potential. See Chapter 4 for further details.

6.2.1 Spin states

In the following, we use the convention on naming the spin states introduced in Chapter 4.2. For the RF spectroscopic measurements, the ^{6}Li atoms forming the spin-polarized Fermi sea were always kept in the lowest hyperfine spin state $F, m_F = (1/2, +1/2)$, simply named Li. As the starting point for the measurements, the K atoms were prepared in an 'ancillary' state $\mathrm{K_{anc}}$, which for ^{41}K corresponds to the third-lowest spin state $(1, +1)$ and for ^{40}K to the lowest state $(9/2, -9/2)$. In our spectroscopic injection scheme, the initial state K0 is represented by the state (1, 0) for ^{41}K and by the state $(9/2, -7/2)$ for ^{40}K. The final Feshbach-resonant state K1 corresponds to $(1, +1)$ for ^{41}K and to the state $(9/2, -5/2)$ for ^{40}K.

6.2.2 Sample preparation and characterization

We prepared our samples as described in Chapter 4.4.1. In particular our Li and K atoms were trapped in a 1064 nm crossed optical dipole trap with averaged trap frequencies of 117 Hz for ^{41}K and 193 Hz for Li (FB mixture), and 158 Hz for ^{40}K and 271 Hz for Li (FF mixture).

After evaporative cooling, in order to obtain a fully polarized sample of Li in the $(1/2, 1/2)$ state, we removed the atoms in the second spin state by applying a resonant 10-μs light pulse at 567 G (1180 G) in the FB (FF) case. Then the magnetic field was ramped close to the FR of interest, near 335 G for the BF mixture, and 155 G for the FF mixture. The trap contained a thermalized sample of roughly 10^5 Li atoms in the lowest hyperfine spin state, and 10^4 K atoms in the K_{anc} state.

In order to vary the impurity concentration in the initial spectroscopy state K0, we transferred the desired amount of atoms from the ancillary state K_{anc} to K0 using a RF pulse. In this way, keeping the total number of K atoms constant in the cooling process, we ensured identical starting conditions for measurements with variable impurity concentration. Note that this is different from what we did in the experiment described in Chapter 5.7, where the impurity concentration was varied mainly by changing the loading time and the evaporation endpoint in our preparation sequence.

After the experimental cycle, we switch off the cross optical dipole trap and let the atomic cloud expand for a typical time of 1 ms after which we detect the atoms by using state-selective absorption imaging. In the case of the FB mixture we can image K0 and K1 directly, using nearly closed optical transitions. In the FF case, however, because of the larger hyperfine structure of ^{40}K in combination with the lower magnetic field, optical transitions for the detection of K0 and K1 are leaky, which compromises the signal-to-noise ratio. Here, we applied a resonant light pulse

in order to remove K1 in 10 μs and applied a 96-μs RF π-pulse transferring atoms from K0 to K_{anc}, which permits imaging via a closed optical transition. In this way, we derived our spectroscopic signal from atoms remaining in K0. For the FB case, to facilitate a direct comparison, we also defined the corresponding spectroscopic signal based on atoms remaining in K0.

The temperature T of the samples was 102 – 137 nK in the FB case, and 190 – 285 nK in the FF case. At these temperatures, the FS was deeply degenerate with $T/T_F \approx 0.14$ (FB) and $T/T_F \approx 0.24$ (FF). The K impurities, instead, remained in the thermal regime.

We determined the temperature of the mixture by ballistic expansion of the thermal K cloud after releasing it from the trap, both in the FB and FF cases. The Fermi energy of the Li cloud and the concentration of the non-interacting impurities were obtained from separate measurements in which we recorded the distributions of the Li and K atoms with the same initial conditions as in the actual polaron measurement. These additional measurements were performed before each main polaron measurement was performed. Typical values of the effective Li density, effective Fermi energy, and reduced temperature were similar for the two mixtures and are reported in Tab. 6.3.

6.2.3 Interaction tuning

We exploit the extraordinary similarity between the FRs in the FB and the FF mixtures discussed in Chapter 4.4.2. The only main difference between these two FRs is their center B_0: in the FB case $B_0 = 335.080(1)$ G, and in the FF case $B_0 = 154.7126(5)$ G.

For both K isotopes in the initial spectroscopy state K0 and the ancillary state K_{anc}, the interaction with the FS remains weak (see Tab. 4.4). This is just enough

for thermalization with the bath in the sympathetic cooling process, but for the spectroscopic scheme this background interaction is fully negligible.

We further note that the weak intraspecies interaction between ^{41}K bosons is characterized by s-wave scattering lengths of about $61\,a_0$ between all the spin states considered [Lys10]; the ^{40}K fermions are characterized by intraspecies scattering lengths of about $170\,a_0$ between different spin states [Lud12] and the interaction between atoms with identical spin states is suppressed due to Pauli exclusion principle (see Tab. 4.5).

6.2.4 Data selection and relevant parameters

In this Section, we discuss how we selected the data presented in this Chapter, and give an overview of typical values for the most relevant experimental parameters obtained in the two mixtures.

We investigated the influence of impurity concentration on the polaron energy for different values of the interaction strength between the impurity and the bath. In order to so, we performed measurements varying the impurity concentration at given values of the magnetic field close to the FR. We took measurements in a range of about $\pm 35\,$mG around the FR centre. This implies that we needed knowledge of our magnetic field on the level of a mG. The main limitation in our system was given by slow drifts in the magnetic field during the measurements. In order to deal with these drifts, we performed magnetic field calibrations before and after each measurement was recorded, and we rejected measurements for which the difference of these two values was larger than $2\,$mG ($1\,$mG) for FB (FF). We thus obtained a large set of measurements, for different magnetic fields and different impurity concentrations. We grouped these measurements in subsets according to the X value obtained from the averaged value of the magnetic field before and after the measurement and the

effective Fermi energy of the FS, extracted before each measurements as discussed in Section 6.2.2. In addition to the effective Fermi energy, before each measurement we also determined the temperature of the sample (Section 6.2.2). While we could measure these parameters, we didn't have precise control over them. Thus, in order to keep the comparison in each subset easier, and to consider the impurity concentration the only parameter varied, each subset contains only post selected measurements that show small variance of these parameters. In Tab. 6.1 and Tab. 6.2 we report the averaged values of some important parameters and their respective standard errors obtained in each subset, which in average contains 9 (7) measurements for the FB (FF) case. In total, the data acquisition took almost one full year of constant measurements[2].

Table 6.1: **Experimental parameters for the FB mixture.** The average values of the interaction parameter X, the effective Fermi energy (in kHz), the temperature (both in nK and in unit of T_F), the dimensionless range parameter, and their respective standard errors are reported for each set of measurements corresponding to different X values in the FB case.

X	err X	ϵ_F/h (kHz)	err ϵ_F/h (kHz)	T (nK)	err T (nK)	T/T_F	err T/T_F	$k_F R^*$	err $k_F R^*$
-2.066	0.004	17.77	0.05	116.5	0.7	0.137	0.001	0.545	0.001
-1.449	0.004	16.64	0.06	137.0	0.1	0.172	0.001	0.527	0.001
-1.11	0.013	15.99	0.16	124.1	0.1	0.162	0.002	0.517	0.003
-1.047	0.006	17.33	0.07	116.8	0.9	0.14	0.001	0.538	0.001
-0.902	0.008	16.79	0.24	118.7	1.5	0.148	0.002	0.529	0.004
-0.716	0.011	17.63	0.09	111.2	1.5	0.132	0.002	0.543	0.001
-0.539	0.012	16.67	0.05	129.4	0.5	0.162	0.001	0.528	0.001
-0.443	0.007	17.14	0.09	118.9	0.8	0.145	0.001	0.535	0.001

[2]This long time for the data acquisition was also due to the degrading performance of our current oven.

-0.363	0.008	17.54	0.05	117.3	0.3	0.139	0.0	0.541	0.001
-0.177	0.005	17.51	0.11	131.7	1.6	0.157	0.001	0.541	0.002
0.165	0.006	17.68	0.19	107.1	2.8	0.126	0.002	0.543	0.003
0.337	0.009	17.58	0.08	118.0	0.8	0.14	0.001	0.542	0.001
0.568	0.012	16.17	0.12	124.4	1.8	0.16	0.003	0.52	0.002
0.615	0.006	18.18	0.1	116.0	0.1	0.133	0.001	0.551	0.002
0.731	0.007	17.66	0.07	112.9	0.9	0.133	0.001	0.543	0.001
0.985	0.006	18.01	0.07	117.0	0.5	0.135	0.001	0.548	0.001
1.502	0.019	16.92	0.22	111.8	0.1	0.138	0.002	0.531	0.003
1.878	0.012	16.82	0.13	114.7	1.3	0.142	0.001	0.53	0.002

Table 6.2: **Experimental parameters for the FF mixture.** The average values of the interaction parameter X, the effective Fermi energy ϵ_F/h (in kHz), the temperature T (both in nK and in unit of T_F), the dimensionless range parameter $k_F R^*$, and their respective standard errors are reported for each set of measurements corresponding to different X values in the FF case.

X	err X	ϵ_F/h (kHz)	err ϵ_F/h (kHz)	T (nK)	err T (nK)	T/T_F	err T/T_F	$k_F R^*$	err $k_F R^*$
-1.997	0.008	21.33	0.05	265.7	1.7	0.26	0.002	0.64	0.001
-1.866	0.006	19.01	0.09	226.1	0.1	0.248	0.001	0.605	0.001
-1.626	0.016	23.34	0.41	246.9	1.9	0.221	0.005	0.67	0.006
-1.489	0.014	19.24	0.24	209.4	1.7	0.227	0.004	0.608	0.004
-1.412	0.012	20.58	0.21	272.9	2.9	0.276	0.005	0.629	0.003
-1.234	0.016	24.91	0.61	233.7	10.8	0.196	0.011	0.692	0.008
-1.241	0.012	21.44	0.34	236.1	0.4	0.23	0.004	0.642	0.005
-0.964	0.003	19.45	0.26	223.1	4.0	0.239	0.006	0.611	0.004
-0.922	0.007	20.08	0.33	223.7	3.0	0.233	0.005	0.621	0.005
-0.65	0.005	20.79	0.35	217.2	5.1	0.218	0.005	0.632	0.005

-0.446	0.014	20.3	0.42	229.1	4.6	0.236	0.01	0.625	0.007
0.468	0.011	20.79	0.2	260.8	1.3	0.262	0.001	0.632	0.003
0.58	0.005	20.95	0.41	235.3	0.8	0.235	0.004	0.635	0.006
0.796	0.013	21.08	0.49	229.2	4.6	0.227	0.002	0.636	0.007
1.084	0.014	20.91	0.66	233.1	6.7	0.233	0.009	0.634	0.01
1.129	0.012	19.21	0.27	227.0	5.9	0.247	0.01	0.608	0.004
1.335	0.014	19.46	0.4	235.0	0.9	0.252	0.005	0.612	0.006
1.487	0.003	20.22	0.08	259.2	0.1	0.267	0.001	0.624	0.001
1.614	0.011	19.63	0.23	225.4	1.3	0.24	0.003	0.614	0.004
1.793	0.007	22.7	0.17	240.9	2.2	0.221	0.003	0.661	0.002
2.046	0.013	18.66	0.25	200.7	4.2	0.224	0.002	0.599	0.004

To summarize these results, in Tab. 6.3, we report the effective Fermi energy ϵ_{F} of the FS, the dimensionless parameter $k_{\mathrm{F}}R^*$, the temperature, both in nK, T, and in unit of Fermi temperature of the FS, T/T_{F}, the K-averaged density of the Li FS, $\bar{n}_{\mathrm{Li}}$, and the concentration of the interacting impurities of K1, $\tilde{\mathcal{C}}$ (see Eq. (6.3) further in the text for the experimental definition of this quantity) for the two mixtures. These values are obtained from averaging over all the measurements presented in this Chapter.

Table 6.3: **Relevant parameters**. Comparison of important parameters in the two mixtures. The errors represent the standard errors.

	ϵ_{F}/h (kHz)	$k_F R^*$	T (nK)	T/T_{F}	$\bar{n}_{\mathrm{Li}}$ (10^{12} cm^{-3})	$\tilde{\mathcal{C}}$
FB	17.3(1)	0.537(1)	102 - 137	0.144(1)	1.48(1)	0.01 - 0.23
FF	20.3(1)	0.624(2)	190 - 285	0.237(2)	2.24(5)	0.01 - 0.20

6.3 EXPERIMENTAL OBSERVATION OF THE MEDIATED POLARON-POLARON INTERACTION

The basic idea of our probing method, which has been introduced in previous Chapter 2.2.2, is an injection scheme, based on the radio frequency (RF) transfer from an impurity spin state K0 to a state K1. The initial state K0 interacted only weakly with the bath, and we considered it effectively non-interacting. The target state K1, instead, featured tunability of the s-wave interaction with the fermionic bath via a magnetically controlled interspecies Feshbach resonance (FR) (see Sec. 6.2.3). As already mentioned, in both FB and FF mixtures, direct interaction between the impurities was negligible since the intraspecies s-wave scattering was off-resonant. We note here that in real experiments the single polaron energy $\mathcal{E}_\downarrow$, and the interaction coefficient $\mathcal{E}'_{\downarrow\downarrow}$, depend not only on the interaction parameter X, but also on the mass ratio and the resonance features. Since in the two mixtures used in our measurements the values of these parameters were almost identical and, in addition, the FRs exploited are in a near-universal regime (see Sec. 6.2.3 and Chap. 4.4.2), the difference in mass ratio and FR had a minor effect, so that the impurity quantum statistics was the only essential difference.

We implemented the RF-spectroscopic probing scheme by applying a 1-ms Blackman-shaped pulse (see Chapter 4.3.2). The pulse duration was chosen as a compromise between the spectral width of the RF pulse ($\sigma_{\mathrm{RF}} \approx 0.7$ kHz) and the shortest polaron lifetime (of the order of few ms for strong repulsion [Koh12; Fri21]). The pulse intensity was adjusted to obtain a resonant π-pulse in the absence of Li atoms. We varied the pulse frequency ν in order to probe the polaron spectrum. Our spectroscopic observable was the number N_{K0} of atoms remaining in K0 after the RF pulse. Note that in the measurements presented in Chapter 5, we had chosen $N_{\mathrm{K1}}/N_{\mathrm{K_{tot}}}$ to extract the signal. However, the absence of a sufficiently closed optical transition impeded

an efficient detection of atoms in K1 in particular for the FF mixture. Moreover, possible losses in the transfer process (though not observed) could have complicated the interpretation of a signal based on N_{K1}. We define the detuning $\Delta\nu = \nu_0 - \nu$ in the FB case, and $\Delta\nu = \nu - \nu_0$ in the FF case, where ν_0 is the bare frequency of the K0→K1 transition in the absence of Li. The opposite sign in the definitions of $\Delta\nu$ takes into account that in our FB mixture K0 has a higher energy than K1, and vice versa in our FF mixture. For both cases, the polaron spectrum is then represented by $N_{\mathrm{K0}}(h\Delta\nu/\epsilon_F)$, where the detuning is normalized by the effective Fermi energy of the bath ϵ_F.

In Fig. 6.2, we summarize the data analysis conducted in the case of the FB mixture, and we use this example to describe our routine. Note that analogous analyses were carried out for the FF mixture, as depicted in Fig. 6.3. In Fig. 6.2a we show a typical RF transfer signal, recorded for bosonic ^{41}K impurities, for two different values of the impurity concentration. The resonant dip corresponds to the polaron peak in the quasi-particle spectrum and its position reveals a small energy shift for the two concentrations shown, which we attribute to mediated interactions. We analyzed the signal by applying a heuristic fit model based on the sum of a Gaussian curve and a linear background, the latter taking into account the weak influence of the incoherent part of the polaron spectrum on the peak position [Cet16; Fri21]. The choice of this fitting function was linked to one key point that permitted us to obtain the results presented in this Chapter: the small variance of the X parameter for different measurements (see Tab. 6.1 and Tab. 6.2). Let's open a small parenthesis to explain this link.

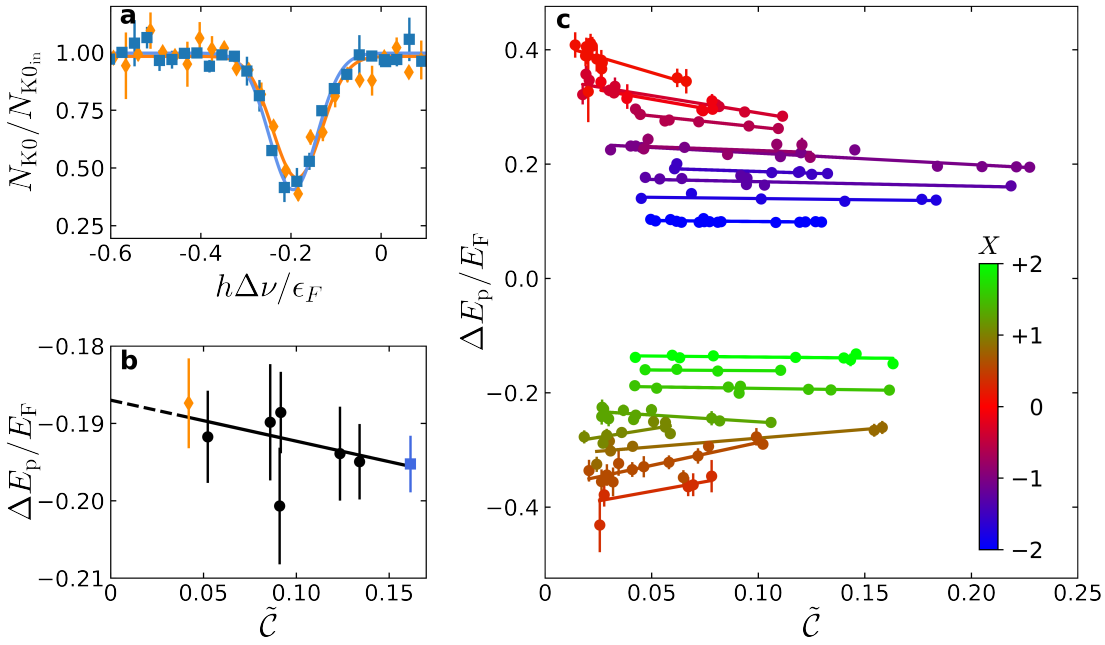

Figure 6.2: **Dependence of the polaron energy shift on the impurity concentration in the FB case. a**, two exemplary spectroscopy signals (normalized to the initial atom number) taken at $X = 0.98$ for different values of the interacting impurity concentration (blue squares $\mathcal{C} = 0.16$, orange diamonds $\mathcal{C} = 0.04$). The solid lines are fits with a Gaussian function plus a linear background (the latter being negligible small in the present data). The error bars represent the standard errors from typical 5-6 measurement repetitions. **b**, Polaron energy shift as a function of concentration for $X = 0.98$, the blue squared and the orange diamond correspond to the exemplary spectra presented in **a**. The black line represents a linear fit to the data with the dashed line showing the extrapolation to zero density. **c**, Polaron energy shift as a function of impurity concentration for different values of the interaction parameter X. From center to top (blue to red) increasing repulsion, from center to bottom (green to red) increasing attraction. Statistical uncertainties are evaluated taking into account errors on the Fermi energy and fit uncertainties from analyzing the spectra.

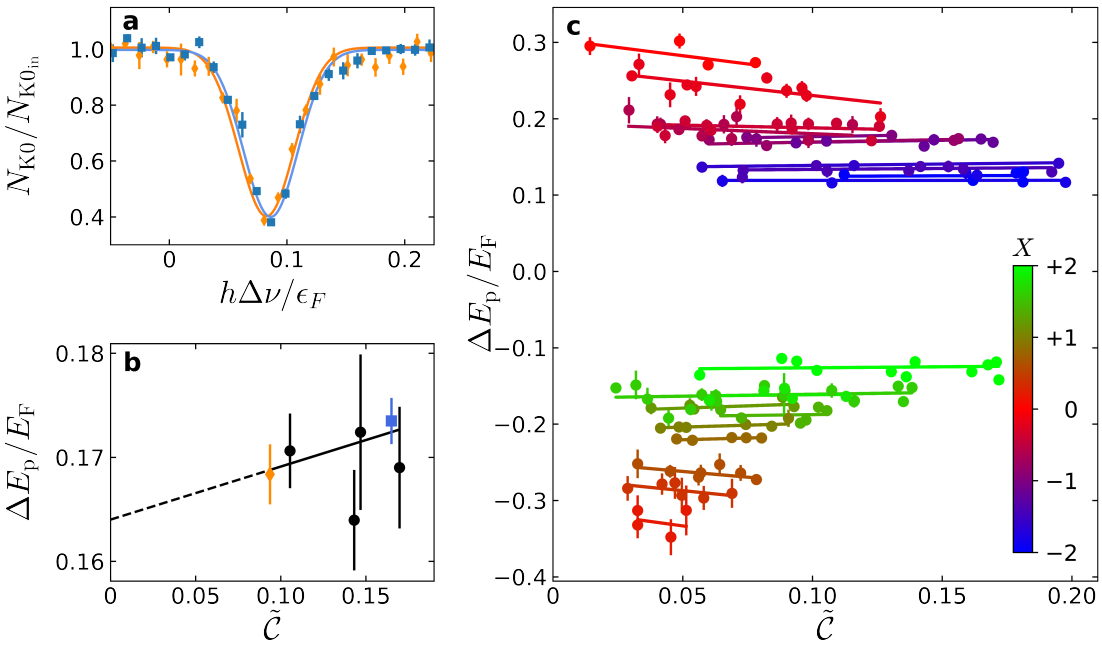

Figure 6.3: **Dependence of the polaron energy on the impurity concentration in the FF case.** **a**, two exemplary spectroscopy signals (normalized to the initial atom number) taken at $X = -1.41$ for different values of the interacting impurity concentration (blue squares $\tilde{\mathcal{C}} = 0.17$, orange diamonds $\tilde{\mathcal{C}} = 0.09$). The solid lines are fits with a Gaussian function plus a linear background. The error bars represent the standard errors from typical 5-6 measurement repetitions. **b**, Polaron energy as a function of concentration for $X = -1.41$, the blue squared and the orange diamond correspond to the exemplary spectra presented in **a**. The black line represents a linear fit to the data with the dashed line showing the extrapolation to zero density. **c**, Polaron energy as a function of impurity concentration for different values of the interaction parameter X. From center to top (blue to red) increasing repulsion, from center to bottom (green to red) increasing attraction. Statistical uncertainties are evaluated taking into account errors on the Fermi energy and fit uncertainties from analyzing the spectra.

As discussed in Section 6.2.4, the main limitation in our system concerning magnetic field stability, was given by slow drifts in the magnetic field during the measurements. In order to deal with this drift, in addition to reject spectra for which the difference in the measured magnetic field before and after the spectrum acquisition was larger

than 2 mG (1 mG) for FB (FF) (see Sec. 6.2.4), we performed the measurements in the shortest time possible and, as a consequence, we sampled the quasi-particle spectrum in a region centered around the polaron peak (typically less than ϵ_F wide), not recording the full background. As a well-established fact, the spectroscopy quasi-particle signal has two component: one due to the polaron, and one due to the presence of an underlying incoherent background [Mas14; Cet16; Fri21]. In previous work [Koh12; Fri21], the broad background was approximated by a Gaussian, so that the complete polaron spectrum could be modeled by a double Gaussian function (see Chapter 5.3). Given the incompleteness of the recorded background in the measurements presented in this Chapter, applying a double Gaussian fit to our spectrum was not possible. To circumvent this, we fitted our signal with a Gaussian combined with a linear background, the latter mimicking the presence of the not fully recorded incoherent background, especially present in the strongly interacting regime, and negligible for weak interactions. We checked that fitting selected spectra taken over a wider range with a Gaussian and a linear fit, and with a double Gaussian led to values of the polaron energy that are in each other error bars (see Fig. 6.4).

Coming back to the discussion of our analysis method, by fitting our spectra with a Gaussian combined with a linear background, we extracted the polaron energy peak position, and we identified it with $\Delta E_p/E_F$. From the fits, we also extracted the maximum transferred fraction of impurities from K0 to K1, $\mathcal{T}_{max}$. Based on the experimental observables, we introduce the effective impurity concentration in the interacting state as

$$\tilde{\mathcal{C}} = \mathcal{C}_{K0} \times \frac{1}{2}\mathcal{T}_{max}, \tag{6.3}$$

where $\mathcal{C}_{K0} = \bar{n}_{K0}/\bar{n}_{Li}$ is the concentration of the non-interacting K0 atoms, given by the ratio between the K-averaged atom number densities of the two species, $\bar{n}_{K0}$ and $\bar{n}_{Li}$. The factor $\frac{1}{2}$ in our definition of $\tilde{\mathcal{C}}$ arises from averaging the number of impurities,

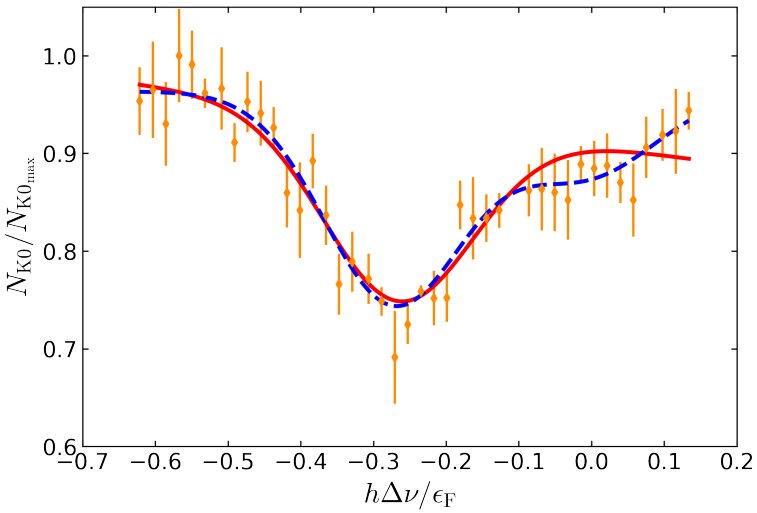

Figure 6.4: **Comparison between two fitting functions**. Spectroscopy signal for an exemplary measurement in the FF case at at $X = 0.75$ and for $\tilde{\mathcal{C}} = 0.08$ fitted by a Gaussian plus linear background (red solid line), and by a double Gaussian (red dashed line). The resulting dip position are at $\Delta E_p = -0.266(7)$ and $\Delta E_p = -0.27(1)$, respectively. The error bars represent the standard errors from typical 5-6 measurement repetitions.

which were gradually injected from 0 to the final value during the RF pulse[3].

In a second step of our data analysis, we considered the dependence of the polaron energy shift $\Delta E_p/E_F$ on the impurity concentration $\tilde{\mathcal{C}}$ for a fixed interaction strength X. In Fig. 6.2b, we present an example of the corresponding procedure for the FB mixture, considering $X \approx 1$. The orange diamond and the blue square represent the polaron energy shift extracted from the spectra in Fig. 6.2a where $\tilde{\mathcal{C}} \approx 0.04$ and $\tilde{\mathcal{C}} \approx 0.16$, respectively. We used a linear dependence to fit the observed behaviour (black line). From the obtained line, we extracted the interaction coefficient $\mathcal{E}'_{\downarrow\downarrow}$ as the slope, and the single impurity polaron energy $\mathcal{E}_\downarrow$ from extrapolation to zero. In Fig. 6.2c, we present the measured polaron energies, and the corresponding fits of the

[3]Note again that here we consider the effect of the RF transfer in defining the concentration while in Ref. [Fri21] and in Chapter 5, this effect was taken into account into the theory.

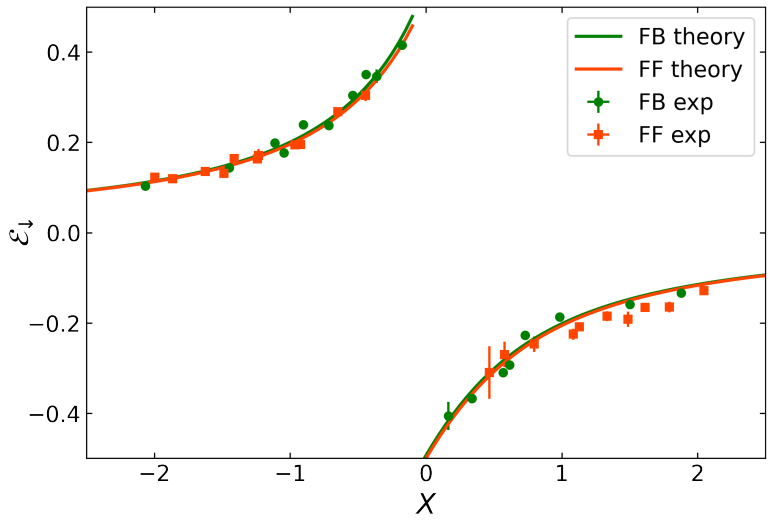

Figure 6.5: **Polaron energy shift in the single-impurity limit.** The experimental results for $\mathcal{E}_\downarrow$ extracted from the linear fits to $\Delta E_\mathrm{p}/E_\mathrm{F}$ *vs* $\tilde{\mathcal{C}}$ for FB (green circles) and FF (orange squares) are compared with the the first term in Eq. (6.1) (green and orange solid lines for FB and FF, respectively) for all the values of the dimensionless interacting strength parameter X considered. Note that the theory lines are almost identical for the FB and the FF case, so that they overlap to a large extent. Error bars for $\mathcal{E}_\downarrow$ correspond to the uncertainties of the linear fit, error bars for X, smaller than the symbol size, represent the standard errors for each set of measurements.

concentration dependence for different X values for the FB case. For all our recorded data, we found the linear dependence to fit the observed behaviour very well, with all deviations staying within the statistical uncertainties. This linear behaviour is in accordance with the expectations from Eq. (6.1).

We can now compare our experimental results with the theory presented in Eq. (6.1). As an important benchmark, we first confront the zero-concentration value $\mathcal{E}_\downarrow$, as obtained from our linear fits, with the first term of Eq. (6.1), representing the polaron energy shift in the single-impurity limit. This comparison is reported in Fig. 6.5 for the whole range of interaction strength values explored in our experiment, demonstrating satisfying agreement between the experimental results and the single polaron

theory presented in Chapter 3.2. Minor deviations, observed for fermionic impurities for $X \gtrsim 1$, are likely due to residual finite-temperature shifts in the FF mixture ($T/T_F \approx 0.24$), which was consistently hotter the the FB mixture ($T/T_F \approx 0.14$). The overall agreement with a well-established limiting case represented a validity check for our measurements and, in particular, for the linear fit of $\Delta E_p/E_F$ vs. $\tilde{\mathcal{C}}$. The impurity quantum statistics cannot play a role in the single-impurity limit, which is in accordance with our experimental results.

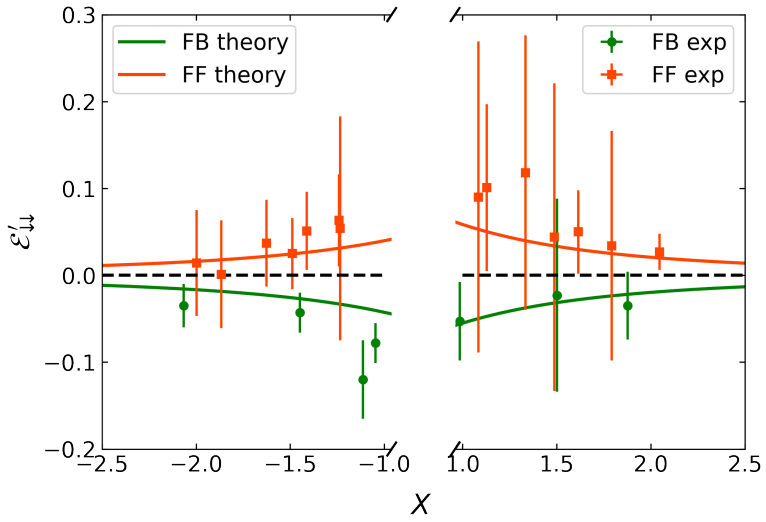

Figure 6.6: **Mediated interaction coefficient in the moderate interaction regime.** The experimental results for $\mathcal{E}'_{\downarrow\downarrow}$ extracted from the linear fit of $\Delta E_p/E_F$ *vs* $\tilde{\mathcal{C}}$ for FB (green circles) and FF (orange squares) are compared with the Eq. (6.2) (green and orange solid lines refer to FB and FF cases, respectively) for interaction values $|X| \gtrsim 1$. Error bars on $\mathcal{E}'_{\downarrow\downarrow}$ correspond to the uncertainties of the linear fit, error bars on X, smaller than the symbol size, represent the standard errors for each set of measurements.

Let us now turn our attention to the main quantity of interest for the mediated interaction: In our linear fits, the slope $\mathcal{E}'_{\downarrow\downarrow}$ quantifies the observed energy shift with increasing impurity concentration, and thus characterizes the interaction between the polarons. We can thus identify this slope with the interaction coefficient in Eq. (6.2),

which in turn represents the main prediction of Fermi-liquid theory from Ref. [Yu12]. The experimental results displayed in Fig. 6.6 for the regime of moderate interaction strength ($|X| \gtrsim 1$) clearly show the expected behaviour of the sign. For bosonic impurities, the downshift ($\mathcal{E}'_{\downarrow\downarrow} < 0$) with increasing concentration reveals attraction on both sides of the resonance. In contrast, for fermionic impurities, the observed interaction between the polarons, manifested in an upshift ($\mathcal{E}'_{\downarrow\downarrow} > 0$), is repulsive on both sides of the resonance. Regarding the magnitude of the rather weak interaction effect, our experimental results are consistent with the prediction. Most importantly, our observations highlighted the essential difference between bosonic and fermionic impurities, which is the opposite sign of polaron-polaron interaction [Yu12].

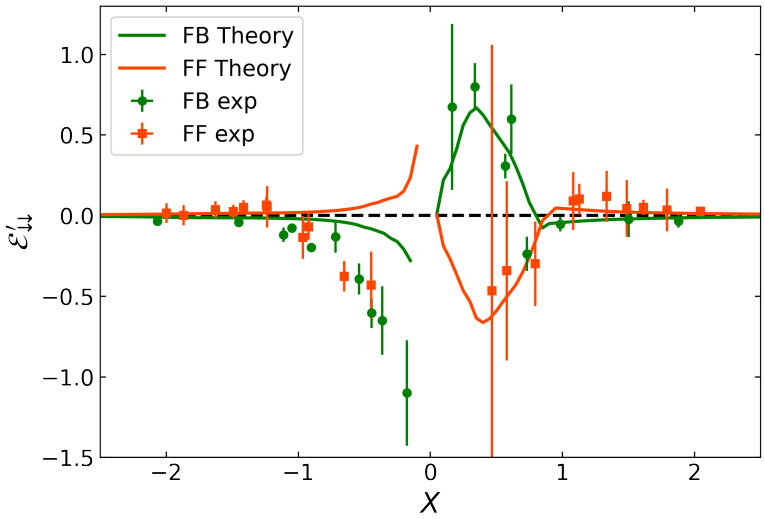

Figure 6.7: **Mediated interaction coefficient along the full resonance.** The experimental results for $\mathcal{E}'_{\downarrow\downarrow}$ for FB (green circles) and FF (orange squares) are compared with the extended theory model discussed in the text, assuming a population of excited molecules with a density equal to 2.5 times the density of the polarons (solid green and orange lines for FB and FF, respectively). Error bars on $\mathcal{E}'_{\downarrow\downarrow}$ correspond to the uncertainties of the linear fit. Error bars on X, smaller than the symbol size, represent the standard errors for each set of measurements.

In Fig. 6.7 we report the observed dependence of $\mathcal{E}'_{\downarrow\downarrow}$ across the full resonance, in

particular exploring the strongly interacting regime ($-1 < X < 1$). We find the linear approximation of Eq. (6.1) to hold for any interaction strength for both the FB and the FF case (see Fig. 6.2 and Fig. 6.3). For strong interactions, however, we observe striking deviations from the Fermi-liquid prediction of Eq. (6.2), which concern not only the magnitude of the effect but also its symmetry behaviour. When the resonance is approached from the lower side ($X < 0$), $\mathcal{E}'_{\downarrow\downarrow}$ acquires large negative values. This means that the repulsive interaction of impurities in the FS is counteracted by mediated interactions, causing an effective attraction. This change appears independent of the impurity quantum statistics, in contrast to the observations for moderate interaction strength. Approaching the resonance from the upper side ($X > 0$), a sign reversal is observed for both the bosonic and the fermionic impurity case. Below $X \approx 1$ the attractive (repulsive) character of the mediated interaction for bosonic (fermionic) impurities turns into a repulsive (attractive) one.

We speculate about two effects that may complicate the interpretation of mediated impurity interactions in the strongly interacting regime. First, the particle character of the polaron, as quantified by the quasi-particle residue, becomes increasingly suppressed near the resonance center (see Chapter 3.2). This raises general questions about the interpretation in terms of interacting quasi-particles, as the incoherent background of particle-hole excitations in the FS may dominate the many-body system, and this may result in the decrease of the mediated interaction strength observed below the resonance center. Above, the system is known to undergo the polaron-molecule transition [Pun09; Tre12; Mas12]. Including thermal broadening effects [Nes20; Par21], dimer formation can be expected below $X \approx 1$. A dimer formed by an impurity atom and an atom from the FS represents a new quasi-particle (molaron) with opposite quantum statistics. This may explain the sign reversal of mediated impurity interactions if significant molecular population is present.

Obviously, a theoretical model beyond Fermi-liquid theory is needed to understand

the intricate interaction physics in the strongly interacting regime. Our theory collaborator Miguel A. Bastarrachea-Magnani developed a model based on a T-matrix approach that takes into account the finite concentration of the impurities, their momentum and the presence of high energy molecular levels on the attractive side. While a detail description of this model is given in Ref.[Bar23], here we just discuss its main predictions.

For $0 < X \lesssim 1$ the model supports the molecular fraction as an explanation for the observed experimental deviation from the Landau's theory when considering, as fit parameter, a density of the high energy molecules 2.5 times higher than the density of the polarons (dashed-dotted lines in Fig. 6.7), value that is reasonable for our experimental conditions. The effect of the high energy molecules can be understood considering that in the FB case, a bosonic impurity can form a dimer with an interacting particle of the FS, creating a fermionic molecule. A finite density of such molecules Fermi blocks the interaction, reducing the negative energy shift due to the attractive polaron mediated interactions and producing repulsion. For $X \to 0^+$, the induced interaction between polarons becomes larger and eventually cancel this repulsive effect, leading to a decrease of $\mathcal{E}'_{\downarrow\downarrow}$ that eventually becomes negative again. Instead, in the FF case, fermionic impurities form bosonic molecules with the particles of the medium. A non-zero molecule density produces Bose-stimulation, decreasing the energy shift and creating an attractive interaction. Similar to the FB case, for $X \to 0^+$, the competition between the increasing polaron-polaron repulsive interaction and the attraction given by the presence of molecules leads to an increase of $\mathcal{E}'_{\downarrow\downarrow}$ that eventually becomes positive again.

For $X < 0$, however, the model does not yield an explanation of the observed behavior and we suspected that the Fermi-liquid theory may fail to describe such strongly repulsive system.

6.4 CONCLUSIONS

In this Chapter we presented the first observation of the mediated polaron-polaron interaction in ultracold atoms experiments. The measurements were performed in both a FB and FF mixture of ^{6}Li and either ^{41}K or ^{40}K. The marvelous similarity of the properties of the two FRs allowed for a direct comparison of the bosonic and fermionic statistics of the impurities.

For weak to moderate interactions between the bath and the impurities we observed the impurity concentration dependent energy shift of the polaron energy and its sign inversion due to impurity statistic, as predicted by Landau's Fermi liquid theory. For strong interspecies interactions, instead, we saw deviation from this theory that could be explained by the ill-definiteness of the polaron in this region and, on the attractive side of the FR, by the presence of high energy molecular levels.

In order to shed light on these deviation a new theoretical model, based on a T-matrix approach that takes into account the finite concentration of the impurities, their momentum and the presence of high energy molecular levels on the attractive side, was presented. While this model fails in reproducing the behaviour on the repulsive side, on the attractive side it qualitatively explains our observations when considering that the density of the high energy molecules is 2.5 times the density of the polarons

Crucial for this observation was the fact that in our system the impurities were thermal. Indeed, the mediated interaction can be masked in the case of degenerate impurities by the creation of a FS of polarons [Gir12], and by the different dispersion relation of the non interacting and interacting state in RF spectroscopy experiments [Sch09; Sca17].

From our observations we concluded that the Landau theory for mediated polaron-polaron interaction is valid in the interaction range $|X| \gtrsim 1$ and, in this region, for

at least all the interacting impurity concentrations achieved in our experiments, up to ~ 0.2.

It would be interesting to observe the effect of the mediated interaction by means of other techniques, such as via Ramsey interferometry [Cet16], which would help in understanding the system dynamics on shorter timescales.

OUTLOOK

In this Thesis, I presented two experiments aimed at investigating the physics of Fermi polarons. New questions have arisen from these measurements and in the following I will discuss some possible experiments that can be performed in FeLi(Bo)Kx. I will start presenting some technical upgrades.

Technical upgrades

New oven. At the moment, as already mentioned, our oven is providing a very low atom flux, and obtaining samples with large atom number is particularly hard. Fortunately, my colleague Erich Dobler has designed a new oven. Together with Adrian König, he is testing [Kön22], and soon will install it, allowing FeLi(Bo)Kx to keep on investigating new interesting physics.

Species-selective potential. In order to enrich the physics that we can investigate in our experiment, we have available an additional laser for K, which operates at a wavelength of about 767 nm. With this laser we could create a species-selective trap for K, with which we could better manipulate the density of the impurities, or a species-selective lattice, with which we could pin down

our impurities. At the moment, my colleague Erich Dobler has installed this laser in a setup that allows to exploit two-photon optical Raman transitions between K hyperfine states. This setup allows to switch between two configurations. In the first, thanks to two co-propagating laser beams, we can transfer atoms between two K hyperfine states without varying their momentum. Due to a higher (and widely tunable) Rabi frequency, this methods allows to obtain shorter π-pulses with respect to our usual RF technique. In the second configuration, thanks to a couple of counter-propagating laser beams, we can transfer atoms between two K hyperfine states while imprinting momentum to them. This technique opens the door to the investigation of momentum effects in the system.

Microscope. Our imaging system could be upgraded by installing a new microscope, designed by Emil Kirilov, which will increase the magnification by a factor of $\sim$8 [Ött19], possibly allowing for the observation of *insitu* distributions. Indeed, for instance, an *insitu* image of a K condensate, obtained with our current setup, is only approximately two pixel wide.

Future projects

Breaking down of the Fermi polaron. In the experiments presented in Chapter 6, limited by the performance of our current oven, we were not able to reach very high concentration of the impurities. With the new oven, and with the possibility to exploit a species-selective potential to match the densities of the two species [Dud23], we should be able to probe the polaron up to the regime where the Fermi polaron picture breaks down.

Probing the mediated interaction with Ramsey spectroscopy. In the measurements discussed in Chapter 6, we probed the mediated interaction between polarons via RF spectroscopy, that is, by injecting the impurities in the Fermi sea with a pulse much longer than the Fermi time, of the order of few μs. Thanks to the recently installed Raman setup in the co-propagating configuration we can probe the influence of the injection time, ranging from Fermi time to arbitrarily long times, thus investigating the behaviour of the system if a large concentration of interacting impurities is quenched or gradually increased into the bath. In this respect, the Raman setup allows to bridge the two approaches available in our experiment: the fairly slow RF transfer and the previously exploited optical shift of the Feshbach resonance [Cet16], which only allowed to quench the system. Further investigations of the mediated interaction can thus be carried out by exploiting a combination of Raman transfer and Ramsey interferometric techniques [Cet16], probing the evolution of the system after different injection times.

Infinite impurity mass. With the possibility to create a species-selective optical lattice, we can pin down our K impurities, effectively creating impurities with infinite mass. With this we could observe Anderson's orthogonality catastrophe [And67].

Bose polarons. As discussed in Chapter 5, in our system both Fermi and Bose polarons can coexist. It would be interesting to further study Bose polarons in our system. In particular, our system would be suitable for observing the BEC instability due to the transition between Bose polarons and Efimov clusters predicted in Ref. [Chr22].

Momentum dependence of the Fermi polaron. Thanks to the implemented Raman setup in the counter-propagating configuration, we can selectively transfer momentum to our K impurities, investigating the effect of moving impurities in a Fermi sea [Hu22]. In particular, we want to probe the stability of the Fermi polaron against the impurity momentum.

Scattering close to a narrow Feshbach resonance. For a narrow resonance, the range parameter R^* plays a not neglible role in the scattering process (see Section 2.1.3). Such parameter enters the scattering amplitude together with the relative momentum between the two particles (Eq. (2.2)). Thus, thanks to the implementation of the Raman setup in the counter-propagating configuration, we could test the influence of R^* in the scattering process for large relative momentum between the scattering particles.

Fermi sea modulation. Thanks to a better imaging system we could be able to observe density modulations in the Li Fermi sea due to the presence of the K impurities [Tre13].

There are many other possible research path that FeLi(Bo)Kx still offers, regardless of its age. Once the new oven will be install, its rejuvenation will be complete, and a new era of intriguing experiments is ready to begin.

LIST OF PUBLICATIONS

Breathing mode of a Bose-Einstein condensate repulsively interacting with a fermionic reservoir
Bo Huang, Isabella Fritsche, Rianne S. Lous, Cosetta Baroni, Jook T. M. Walraven, Emil Kirilov, and Rudolf Grimm
Phys. Rev. A 99, 041602(R) (2019); 10.1103/PhysRevA.99.041602

Effect of Inter-Well Interactions on Non-Linear Beam Splitters for Matter-Wave Interferometers [1]
Cosetta Baroni, Giacomo Gori, Maria Luisa Chiofalo, Andrea Trombettoni
Condens. Matter 5(2), 31 (2020); 10.3390/condmat5020031

Stability and breakdown of Fermi polarons in a strongly interacting Fermi-Bose mixture
Isabella Fritsche, Cosetta Baroni, Erich Dobler, Emil Kirilov, Bo Huang, Rudolf Grimm, Georg M. Bruun, and Pietro Massignan
Phys. Rev. A 103, 053314 (2021); 10.1103/PhysRevA.103.053314

Mediated interactions between Fermi polarons and the role of impurity quantum statistics
Cosetta Baroni, Erich Dobler, Isabella Fritsche, Bo Huang, Rudolf Grimm, Pietro Massignan, Georg M. Bruun, and Miguel Bastarrachea-Magnani
In preparation

[1] These results concern my Master thesis work and, even though the manuscript was completed in parallel to my PhD work, they are unrelated to my PhD project.

BIBLIOGRAPHY

[Adl20] H. S. Adlong, W. E. Liu, F. Scazza, M. Zaccanti, N. D. Oppong, S. Fölling, M. M. Parish and J. Levinsen, "Quasiparticle Lifetime of the Repulsive Fermi Polaron", Phys. Rev. Lett. 125 (2020), p. 133401 (cit. on p. 44).

[Alt21] E. Altman, K. R. Brown, G. Carleo, L. D. Carr, E. Demler, C. Chin, B. DeMarco, S. E. Economou, M. A. Eriksson, K.-M. C. Fu, M. Greiner, K. R. Hazzard, R. G. Hulet, A. J. Kollár, B. L. Lev, M. D. Lukin, R. Ma, X. Mi, S. Misra, C. Monroe, K. Murch, Z. Nazario, K.-K. Ni, A. C. Potter, P. Roushan, M. Saffman, M. Schleier-Smith, I. Siddiqi, R. Simmonds, M. Singh, I. Spielman, K. Temme, D. S. Weiss, J. Vučković, V. Vuletić, J. Ye and M. Zwierlein, "Quantum Simulators: Architectures and Opportunities", PRX Quantum 2 (2021), p. 017003 (cit. on p. 3).

[And67] P. W. Anderson, "Infrared Catastrophe in Fermi Gases with Local Scattering Potentials", Phys. Rev. Lett. 18 (1967), p. 1049 (cit. on pp. 5, 119).

[And95] M. H. Anderson, J. R. Ensher, M. R. Matthews, C. E. Wieman and E. A. Cornell, "Observation of Bose-Einstein condensation in dilute atomic vapor", Science 269 (1995), p. 198 (cit. on p. 2).

[And97] M. R. Andrews, D. M. Kurn, H.-J. Miesner, D. S. Durfee, C. G. Townsend, S. Inouye and W. Ketterle, "Propagation of Sound in a Bose-Einstein Condensate", Phys. Rev. Lett. 79 (1997), p. 553 (cit. on p. 3).

[App68] J. Appel, "Polarons", ed. by F. Seitz, D. Turnbull and H. Ehrenreich. Vol. 21. Solid State Physics. Academic Press, 1968, p. 193 (cit. on p. 3).

[Baa10] J. E. Baarsma, K. B. Gubbels and H. T. C. Stoof, "Population and mass imbalance in atomic Fermi gases", Phys. Rev. A 82 (2010), p. 013624 (cit. on p. 5).

[Baa12] J. E. Baarsma, J. Armaitis, R. A. Duine and H. T. C. Stoof, "Polarons in extremely polarized Fermi gases: The strongly interacting ^{6}Li-^{40}K mixture", Phys. Rev. A 85 (2012), p. 033631 (cit. on p. 5).

[Baa13] J. E. Baarsma and H. T. C. Stoof, "Inhomogeneous superfluid phases in ^{6}Li-^{40}K mixtures at unitarity", Phys. Rev. A 87 (2013), p. 063612 (cit. on p. 47).

[Bak99] G. A. Baker, "Neutron matter model", Phys. Rev. C 60 (1999), p. 054311 (cit. on p. 3).

[Bal08] M. Baldo and C. Maieron, "Neutron matter at low density and the unitary limit", Phys. Rev. C 77 (2008), p. 015801 (cit. on p. 3).

[Bar23] C. Baroni, E. Dobler, I. Fritsche, B. Huang, E. Kirilov, R. Grimm, P. Massignan, G. Bruun and M. Bastarrachea-Magnani, "In preparation", (2023) (cit. on pp. 5, 6, 25, 44, 47, 57, 58, 63, 91, 113).

[Blo08] I. Bloch, J. Dalibard and W. Zwerger, "Many-body physics with ultracold gases", Rev. Mod. Phys. 80 (2008), p. 885 (cit. on pp. 2, 4).

[Blo12] I. Bloch, J. Dalibard and S. Nascimbène, "Quantum simulations with ultracold quantum gases", Nat. Phys. 8 (2012), p. 267 (cit. on p. 3).

[Blo99] I. Bloch, T. W. Hänsch and T. Esslinger, "Atom Laser with a cw Output Coupler", Phys. Rev. Lett. 82 (1999), p. 3008 (cit. on p. 3).

[Bot22] S. Botsi, A. Yang, M. M. Lam, S. B. Pal, S. Kumar, M. Debatin and K. Dieckmann, "Empirical LiK excited state potentials: connecting short range and near dissociation expansions", Phys. Chem. Chem. Phys. 24 (2022), p. 3933 (cit. on p. 48).

[Bra95] C. C. Bradley, C. A. Sackett, J. J. Tollett and R. G. Hulet, "Evidence of Bose-Einstein condensation in an atomic gas with attractive interactions", Phys. Rev. Lett. 75 (1995), p. 1687 (cit. on p. 2).

[Bro25] L. de Broglie, "Recherces sur la théorie des Quanta", Ann. Phys. 10 (1925), p. 22 (cit. on p. 1).

[Bru04] G. M. Bruun, "Universality of a two-component Fermi gas with a resonant interaction", Phys. Rev. A 70, 053602 (2004), p. 053602 (cit. on p. 17).

[Bru05] G. M. Bruun, A. D. Jackson and E. E. Kolomeitsev, "Multichannel scattering and Feshbach resonances: Effective theory, phenomenology, and many-body effects", Phys. Rev. A 71 (2005), p. 052713 (cit. on p. 17).

[Bru10] G. M. Bruun and P. Massignan, "Decay of Polarons and Molecules in a Strongly Polarized Fermi Gas", Phys. Rev. Lett. 105 (2010), p. 020403 (cit. on p. 36).

[Bur14] A. Burchianti, G. Valtolina, J. A. Seman, E. Pace, M. De Pas, M. Inguscio, M. Zaccanti and G. Roati, "Efficient all-optical production of large ^{6}Li quantum gases using D_1 gray-molasses cooling", Phys. Rev. A 90 (2014), p. 043408 (cit. on p. 53).

[Cam18a] A. Camacho-Guardian and G. M. Bruun, "Landau Effective Interaction between Quasiparticles in a Bose-Einstein Condensate", Phys. Rev. X 8 (2018), p. 031042 (cit. on pp. 42, 64).

[Cam18b] A. Camacho-Guardian, L. A. Peña Ardila, T. Pohl and G. M. Bruun, "Bipolarons in a Bose-Einstein Condensate", Phys. Rev. Lett. 121 (2018), p. 013401 (cit. on p. 64).

[Cet15] M. Cetina, M. Jag, R. S. Lous, J. T. M. Walraven, R. Grimm, R. S. Christensen and G. M. Bruun, "Decoherence of Impurities in a Fermi Sea of Ultracold Atoms", Phys. Rev. Lett. 115 (2015), p. 135302 (cit. on pp. 44, 46, 54, 55, 59).

[Cet16] M. Cetina, M. Jag, R. S. Lous, I. Fritsche, J. T. M. Walraven, R. Grimm, J. Levinsen, M. M. Parish, R. Schmidt, M. Knap and E. Demler, "Ultrafast many-body interferometry of impurities coupled to a Fermi sea", Science 354.6308 (2016), p. 96 (cit. on pp. 44, 46, 47, 59, 93, 104, 107, 115, 119).

[Cha62] B. S. Chandrasekhar, "A note on the maximum critical field of high-field superconductors", Appl. Phys. Lett.s 1.1 (1962), p. 7 (cit. on p. 4).

[Che06a] F. Chevy, "Density Profile of a Trapped Strongly Interacting Fermi Gas with Unbalanced Spin Populations", Phys. Rev. Lett. 96.13, 130401 (2006), p. 130401 (cit. on p. 29).

[Che06b] F. Chevy, "Universal phase diagram of a strongly interacting Fermi gas with unbalanced spin populations", Phys. Rev. A 74 (2006), p. 063628 (cit. on pp. 4, 28, 29, 31, 93).

[Chi04] C. Chin, M. Bartenstein, A. Altmeyer, S. Riedl, S. Jochim, J. Hecker Denschlag and R. Grimm, "Observation of the Pairing Gap in a Strongly Interacting Fermi Gas", Science 305 (2004), p. 1128 (cit. on p. 24).

[Chi05] C. Chin and P. S. Julienne, "Radio-frequency transitions on weakly bound ultracold molecules", Phys. Rev. A 71, 012713 (2005), p. 012713 (cit. on p. 59).

[Chi10] C. Chin, R. Grimm, P. S. Julienne and E. Tiesinga, "Feshbach resonances in ultracold gases", Rev. Mod. Phys. 82 (2010), p. 1225 (cit. on pp. 2, 10, 14, 15, 17, 56).

[Chr22] A. Christianen, J. I. Cirac and R. Schmidt, "Chemistry of a Light Impurity in a Bose-Einstein Condensate", Phys. Rev. Lett. 128 (2022), p. 183401 (cit. on p. 119).

[Clo62] A. M. Clogston, "Upper Limit for the Critical Field in Hard Superconductors", Phys. Rev. Lett. 9 (1962), p. 266 (cit. on p. 4).

[Coh98a] C. Cohen-Tannoudji, J. Dupont-Roc and G. Grynberg, *Atom-Photon Interactions: Basic Processes and Applications*. John Wiley & Sons, Inc, 1998 (cit. on pp. 18, 22).

[Coh98b] C. N. Cohen-Tannoudji, "Nobel Lecture: Manipulating atoms with photons", Rev. Mod. Phys. 70 (1998), p. 707 (cit. on p. 22).

[Com07] R. Combescot, A. Recati, C. Lobo and F. Chevy, "Normal state of highly polarized Fermi gases: Simple many-body approaches", Phys. Rev. Lett. 98 (2007), p. 180402 (cit. on pp. 28, 33, 93).

[Com08] R. Combescot and S. Giraud, "Normal state of highly polarized Fermi gases: Full many-body treatment", Phys. Rev. Lett. 101 (2008), p. 050404 (cit. on pp. 28, 29, 32, 93).

[Com10] R. Combescot, S. Giraud and X. Leyronas, "Analytical theory of the dressed bound state in highly polarized Fermi gases", Europhys. Lett. 88.6 (2010), p. 60007 (cit. on p. 36).

[Dal89] J. Dalibard and C. Cohen-Tannoudji, "Laser cooling below the Doppler limit by polarization gradients: simple theoretical models", J. Opt. Soc. Am. B 6 (1989), p. 2023 (cit. on p. 13).

[Dal98] J. Dalibard, *Collisional dynamics of ultra-cold atomic gases*. Proceedings of the International School of Physics Enrico Fermi (M. Inguscio, S. Stringari, and C. Wieman, eds.), 1998 (cit. on p. 12).

[Dal99] F. Dalfovo, S. Giorgini, L. P. Pitaevskii and S. Stringari, "Theory of Bose-Einstein condensation in trapped gases", Rev. Mod. Phys. 71 (1999), p. 463 (cit. on p. 4).

[Dan17] I. Danshita, M. Hanada and M. Tezuka, "Creating and probing the Sachdev–Ye–Kitaev model with ultracold gases: Towards experimental studies of quantum gravity", Prog. Theor. Exp. Phys. 2017.8 (2017). 083I01 (cit. on p. 3).

[Dao07] T.-L. Dao, A. Georges, J. Dalibard, C. Salomon and I. Carusotto, "Measuring the One-Particle Excitations of Ultracold Fermionic Atoms by Stimulated Raman Spectroscopy", Phys. Rev. Lett. 98 (2007), p. 240402 (cit. on p. 23).

[Dao09] T.-L. Dao, I. Carusotto and A. Georges, "Probing quasiparticle states in strongly interacting atomic gases by momentum-resolved Raman photoemission spectroscopy", Phys. Rev. A 80 (2009), p. 023627 (cit. on p. 23).

[Dav95] K. B. Davis, M. O. Mewes, M. R. Andrews, N. J. van Druten, D. S. Durfee, D. M. Kurn and W. Ketterle, "Bose-Einstein condensation in a gas of sodium atoms", Phys. Rev. Lett. 75 (1995), p. 3969 (cit. on p. 2).

[DeM99] B. DeMarco and D. S. Jin, "Onset of Fermi Degeneracy in a Trapped Atomic Gas", Science 285 (1999), p. 1703 (cit. on p. 2).

[DeS19] B. DeSalvo, K. Patel, G. Cai and C. Cheng, "Observation of fermion-mediated interactions between bosonic atoms", Nature 568 (2019), p. 61 (cit. on p. 64).

[Dor12] R. Dorner, J. Goold and V. Vedral, "Towards quantum simulations of biological information flow", Interface Focus 2.4 (2012), p. 522 (cit. on p. 3).

[Dud23] M. Duda, X.-Y. Chen, A. Schindewolf, R. Bause, J. von Milczewski, R. Schmidt, I. Bloch and X.-Y. Luo, "Transition from a polaronic condensate to a degenerate Fermi gas of heteronuclear molecules", Nat. Phys. (2023) (cit. on p. 118).

[Eag69] D. M. Eagles, "Possible pairing without superconductivity at low carrier concentrations in bulk and thin-film superconducting semiconductors", Phys. Rev. 186 (1969), p. 456 (cit. on p. 4).

[Eam90] C. Eames and E. Ray, *A Computer Perspective: Background to the Computer Age*. Harvard University Press, 1990 (cit. on p. 3).

[Edr20] H. Edri, B. Raz, N. Matzliah, N. Davidson and R. Ozeri, "Observation of Spin-Spin Fermion-Mediated Interactions between Ultracold Bosons", Phys. Rev. Lett. 124 (2020), p. 163401 (cit. on p. 64).

[Fed96] P. O. Fedichev, Y. Kagan, G. V. Shlyapnikov and J. T. M. Walraven, "Influence of nearly resonant light on the scattering length in low-temperature atomic gases", Phys. Rev. Lett. 77 (1996), p. 2913 (cit. on p. 16).

[For14] M. M. Forbes, A. Gezerlis, K. Hebeler, T. Lesinski and A. Schwenk, "Neutron polaron as a constraint on nuclear density functionals", Phys. Rev. C 89 (2014), p. 041301 (cit. on p. 28).

[Fra10] E. Fratini and P. Pieri, "Pairing and condensation in a resonant Bose-Fermi mixture", Phys. Rev. A 81 (2010), p. 051605 (cit. on p. 92).

[Fri15] I. Fritsche, *Sub-Doppler cooling of fermionic lithium*. Master thesis. 2015 (cit. on p. 53).

[Fri21] I. Fritsche, C. Baroni, E. Dobler, E. Kirilov, B. Huang, R. Grimm, G. M. Bruun and P. Massignan, "Stability and breakdown of Fermi polarons in a strongly interacting Fermi-Bose mixture", Phys. Rev. A 103 (2021), p. 053314 (cit. on pp. 5, 6, 25, 32, 33, 38, 39, 44, 47, 57, 61, 64, 68, 70, 71, 73, 76, 78, 82, 83, 86, 92–94, 103, 104, 107, 108).

[Ful64] P. Fulde and R. A. Ferrell, "Superconductivity in a Strong Spin-Exchange Field", Phys. Rev. 135.3A (1964), A550 (cit. on p. 4).

[Gez08] A. Gezerlis and J. Carlson, "Strongly paired fermions: Cold atoms and neutron matter", Phys. Rev. C 77 (2008), p. 032801 (cit. on p. 3).

[Gez11] A. Gezerlis, "Spin-polarized low-density neutron matter", Phys. Rev. C 83 (2011), p. 065801 (cit. on p. 3).

[Gez12] Gezerlis, Alexandros and Sharma, Rishi, "Phase separation in low-density neutron matter", Phys. Rev. C 85 (2012), p. 015806 (cit. on p. 3).

[Gio08] S. Giorgini, L. P. Pitaevskii and S. Stringari, "Theory of ultracold atomic Fermi gases", Rev. Mod. Phys. 80 (2008), p. 1215 (cit. on p. 4).

[Gir12] S. Giraud and R. Combescot, "Interaction between polarons and analogous effects in polarized Fermi gases", Phys. Rev. A 85 (2012), p. 013605 (cit. on pp. 38, 43, 93, 96, 114).

[Goo11] J. Goold, T. Fogarty, N. Lo Gullo, M. Paternostro and T. Busch, "Orthogonality catastrophe as a consequence of qubit embedding in an ultracold Fermi gas", Phys. Rev. A 84 (2011), p. 063632 (cit. on p. 5).

[Gre03] M. Greiner, C. A. Regal and D. S. Jin, "Emergence of a Molecular Bose-Einstein Condensate from a Fermi Gas", Nature 426 (2003), p. 537 (cit. on p. 4).

[Gri07] R. Grimm, "Ultracold Fermi gases in the BEC-BCS crossover: a review from the Innsbruck perspective", arXiv preprint (2007) (cit. on p. 4).

[Gub09] K. B. Gubbels, J. E. Baarsma and H. T. C. Stoof, "Lifshitz Point in the Phase Diagram of Resonantly Interacting ^{6}Li-^{40}**K** Mixtures", Phys. Rev. Lett. 103 (2009), p. 195301 (cit. on p. 5).

[Gub13] K. Gubbels and H. Stoof, "Imbalanced Fermi gases at unitarity", Phys. Rep. 525.4 (2013), p. 255 (cit. on p. 92).

[Gur07] V. Gurarie and L. Radzihovsky, "Resonantly paired fermionic superfluids", Ann. Phys. (NY) 322.1 (2007), p. 2 (cit. on p. 17).

[Han10] T. Hanna and E. Tiesinga, Private communication (2010) (cit. on p. 57).

[Hew93] A. C. Hewson, *The Kondo Problem to Heavy Fermions*. Cambridge University Press, 1993 (cit. on p. 5).

[Hol21] M. Holten, L. Bayha, K. Subramanian, C. Heintze, P. M. Preiss and S. Jochim, "Observation of Pauli Crystals", Phys. Rev. Lett. 126 (2021), p. 020401 (cit. on p. 2).

[Hu16] M.-G. Hu, M. J. Van de Graaff, D. Kedar, J. P. Corson, E. A. Cornell and D. S. Jin, "Bose Polarons in the Strongly Interacting Regime", Phys. Rev. Lett. 117 (2016), p. 055301 (cit. on pp. 65, 76, 87).

[Hu18] H. Hu, B. C. Mulkerin, J. Wang and X.-J. Liu, "Attractive Fermi polarons at nonzero temperatures with a finite impurity concentration", Phys. Rev. A 98 (2018), p. 013626 (cit. on pp. 38, 64).

[Hu22] H. Hu and X.-J. Liu, "Raman spectroscopy of Fermi polarons", Phys. Rev. A 106 (2022), p. 063306 (cit. on pp. 23, 120).

[Hua19] B. Huang, I. Fritsche, R. S. Lous, C. Baroni, J. T. M. Walraven, E. Kirilov and R. Grimm, "Breathing mode of a Bose-Einstein condensate repulsively interacting with a fermionic reservoir", Phys. Rev. A 99 (2019), p. 041602 (cit. on pp. 47, 77, 80).

[Ing08] M. Inguscio, W. Ketterle and C. Salomon, eds., *Ultra-cold Fermi Gases, Proceedings of the International School of Physics "Enrico Fermi", Course CLXIV, Varenna, June 2006*. IOS Press, Amsterdam, 2008 (cit. on p. 46).

[Ino04] S. Inouye, J. Goldwin, M. L. Olsen, C. Ticknor, J. L. Bohn and D. S. Jin, "Observation of Heteronuclear Feshbach Resonances in a Mixture of Bosons and Fermions", Phys. Rev. Lett. 93, 183201 (2004), p. 183201 (cit. on p. 46).

[Jag16] M. Jag, M. Cetina, R. S. Lous, R. Grimm, J. Levinsen and D. S. Petrov, "Lifetime of Feshbach dimers in a Fermi-Fermi mixture of ^{6}Li and ^{40}K", Phys. Rev. A 94 (2016), p. 062706 (cit. on pp. 47, 85).

[Jin96] D. S. Jin, J. R. Ensher, M. R. Matthews, C. E. Wieman and E. A. Cornell, "Collective Excitations of a Bose-Einstein Condensate in a Dilute Gas", Phys. Rev. Lett. 77 (1996), p. 420 (cit. on p. 3).

[Joc03] S. Jochim, M. Bartenstein, A. Altmeyer, G. Hendl, S. Riedl, C. Chin, J. Hecker Denschlag and R. Grimm, "Bose-Einstein Condensation of Molecules", Science 302 (2003), p. 2101 (cit. on p. 4).

[Jør16] N. B. Jørgensen, L. Wacker, K. T. Skalmstang, M. M. Parish, J. Levinsen, R. S. Christensen, G. M. Bruun and J. J. Arlt, "Observation of Attractive and Repulsive Polarons in a Bose-Einstein Condensate", Phys. Rev. Lett. 117 (2016), p. 055302 (cit. on pp. 65, 76, 87).

[Kas22] V. Kasper, D. González-Cuadra, A. Hegde, A. Xia, A. Dauphin, F. Huber, E. Tiemann, M. Lewenstein, F. Jendrzejewski and P. Hauke, "Universal quantum computation and quantum error correction with ultracold atomic mixtures", Quantum Sci. Technol. 7.1 (2022), p. 015008 (cit. on p. 3).

[Ket08] W. Ketterle and M. W. Zwierlein, "Making, probing and understanding ultracold Fermi gases", Riv. del Nuovo Cim. 31 (2008), p. 247 (cit. on p. 23).

[Kna12] M. Knap, A. Shashi, Y. Nishida, A. Imambekov, D. A. Abanin and E. Demler, "Time-Dependent Impurity in Ultracold Fermions: Orthogonality Catastrophe and Beyond", Phys. Rev. X 2 (2012), p. 041020 (cit. on p. 5).

[Köh06] T. Köhler, K. Goral and P. S. Julienne, "Production of cold molecules via magnetically tunable Feshbach resonances", Rev. Mod. Phys. 78 (2006), p. 1311 (cit. on p. 17).

[Koh12] C. Kohstall, M. Zaccanti, M. Jag, A. Trenkwalder, P. Massignan, G. M. Bruun, F. Schreck and R. Grimm, "Metastability and coherence of repulsive polarons in a strongly interacting Fermi mixture", Nature 485 (2012), p. 615 (cit. on pp. 25, 32, 36, 44, 46, 47, 56, 59, 63, 67, 72, 74, 81, 82, 84, 93, 96, 103, 107).

[Kok15] S. Kokkelmans, "Feshbach Resonances in Ultracold Gases", *Quantum Gas Experiments*. Ed. by P. Törma and K. Sengstock. Imperial College Press, 2015, p. 63 (cit. on pp. 2, 10, 14).

[Kön22] A. König, *Characterization of a New Dual-Species Atomic Source for Lithium and Potassium*. Master thesis. 2022 (cit. on p. 117).

[Kon64] J. Kondo, "Resistance Minimum in Dilute Magnetic Alloys", Prog. Theor. Phys. 32.1 (1964), p. 37 (cit. on p. 5).

[Kos12] M. Koschorreck, D. Pertot, E. Vogt, B. Frölich, M. Feld and M. Köhl, "Attractive and repulsive Fermi polarons in two dimensions", Nature 485 (2012), p. 619 (cit. on p. 36).

[Krü15] T. Krüger, K. Hebeler and A. Schwenk, "To which densities is spin-polarized neutron matter a weakly interacting Fermi gas?", Physics Letters B 744 (2015), p. 18 (cit. on p. 3).

[Lan14] Z. Lan and C. Lobo, "A single impurity in an ideal atomic Fermi gas: current understanding and some open problems", J. Indian Inst. Sci. 94.2 (2014) (cit. on pp. 29, 31–33).

[Lan33] L. Landau, "Uber die Bewegung der Elektronen in Kristalgitter", Phys. Z. Sowjetunion 3 (1933), p. 644 (cit. on pp. 3, 27, 28).

[Lar65] A. I. Larkin and Y. N. Ovchinnikov, "Inhomogeneous state of superconductors", Sov. Phys. JETP 20 (1965), p. 762 (cit. on p. 4).

[LeB07] L. J. LeBlanc and J. H. Thywissen, "Species-specific optical lattices", Phys. Rev. A 75 (2007), p. 053612 (cit. on p. 5).

[Leg80] A. J. Leggett, *Modern Trends in the Theory of Condensed Matter*. Ed. by A. Pekalski and R. Przystawa. Vol. 115. Lecture Notes in Physics. Springer Verlag, Berlin, 1980, p. 13 (cit. on p. 4).

[Lev11] J. Levinsen and D. Petrov, "Atom-dimer and dimer-dimer scattering in fermionic mixtures near a narrow Feshbach resonance", Eur. Phys. J. D 65.1-2 (2011), p. 67 (cit. on p. 58).

[Lew07] M. Lewenstein, A. Sanpera, V. Ahufinger, B. Damski, A. Sen and U. Sen, "Ultracold atomic gases in optical lattices: mimicking condensed matter physics and beyond", Adv. Phys. 56 (2007), p. 243 (cit. on p. 3).

[Liu18] X.-P. Liu, X.-C. Yao, R. Qi, X.-Q. Wang, Y.-X. Wang, Y.-A. Chen and J.-W. Pan, "Feshbach spectroscopy of an ultracold ^{41}K$-^{6}$Li mixture and ^{41}K atoms", Phys. Rev. A 98 (2018), p. 022704 (cit. on p. 48).

[Liu20a] W. E. Liu, Z. Shi, M. M. Parish and J. Levinsen, "Theory of Radio-Frequency Spectroscopy of Impurities in Quantum Gases", Phys. Rev. A 102 (2020), p. 023304 (cit. on p. 25).

[Liu20b] W. E. Liu, Z.-Y. Shi, J. Levinsen and M. M. Parish, "Radio-Frequency Response and Contact of Impurities in a Quantum Gas", Phys. Rev. Lett. 125 (2020), p. 065301 (cit. on p. 25).

[Lob06] C. Lobo, A. Recati, S. Giorgini and S. Stringari, "Normal State of a Polarized Fermi Gas at Unitarity", Phys. Rev. Lett. 97 (2006), p. 200403 (cit. on pp. 4, 28, 29, 93).

[Lof02] T. Loftus, C. A. Regal, C. Ticknor, J. L. Bohn and D. S. Jin, "Resonant Control of Elastic Collisions in an Optically Trapped Fermi Gas of Atoms", Phys. Rev. Lett. 88 (2002), p. 173201 (cit. on p. 57).

[Lou00] R. Loudon, *The Quantum Theory of Light, 3rd ed.* Oxford University Press, USA, 2000 (cit. on pp. 18, 22).

[Lou17] R. S. Lous, I. Fritsche, M. Jag, B. Huang and R. Grimm, "Thermometry of a deeply degenerate Fermi gas with a Bose-Einstein condensate", Phys. Rev. A 95 (2017), p. 053627 (cit. on pp. 47, 53, 55).

[Lou18a] R. Lous, "Tunable Bose-Fermi and Fermi-Fermi mixtures of potassium and lithium: phase separation, polarons and molecules". PhD thesis. Innsbruck University, 2018 (cit. on pp. 47, 49).

[Lou18b] R. S. Lous, I. Fritsche, M. Jag, F. Lehmann, E. Kirilov, B. Huang and R. Grimm, "Probing the Interface of a Phase-Separated State in a Repulsive Bose-Fermi Mixture", Phys. Rev. Lett. 120 (2018), p. 243403 (cit. on pp. 47, 54, 55, 57, 59, 77, 80).

[Lud11] D. Ludwig, S. Floerchinger, S. Moroz and C. Wetterich, "Quantum phase transition in Bose-Fermi mixtures", Phys. Rev. A 84 (2011), p. 033629 (cit. on p. 92).

[Lud12] A. Ludewig, "Feshbach Resonances in ^{40}K". PhD thesis. University of Amsterdam, The Netherlands, 2012 (cit. on pp. 57, 99).

[Lys10] M. Lysebo and L. Veseth, "Feshbach resonances and transition rates for cold homonuclear collisions between ^{39}K and ^{41}K atoms", Phys. Rev. A 81 (2010), p. 032702 (cit. on pp. 57, 99).

[Mac05] M. Mackie and J. Piilo, "Feshbach-Resonant Interactions in ^{40}K and ^{6}Li Degenerate Fermi Gases", Phys. Rev. Lett. 94 (2005), p. 060403 (cit. on p. 47).

[Mas11] P. Massignan and G. M. Bruun, "Repulsive polarons and itinerant ferromagnetism in strongly polarized Fermi gases", Eur. Phys. J. D 65 (2011), p. 83 (cit. on pp. 33, 36, 40, 67, 81, 93).

[Mas12] P. Massignan, "Polarons and dressed molecules near narrow Feshbach resonances", Europhys. Lett. 98 (2012), p. 10012 (cit. on pp. 36, 79, 112).

[Mas14] P. Massignan, M. Zaccanti and G. M. Bruun, "Polarons, dressed molecules and itinerant ferromagnetism in ultracold Fermi gases", Rep. Prog. Phys. 77 (2014), p. 034401 (cit. on pp. 10, 17, 24, 25, 29, 81, 107).

[Mas20] P. Massignan, private communication (2020) (cit. on pp. 30, 35, 40).

[Mat11] C. J. M. Mathy, M. M. Parish and D. A. Huse, "Trimers, Molecules, and Polarons in Mass-Imbalanced Atomic Fermi Gases", Phys. Rev. Lett. 106 (2011), p. 166404 (cit. on p. 5).

[Mat99] M. R. Matthews, B. P. Anderson, P. C. Haljan, D. S. Hall, C. E. Wieman and E. A. Cornell, "Vortices in a Bose-Einstein Condensate", Phys. Rev. Lett. 83 (1999), p. 2498 (cit. on p. 3).

[Mis22] S. I. Mistakidis, A. G. Volosniev, R. E. Barfknecht, T. Fogarty, T. Busch, A. Foerster, P. Schmelcher and N. T. Zinner, "Cold atoms in low dimensions – a laboratory for quantum dynamics", arXiv preprint (2022) (cit. on p. 2).

[Moe95] A. J. Moerdijk, B. J. Verhaar and A. Axelsson, "Resonances in ultracold collisions of 6Li, ^{7}Li, and ^{23}Na", Phys. Rev. A 51 (1995), p. 4852 (cit. on p. 16).

[Mor09] C. Mora and F. Chevy, "Ground state of a tightly bound composite dimer immersed in a Fermi sea", Phys. Rev. A 80 (2009), p. 033607 (cit. on pp. 32, 36).

[Mor10] C. Mora and F. Chevy, "Normal Phase of an Imbalanced Fermi Gas", Phys. Rev. Lett. 104 (2010), p. 230402 (cit. on pp. 39, 42, 64).

[Mui22] J. Muir, J. Levinsen, S. Earl, M. A. Conway, J. H. Cole, M. Wurdack, R. Mishra, D. J. Ing, E. Estrecho, Y. Lu, D. K. Efimkin, J. O. Tollerud, E. A. Ostrovskaya, M. M. Parish and J. A. Davis, "Interactions between Fermi polarons in monolayer WS_2", Nat. Commun. 13 (2022), p. 6164 (cit. on p. 28).

[Nai11] D. Naik, A. Trenkwalder, C. Kohstall, F. M. Spiegelhalder, M. Zaccanti, G. Hendl, F. Schreck, R. Grimm, T. Hanna and P. Julienne, "Feshbach resonances in the ^{6}Li-^{40}K Fermi-Fermi mixture: Elastic versus inelastic interactions", Eur. Phys. J. D 65 (2011), p. 55 (cit. on pp. 46, 57).

[Nak20] E. Nakano, K. Iida and W. Horiuchi, "Quasiparticle properties of a single α particle in cold neutron matter", Phys. Rev. C 102 (2020), p. 055802 (cit. on p. 28).

[Nas09] S. Nascimbène, N. Navon, K. J. Jiang, L. Tarruell, M. Teichmann, J. McKeever, F. Chevy and C. Salomon, "Collective Oscillations of an Imbalanced Fermi Gas: Axial Compression Modes and Polaron Effective Mass", Phys. Rev. Lett. 103 (2009), p. 170402 (cit. on pp. 36, 44).

[Nav10] N. Navon, S. Nascimbène, F. Chevy and C. Salomon, "The Equation of State of a Low-Temperature Fermi Gas with Tunable Interactions", Science 328.5979 (2010), p. 729 (cit. on p. 44).

[Nes20] G. Ness, C. Shkedrov, Y. Florshaim, O. K. Diessel, J. von Milczewski, R. Schmidt and Y. Sagi, "Observation of a Smooth Polaron-Molecule Transition in a Degenerate Fermi Gas", Phys. Rev. X 10 (2020), p. 041019 (cit. on pp. 29, 44, 112).

[Nis13] Y. Nishida, "SU(3) Orbital Kondo Effect with Ultracold Atoms", Phys. Rev. Lett. 111 (2013), p. 135301 (cit. on p. 5).

[Noz85] P. Nozières and S. Schmitt-Rink, "Bose condensation in an attractive fermion gas: From weak to strong coupling superconductivity", J. Low Temp. Phys. 59 (1985), p. 195 (cit. on p. 4).

[OHa02] K. M. O'Hara, S. L. Hemmer, M. E. Gehm, S. R. Granade and J. E. Thomas, "Observation of a Strongly Interacting Degenerate Fermi Gas", Science 298 (2002), p. 2179 (cit. on p. 4).

[Opa13] B. Opanchuk, R. Polkinghorne, O. Fialko, J. Brand and P. D. Drummond, "Quantum simulations of the early universe", Ann. Phys. 525.10-11 (2013), p. 866 (cit. on p. 3).

[Ött19] T. Öttl, *Designing and Testing an Objective for Imaging Ultracold Quantum Gases*. Master thesis. 2019 (cit. on p. 118).

[Par21] M. M. Parish, H. S. Adlong, W. E. Liu and J. Levinsen, "Thermodynamic signatures of the polaron-molecule transition in a Fermi gas", Phys. Rev. A 103 (2021), p. 023312 (cit. on p. 112).

[Peñ19] L. A. Peña Ardila, N. B. Jørgensen, T. Pohl, S. Giorgini, G. M. Bruun and J. J. Arlt, "Analyzing a Bose polaron across resonant interactions", Phys. Rev. A 99 (2019), p. 063607 (cit. on p. 76).

[Pet03] D. S. Petrov, "Three-body problem in Fermi gases with short-range interparticle interaction", Phys. Rev. A 67, 010703 (2003), 010703(R) (cit. on pp. 37, 82).

[Pet04] D. S. Petrov, "Three-boson problem near a narrow Feshbach resonance", Phys. Rev. Lett. 93 (2004), p. 143201 (cit. on pp. 17, 58).

[Pin21] M. Pini, P. Pieri, R. Grimm and G. C. Strinati, "Beyond-mean-field description of a trapped unitary Fermi gas with mass and population imbalance", Phys. Rev. A 103 (2021), p. 023314 (cit. on p. 92).

[Pit16] L. Pitaevskii and S. Stringari, *Bose-Einstein Condensation and Superfluidity*. Oxford University Press, 2016 (cit. on p. 55).

[Pro08] N. Prokof'ev and B. Svistunov, "Fermi-polaron problem: Diagrammatic Monte Carlo method for divergent sign-alternating series", Phys. Rev. B 77 (2008), p. 020408 (cit. on pp. 36, 93).

[Pun09] M. Punk, P. T. Dumitrescu and W. Zwerger, "Polaron-to-molecule transition in a strongly imbalanced Fermi gas", Phys. Rev. A 80 (2009), p. 053605 (cit. on pp. 32, 36, 112).

[Qi12] R. Qi and H. Zhai, "Highly polarized Fermi gases across a narrow Feshbach resonance", Phys. Rev. A 85 (2012), 041603(R) (cit. on pp. 33, 36).

[Reg03] C. A. Regal and D. S. Jin, "Measurement of Positive and Negative Scattering Lengths in a Fermi Gas of Atoms", Phys. Rev. Lett. 90, 230404 (2003), p. 230404 (cit. on p. 57).

[Rid11] A. Ridinger, S. Chaudhuri, T. Salez, D. R. Fernandes, N. Bouloufa, O. Dulieu, C. Salomon and F. Chevy, "Photoassociative creation of ultracold heteronuclear 6Li40K* molecules", Europhys. Lett. 96.3 (2011), p. 33001 (cit. on pp. 47, 48).

[Sac97] C. Sackett, C. Bradley, M. Welling and R. Hulet, "Bose–Einstein condensation of lithium", App. Phys. B 65 (1997), p. 433 (cit. on p. 2).

[Saf13] M. S. Safronova, U. I. Safronova and C. W. Clark, "Magic wavelengths for optical cooling and trapping of potassium", Phys. Rev. A 87 (2013), p. 052504 (cit. on p. 47).

[San08] D. H. Santamore and E. Timmermans, "Fermion-mediated interactions in a dilute Bose-Einstein condensate", Phys. Rev. A 78 (2008), p. 013619 (cit. on p. 64).

[Sar63] G. Sarma, "On the influence of a uniform exchange field acting on the spins of the conduction electrons in a superconductor", J. Phys. Chem. Solids 24.8 (1963), p. 1029 (cit. on p. 4).

[Sca17] F. Scazza, G. Valtolina, P. Massignan, A. Recati, A. Amico, A. Burchianti, C. Fort, M. Inguscio, M. Zaccanti and G. Roati, "Repulsive Fermi Polarons in a Resonant Mixture of Ultracold ^{6}Li Atoms", Phys. Rev. Lett. 118 (2017), p. 083602 (cit. on pp. 25, 36, 43, 44, 82, 93, 96, 114).

[Sca22] F. Scazza, F. Zaccanti, P. Massignan, M. M. Parish and J. Jesper, "Repulsive Fermi and Bose Polarons in Quantum Gases", Atoms 10 (2022), p. 55 (cit. on pp. 38, 43, 94).

[Sch05] A. Schwenk and C. J. Pethick, "Resonant Fermi Gases with a Large Effective Range", Phys. Rev. Lett. 95 (2005), p. 160401 (cit. on p. 3).

[Sch09] A. Schirotzek, C.-H. Wu, A. Sommer and M. W. Zwierlein, "Observation of Fermi polarons in a tunable Fermi liquid of ultracold atoms", Phys. Rev. Lett. 102 (2009), p. 230402 (cit. on pp. 24, 29, 32, 36, 44, 93, 96, 114).

[Sch18] R. Schmidt, M. Knap, D. A. Ivanov, J.-S. You, M. Cetina and E. Demler, "Universal many-body response of heavy impurities coupled to a Fermi sea: a review of recent progress", Rep. Prog. Phys. 81 (2018), p. 024401 (cit. on pp. 5, 24, 25, 93).

[Sch20] F. Schäfer, T. Fukuhara, S. Sugawa, Y. Takasu and Y. Takahashi, "Tools for quantum simulation with ultracold atoms in optical lattices", Nat. Rev. Phys. 2 (2020), p. 411 (cit. on p. 3).

[Shi07] Y. Shin, C. H. Schunck, A. Schirotzek and W. Ketterle, "Tomographic rf Spectroscopy of a Trapped Fermi Gas at Unitarity", Phys. Rev. Lett. 99 (2007), p. 090403 (cit. on p. 24).

[Sid17] M. Sidler, P. Back, O. Cotlet, a. Srivastava, T. Fink, M. Kroner, E. Demler and A. Imamoglu, "Fermi polaron-polaritons in charge-tunable atomically thin semiconductors", Nat. Phys. 13 (2017), p. 255 (cit. on p. 28).

[Sie15] F. Sievers, N. Kretzschmar, D. R. Fernandes, D. Suchet, M. Rabinovic, S. Wu, C. V. Parker, L. Khaykovich, C. Salomon and F. Chevy, "Simultaneous sub-Doppler laser cooling of fermionic ^{6}Li and ^{40}K on the D_1 line: Theory and experiment", Phys. Rev. A 91 (2015), p. 023426 (cit. on p. 48).

[Sin13] A. Sindona, J. Goold, N. Lo Gullo, S. Lorenzo and F. Plastina, "Orthogonality Catastrophe and Decoherence in a Trapped-Fermion Environment", Phys. Rev. Lett. 111 (2013), p. 165303 (cit. on p. 5).

[Sko21] M. G. Skou, T. G. Skov, N. B. Jørgensen, K. K. Nielsen, A. Camacho-Guardian, T. Pohl, G. M. Bruun and J. J. Arlt, "Non-equilibrium quantum dynamics and formation of the Bose polaron", Nat. Phys. (2021), p. 731 (cit. on p. 76).

[Spi09] F. M. Spiegelhalder, A. Trenkwalder, D. Naik, G. Hendl, F. Schreck and R. Grimm, "Collisional stability of ^{40}K immersed in a strongly interacting Fermi Gas of ^{6}Li", Phys. Rev. Lett. 103 (2009), p. 223203 (cit. on p. 46).

[Spi10] F. M. Spiegelhalder, A. Trenkwalder, D. Naik, G. Kerner, E. Wille, G. Hendl, F. Schreck and R. Grimm, "All-optical production of a degenerate mixture of ^{6}Li and ^{40}K and creation of heteronuclear molecules", Phys. Rev. A 81 (2010), p. 043637 (cit. on pp. 46, 49, 53).

[Sta04] C. A. Stan, M. W. Zwierlein, C. H. Schunck, S. M. F. Raupach and W. Ketterle, "Observation of Feshbach Resonances between Two Different Atomic Species", Phys. Rev. Lett. 93, 143001 (2004) (cit. on p. 46).

[Ste08] J. T. Stewart, J. P. Gaebler and D. S. Jin, "Using photoemission spectroscopy to probe a strongly interacting Fermi gas", Nature 454 (2008), p. 744 (cit. on p. 24).

[Suc16] D. Suchet, M. Rabinovic, T. Reimann, N. Kretschmar, F. Sievers, C. Salomon, J. Lau, O. Goulko, C. Lobo and F. Chevy, "Analog simulation of Weyl particles with cold atoms", Europhys. Lett. 114.2 (2016), p. 26005 (cit. on p. 48).

[Tag08] M. Taglieber, A. C. Voigt, T. Aoki, T. W. Hänsch and K. Dieckmann, "Quantum Degenerate Two-Species Fermi-Fermi Mixture Coexisting with a Bose-Einstein Condensate", Phys. Rev. Lett. 100, 010401 (2008), p. 010401 (cit. on p. 48).

[Taj18] H. Tajima and S. Uchino, "Many Fermi polarons at nonzero temperature", New J. Phys. 20 (2018), p. 073048 (cit. on pp. 38, 64).

[Taj21] H. Tajima, J. Takahashi, S. I. Mistakidis, E. Nakano and K. Iida, "Polaron Problems in Ultracold Atoms: Role of a Fermi Sea across Different Spatial Dimensions and Quantum Fluctuations of a Bose Medium", Atoms 9.1 (2021) (cit. on p. 43).

[Tan10] L.-Y. Tang, Z.-C. Yan, T.-Y. Shi and J. Mitroy, "Dynamic dipole polarizabilities of the Li atom and the Be^+ ion", Phys. Rev. A 81 (2010), p. 042521 (cit. on p. 47).

[Tie10] T. G. Tiecke, M. R. Goosen, A. Ludewig, S. D. Gensemer, S. Kraft, S. J. J. M. F. Kokkelmans and J. T. M. Walraven, "Broad Feshbach resonance in the ^{6}Li-^{40}K mixture", Phys. Rev. Lett. 104 (2010), p. 053202 (cit. on p. 48).

[Tör00] P. Törmä and P. Zoller, "Laser Probing of Atomic Cooper Pairs", Phys. Rev. Lett. 85 (2000), p. 487 (cit. on p. 23).

[Tör15] P. Törma, "Spectroscopies - Theory", *Quantum Gas Experiments*. Ed. by P. Törma and K. Sengstock. Imperial College Press, 2015, p. 63 (cit. on pp. 4, 23, 24).

[Tör16] P. Törmä, "Physics of ultracold Fermi gases revealed by spectroscopies", Physica Scripta 91.4 (2016), p. 043006 (cit. on p. 24).

[Tre11] A. Trenkwalder, C. Kohstall, M. Zaccanti, D. Naik, A. I. Sidorov, F. Schreck and R. Grimm, "Hydrodynamic Expansion of a Strongly Interacting Fermi-Fermi Mixture", Phys. Rev. Lett. 106 (2011), p. 115304 (cit. on p. 46).

[Tre12] C. Trefzger and Y. Castin, "Impurity in a Fermi sea on a narrow Feshbach resonance: A variational study of the polaronic and dimeronic branches", Phys. Rev. A 85 (2012), p. 053612 (cit. on pp. 29, 33, 36, 93, 112).

[Tre13] C. Trefzger and Y. Castin, "Polaron residue and spatial structure in a Fermi gas", Europhys. Lett. 101.3 (2013), p. 30006 (cit. on p. 120).

[Vid21] I. Vidaña, "Fermi polaron in low-density spin-polarized neutron matter", Phys. Rev. C 103 (2021), p. L052801 (cit. on p. 28).

[Voi09] A.-C. Voigt, M. Taglieber, L. Costa, T. Aoki, W. Wieser, T. W. Hänsch and K. Dieckmann, "Ultracold heteronuclear Fermi-Fermi molecules", Phys. Rev. Lett. 102 (2009). *ibid.* **105**, 269904(E) (2010)., p. 020405 (cit. on pp. 47, 48).

[Wal19] J. Walraven, *Elastic collisions in ultracold atomic gases*. Lecture Notes at ICTP-SAIFR School on Interaction of Light with Cold Atoms. 2019 (cit. on p. 10).

[Wil08] E. Wille, F. M. Spiegelhalder, G. Kerner, D. Naik, A. Trenkwalder, G. Hendl, F. Schreck, R. Grimm, T. G. Tiecke, J. T. M. Walraven, S. J. J. M. F. Kokkelmans, E. Tiesinga and P. S. Julienne, "Exploring an ultracold Fermi-Fermi mixture: Interspecies Feshbach resonances and scattering properties of ^{6}Li and ^{40}K", Phys. Rev. Lett. 100, 053201 (2008), p. 053201 (cit. on p. 46).

[Wil09] E. Wille, "Preparation of an Optically Trapped Fermi-Fermi Mixture of ^{6}Li and ^{40}K Atoms and Characterization of the Interspecies Interactions by Feshbach Spectroscopy". PhD thesis. Innsbruck University, 2009 (cit. on pp. 46, 49).

[Wu11] C.-H. Wu, I. Santiago, J. W. Park, P. Ahmadi and M. W. Zwierlein, "Strongly interacting isotopic Bose-Fermi mixture immersed in a Fermi sea", Phys. Rev. A 84 (2011), p. 011601 (cit. on p. 48).

[Wu17] Y. Wu, X. Yao, H. Chen, X. Liu, X. Wang, Y. Chen and J. Pan, "A quantum degenerate Bose–Fermi mixture of 41K and 6Li", Journal of Physics B: Atomic, Molecular and Optical Physics 50.9 (2017), p. 094001 (cit. on p. 48).

[Wu18] Y.-P. Wu, X.-C. Yao, X.-P. Liu, X.-Q. Wang, Y.-X. Wang, H.-Z. Chen, Y. Deng, Y.-A. Chen and J.-W. Pan, "Coupled dipole oscillations of a mass-imbalanced Bose-Fermi superfluid mixture", Phys. Rev. B 97 (2018), p. 020506 (cit. on p. 48).

[Yan19] Z. Yan, P. B. Patel, B. Mukherjee, R. J. Fletcher, J. Struck and M. W. Zwierlein, "Boiling a Unitary Fermi Liquid", Phys. Rev. Lett. 122 (2019), p. 093401 (cit. on pp. 44, 93).

[Yan20a] Z. Z. Yan, Y. Ni, C. Robens and M. W. Zwierlein, "Bose polarons near quantum criticality", Science 368 (2020), p. 6487 (cit. on p. 76).

[Yan20b] A. Yang, S. Botsi, S. Kumar, S. B. Pal, M. M. Lam, I. Čepait ė, A. Laugharn and K. Dieckmann, "Singlet Pathway to the Ground State of Ultracold Polar Molecules", Phys. Rev. Lett. 124 (2020), p. 133203 (cit. on pp. 47, 48).

[Yao16] X.-C. Yao, H.-Z. Chen, Y.-P. Wu, X.-P. Liu, X.-Q. Wang, X. Jiang, Y. Deng, Y.-A. Chen and J.-W. Pan, "Observation of Coupled Vortex Lattices in a Mass-Imbalance Bose and Fermi Superfluid Mixture", Phys. Rev. Lett. 117 (2016), p. 145301 (cit. on p. 48).

[Yi06] W. Yi and L.-M. Duan, "BCS-BEC crossover and quantum phase transition for ^{6}Li and ^{40}K atoms across the Feshbach resonance", Phys. Rev. A 73 (2006), p. 063607 (cit. on p. 47).

[Yu10] Z. Yu, S. Zöllner and C. J. Pethick, "Comment on "Normal Phase of an Imbalanced Fermi Gas"", Phys. Rev. Lett. 105 (2010), p. 188901 (cit. on pp. 39, 42, 64).

[Yu11] Z.-Q. Yu, S. Zhang and H. Zhai, "Stability condition of a strongly interacting boson-fermion mixture across an interspecies Feshbach resonance", Phys. Rev. A 83 (2011), p. 041603 (cit. on p. 92).

[Yu12] Z. Yu and C. J. Pethick, "Induced interactions in dilute atomic gases and liquid helium mixtures", Phys. Rev. A 85 (2012), p. 063616 (cit. on pp. 38–40, 42, 64, 93, 94, 111).

[Zwi03] M. W. Zwierlein, C. A. Stan, C. H. Schunck, S. M. F. Raupach, S. Gupta, Z. Hadzibabic and W. Ketterle, "Observation of Bose-Einstein Condensation of Molecules", Phys. Rev. Lett. 91 (2003), p. 250401 (cit. on p. 4).

[Zwi05] M. W. Zwierlein, J. R. Abo-Shaeer, A. Schirotzek, C. H. Schunck and W. Ketterle, "Vortices and Superfluidity in a Strongly Interacting Fermi Gas", Nature 435 (2005), p. 1047 (cit. on p. 4).

[Zwi06] M. W. Zwierlein, A. Schirotzek, C. H. Schunck and W. Ketterle, "Fermionic Superfluidity with Imbalanced Spin Populations", Science 311 (2006), p. 492 (cit. on p. 4).

ACKNOWLEDGEMENTS

There are good ships and wood ships, ships that sail the sea,
but the best ships are friendships,
and may they always be!
Irish proverb

Working in an university environment is a bit like working in a harbor: You meet a lot of people, you enjoy time with them, but soon, in a way or another, they will leave for other seas. I hope that some of the bonds we built during this years will survive the distance. There are many people that made my PhD time easier and nicer, both inside and outside the lab, and here I want to thank them.

At the beginning of my PhD I knew very little of how to work in a lab is, and I am really grateful to Andrea, Rianne, and Isabella for the patience they showed in answering all my questions and teaching me how to do a lot of things. In particular, I want to thank Isabella, for having been a solid column in my first two years, when everything in the lab was breaking apart, for all the physics discussions, and for being a friend outside the lab. Thanks to Erich, who is upgrading our experiment so that we can run new exciting experiments, and to Gregor, who was always available to help for any issues we had with our softwares and bus system. Thanks to Emil, for being a reference figure for both scientific and personal discussions. Thanks to Erich

Wille, for having written such a complete PhD thesis that we still use like a bible in our experiment. Thanks to the DyK team, and in general to all the ultracold groups here in Innsbruck, for sharing equipment and knowledge.

A special thanks goes to the people of the administrative and of the workshop team: Elisabeth, Klaus, Mr. Knabl, Christine, Silvia, Barbara, Verena, Valentin, David, Gerhard, Bernhard, Andreas, and David, who are always the most helpful and friendly, even when asked for unusual and badly posed questions.

Even though I spent these five years mostly in the lab, I also enjoyed the company of very nice people outside it. Thanks to Isabella, Erich, and Gregor, for the fun we had together in and outside the lab and the office. Thanks to Vincent for all the mountain experiences we enjoyed during these years. I want to thank all our ultracold Italian community: Elisa, Deborah, Claudia, Gabriele, Elvia, and Lorenzo, for all the nice hikes and the tasty dinners. A special thanks to Elisa, who, together with Pietro and Luisa, made Völs a much funnier place, and to Deborah for supporting me on a daily basis. Moreover thanks to my family, for the support it always gave me.

Finally, a special thanks to Viktor, for all the physics discussions and for sharing with me all the good and bad moments.